



Durham E-Theses

Transport properties of HgTe - In(₂)Te(₃) alloys

Lewis, John Eric

How to cite:

Lewis, John Eric (1965) *Transport properties of HgTe - In(₂)Te(₃) alloys*, Durham theses, Durham University. Available at Durham E-Theses Online: <http://etheses.dur.ac.uk/8553/>

Use policy

The full-text may be used and/or reproduced, and given to third parties in any format or medium, without prior permission or charge, for personal research or study, educational, or not-for-profit purposes provided that:

- a full bibliographic reference is made to the original source
- a [link](#) is made to the metadata record in Durham E-Theses
- the full-text is not changed in any way

The full-text must not be sold in any format or medium without the formal permission of the copyright holders.

Please consult the [full Durham E-Theses policy](#) for further details.

Transport Properties of HgTe - In₂Te₃ Alloys

by

John Eric Lewis, B. Eng.

Thesis submitted for the degree of Doctor of Philosophy

University of Durham

1965



Acknowledgements

The work presented in this thesis forms part of a programme of research into semiconducting compounds and alloys being carried out at Durham University under the guidance of Professor D. A. Wright, to whom I am grateful for his continued help and encouragement, for providing the initial ideas, and for the use of the facilities of the Department of Applied Physics.

I am indebted to the Science Research Council (formerly the D.S.I.R.) for providing me with a maintenance grant over this period.

I have drawn greatly on the knowledge and experience of members of the Department, especially Dr. P.M. Spencer and Dr. W. Giriat, who preceded me in this research programme.

I would also like to thank Frank Spence and the workshop staff for their tolerance and understanding, and for their skill in building the apparatus. The thesis was typed by Miss F. Harland and duplicated by Xerox Copier 914 in the Department of Geography by Miss C. Gyll.

Introduction

This thesis is concerned with the production of single crystals of particular compositions of the alloy system indium sesquitelluride (In_2Te_3) and mercury telluride (HgTe) and the investigation of their electrical, galvanomagnetic, and thermomagnetic properties. The effects of annealing on these alloys was also investigated to some extent.

The alloys chosen were mercury telluride, HgTe ; 7% InTe_3 in HgTe ; 10%; 30%; 37.5%; 40% and 50% In_2Te_3 in HgTe . The first three were chosen as it is in this region of the system that the energy gap changes from an overlap (at HgTe) to a gap proper. The 37.5% composition was known to exist in an ordered superlattice form, of some interest, and could possibly represent the largest alloy composition having the band structure of HgTe . The 50% composition was chosen as its crystal structure had not been fully resolved, there being some argument as to whether it was ordered or disordered. It was also thought to have quite a different band structure than the lower compositions, hence different properties. The 30% and 40% compositions were added later in an attempt to investigate what was happening between these three regions.

In_2Te_3 has a low electronic mobility and an energy gap of about 1.1eV. Subject to the correct heat treatment its vacancies form an ordered superstructure which produces changes

in its energy gap, electronic mobility and thermal conductivity. However large single crystals of this material are difficult to produce so little valid work has been done on it, and there is disagreement in the results quoted for each different sample.

HgTe, on the other hand, has had considerable work carried out on it. Single crystals have been produced using standard techniques and most of its transport properties have been measured by various workers. However these properties are extremely sensitive to the previous heat treatment of the sample, especially if the sample has been treated in mercury vapour. Very high electronic mobilities are observed when the sample is appropriately annealed. Due to the high number of carriers at room temperature and liquid helium temperatures, HgTe is now considered to be a semi-metal with an overlap in energy between the conduction band and the valence band. Many of the results published for HgTe must be open to query on the grounds that the material has not been annealed to produce optimum properties or stoichiometry. For valid results measurements should only be carried out on single crystals on which the appropriate annealing technique has been performed.

Chapter I is a summary of relevant semiconductor physics required for this thesis. The first half of the chapter is a general introduction to the physics of semiconductors. The second half contains a more specialised treatment of the theory of the transport equations and the galvanomagnetic phenomena in general, sufficient for this thesis.

Chapter 2 contains a review of the properties of HgTe, which has had a considerable amount of work carried out in it, and of In_2Te_3 . Previous studies of the alloy system (HgTe - In_2Te_3) are also mentioned.

Chapter 3 describes the apparatus used and experimental techniques employed. This chapter is somewhat more detailed than is usual as it is felt that little is normally said about this side of research work although knowledge of techniques and apparatus is of the first importance to any research worker in this field of study.

The results of the experimental work are presented in chapters 4 and 5. In chapter 4 the results for HgTe are presented exclusively, the first half being concerned with the electrical properties, and results deduced from these, the second half being concerned with the galvanomagnetic and thermomagnetic measurements carried out on this compound. Chapter 5 deals with the alloy compositions, and sections treat each composition separately. After the results for the galvanomagnetic and thermomagnetic measurements have been presented, a further section deals with the alloy system as a whole, including HgTe. The chapter ends with a discussion of the effective mass of the carriers and the band-structure of the system in general.

Contents

Acknowledgements	i
Introduction	ii

Chapter 1

Relevant Theory

Introduction	1
Interatomic Bonding	1
The Ionic Bond	1
The Covalent Bond	2
Mixed Bonding	3
The Energy Gap	5
Impurities in Semiconductors	6
Band Theory of Solids	7
Form of the Energy Bands for a Semiconductor	11
The Effective Mass	13
Intrinsic Semiconduction	17
Impurity Semiconduction	21
General Equations for the Transport Properties in any Magnetic Field	25
Electrical Conductivity	32
The Hall Effect	33
The Seebeck Effect	36
Magnetoconductivity	38
The Hall Effect with Induction	41

Contents - continued

Magnetoseebeck Effect	42
Inhomogeneities	43
Scattering Mechanisms in Semiconductors	46
Lattice Scattering	48
Ionised Impurity Scattering	49
Dislocation Scattering	50
Alloy Scattering	51

Chapter 2

Previous Studies of the Materials

Introduction..	52
The Mercury-Tellurium Binary Alloy System	52
The Preparation and Electrical Properties of HgTe	54
The Band Structure of HgTe	61
Scattering Mechanisms in HgTe...	64
Other Properties of HgTe..	65
Summary of the Properties of HgTe	67
The Indium-Tellurium Binary Alloy System	70
The Compound In_2Te_3	71
The Structure of In_2Te_3	72
Optical and Photoelectrical Properties of In_2Te_3	73
Electrical Properties of In_2Te_3	74
Thermal Conductivity of In_2Te_3	77
The Effects of Ordering in In_2Te_3	78
Summary of the Properties of In_2Te_3	78

Contents - continued

The HgTe - In₂Te₃ Pseudo-Binary Alloy System 81

Chapter 3

Apparatus and Experimental Technique

Introduction.. 84

Furnace Technique 84

Preparation of the Materials 87

Preparation of the Charge 88

The Single Crystal Growing Furnace 90

Cutting, Grinding and Polishing of Samples.. 92

X - ray Technique... .. 94

Determination of the Lattice Parameter 96

Sample Holders 98

The Magnet 102

Experimental Arrangement and Procedure 102

Chapter 4

The Properties of Mercury Telluride

Introduction 108

Electrical Measurements on Unannealed Samples 109

Electrical Measurements on Annealed Samples 112

The Variation of the Hall Mobility with Temperature ... 116

The Effective Mass 118

Magnetoconductivity Measurements 120

Magnetoseebeck Measurements 124

Contents - continued

Chapter 5

The Properties of Some Alloys of HgTe and In_2Te_3

Introduction..	128
Electrical Properties of the Alloys	131
7% In_2Te_3 in HgTe	131
10% In_2Te_3 in HgTe	135
30% and 40% In_2Te_3 in HgTe	138
37.5% In_2Te_3 in HgTe	141
50% In_2Te_3 in HgTe	142
Magnetoconductivity and Magnetosebeck Measurements	144
The Alloy System HgTe - In_2Te_3	147
References	150

CHAPTER I

Relevant Theory

Introduction

This chapter falls into two distinct halves, the first half being an introduction to the physics of semiconductors, the second being a more specialised theory of the transport equations and the phenomena associated with them.

Interatomic Bonding

The atoms which combine to form a solid are bound to each other by means of their electrons. These electrons can form bonds in many different ways, the bonding of one solid never being quite the same as the bonding of another. These bonds can be categorised into four main types, the metallic bond, the ionic bond, the covalent bond and the Van der Waals bond (1). For most semiconductors, however, only the ionic or covalent type of bonding is predominant, or a combination of the two, known as 'mixed' bonding.

The Ionic Bond

The basic need of any atom is to achieve the stable configuration of a closed outer shell of electrons, the most important of these shells being that made up of eight electrons, two in s-states and six in p-states. When atoms of small ionisation

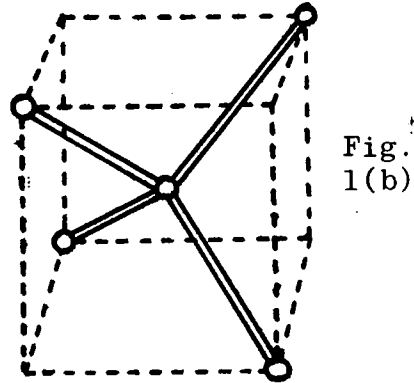
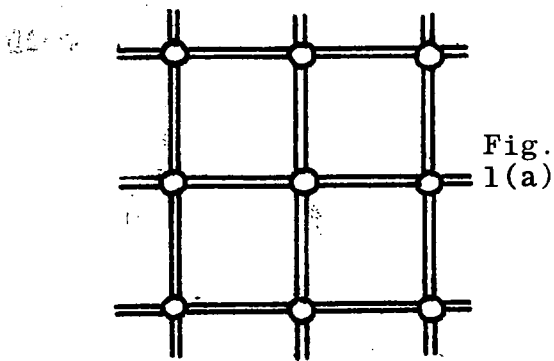


energy bond with ones of high ionisation energy, the latter do not lose their electrons but attempt to complete their valence octet at the expense of the former, that is, to achieve the electronic structure of the rare gas following them in the periodic table. The atoms of the resulting solid are so arranged that the attraction of the positive and negative ions just balances the repulsion of their electron clouds. The two common crystal structures found for ionic solids are typified by the compounds sodium chloride and caesium chloride. Caesium chloride forms a body centred cubic structure, as the ions are of similar size, whereas sodium chloride has a simple cubic structure, its ions being of unequal size. The simple cubic structure is found in some semiconductors, such as the sulphide, selenide, and telluride of lead, although the bonding here is not completely ionic in character (2).

The Covalent Bond

It has been shown by Heitler and London (3) that when two electrons are shared between two identical atoms they provide a strong binding force provided their spins are anti-parallel. Parallel spins provide a strong repulsive force. This concept of a double electron bond, together with the closed shell of eight electrons enables the bonding of an important group of semiconductors, the elements silicon, germanium, grey tin, and diamond, to be described. These elements, known as the Group IV Semiconductors, all belong to the fourth column of the

periodic table and each has four valence electrons. When a solid is formed these electrons are shared with nearest neighbours. Thus an association of eight electrons with each atom is achieved, a stable structure. This is illustrated schematically in Fig. 1(a). Each of the bond lines represents a shared electron, which is arranged with a pair of opposite spin. From symmetry considerations of such a system, the atoms would be expected to arrange themselves at the apexes of regular tetrahedrons, with one atom at the centre of each tetrahedron, as in Fig. 1(b). A regular lattice, the



diamond lattice, may be constructed in this way. All the elements mentioned form this structure.

Mixed Bonding

Only the Group IV semiconductors have bonds which are exclusively covalent. Most other semiconductors have bonds which are a mixture of the covalent and ionic type. The principal characteristics of the bonding will depend on which type is predominant. The III - IV group of semiconductors composed of compounds formed from elements in the third and fifth column

of the periodic table, is predominantly covalent in character. This is most clearly seen in that their crystal structure is very similar to that of the group IV semiconductors. Their structure is known as the zincblende structure.

The lead salts, PbS, PbSe, and PbTe, are an example of a class of semiconductors which have predominantly ionic bonding. These form a simple cubic structure. Generally, substances with predominantly covalent bonding form crystals with the zincblende structure, or a closely related type, whereas those with predominantly ionic bonding form crystals with simple cubic structures.

The mixed bonding with predominantly covalent characteristics, as in the group III - V semiconductors, also exists in the II - VI and I - VI compounds. Compounds of the more complicated type $\text{III}_2 \square \text{VI}_3$, where \square indicates an unoccupied lattice site, are also included in this type of bonding. They are known as defect semiconductors. $\text{In}_2 \square \text{Te}_3$ being a well known example.

The II - VI group of semiconductors, such as zinc sulphide and cadmium sulphide, have a hexagonal wurzite structure, which is closely allied to that of zincblende. The difference in the two structures is mainly in the number of nearest neighbours, the bonding of wurzite being slightly more ionic in nature than that of zincblende. It must be emphasised however, that for semiconductors, the nature of the bond, rather than the crystal structure, is the predominant feature in determining its physical properties. Also, in predicting new semiconducting

compounds, the rule of eight electrons in the outer shell is more successful than bond structure calculations based on crystal symmetry.

The Energy Gap

In a perfect covalent lattice at absolute zero, as typified by a group IV semiconductor, all the valence electrons are associated with the binding of the atoms into a solid. There are no extra electrons, 'free' electrons, which would be needed for conduction through the solid. This state can be considered as two bands, the valence band, which is completely filled with electrons, and the conduction band, which is completely empty of electrons. The two bands are separated in energy space by a gap, known as the energy gap, which is directly proportional to the minimum energy required to remove an electron from the bond and place it on a distant atom of the crystal. As the disrupted bond tries successively to complete itself, the deficit appears to move from one atom to another without energy change and corresponds to a hole in the valence band. The extra electron on the remote atom also moves through the crystal without energy change as the bond which it has disturbed tries to restore itself to its former covalency. This corresponds to an electron in the conduction band and the complete process is known as hole-electron formation. After some time the electron will recombine with the hole to restore the crystal to its former perfection and for any given temperature an equilibrium will be established between the thermal rate of formation of hole-electron

pairs and the rate of their recombination. The formation of a hole-electron pair is schematically represented in Fig 2.

At higher temperatures, thermal energy alone may be sufficient to break some bonds, although for diamond, the energy gap of 5.6 e.V is too great to allow an appreciable number of bonds to be broken. Thus diamond is an insulator, whereas germanium, with a gap of only 0.67 eV, has noticeable room temperature conductivity, albeit poor.

Impurities in Semiconductors

Any deviation from a perfect lattice will mean that some bonds are weakened and can provide more conduction electrons at a particular temperature than the perfect lattice. These defects have numerous causes, the main ones being substitutional atoms, interstitial atoms, vacancies in the lattice, surface atoms, dislocations in the crystal, and any combination of these (4). Well known examples of substitutional atoms in a crystal are the replacement of group V or III in a group IV semiconductor (5). Substituting a group V atom causes an extra free electron in the lattice which is easily removed from its parent atom, leaving an ionised atom in the lattice, which acts now as a scattering centre. Similarly group III atoms cause vacancies in the valence band, holes, leaving an ionised scattering centre in the lattice. Both these impurities require some energy to provide electrons in the conduction band or holes in the valence band, though much less than that required to break the normal bond and create a hole-electron pair (6). This is shown diagrammatically in Fig. 3, where the impurity centres are situated in the energy gap, at an energy level

below the conduction band (for donors) or above the valence band (for acceptors) corresponding to the energy required to ionise them in the lattice.

These impurity atoms, by being virtually all ionised at room temperature, can completely swamp the intrinsic behaviour of the pure semiconductor. Only minute amounts of such an impurity are required to do this, hence high standards of cleanliness and purity of materials are needed when attempting to produce an intrinsic, pure semiconductor.

For greater detail and theory on semiconductor chemistry, the reader is referred to references (7), (8), (9) and (10) and for extensive information on the chemistry of imperfect crystals, to reference (11).

Band Theory of Solids

To explain the physical properties of solids several models of the behaviour of electrons in the solid have been proposed. The earliest to be treated by quantum principles, that of Sommerfield (12) is known as the free electron model. In this the crystalline potential is averaged and the electrons are assumed to move independently in a field-free space, bounded by the surface of the solid. The motion of an electron in a solid is described, according to wave theory, by Schrödinger's equation.

$$\nabla^2 \psi + \frac{8\pi^2 m}{h^2} (E - V) \psi = 0 \quad \dots\dots(1)$$

where ψ is the wave function for the electron, E its energy and V the potential of the electron in the force field. For a field

free space, $V \equiv 0$ and for a one dimensional motion of an electron solutions of (1) are of the form

$$\Psi_k = A \frac{\sin}{\cos} (kx) \dots\dots\dots(2)$$

where the electron momentum is $\frac{hk}{2\pi}$, k acting as a set of quantum numbers describing the state of the electron.

This form of the wave function Ψ_k is inconvenient for many purposes as it depends entirely on the nature of the conditions at the boundary of the solid. Considerable understanding of the motion of electrons is gained by this approach and many of the properties of metals can be explained on this model. But the free electron model has many serious defects and can not begin to explain the differences in conductivity between insulators, semi-conductors and metals. This was only achieved when Bloch extended the free electron model to take into account the interactions of the electrons with the periodic lattice (13). It must be emphasised that this approach is again a simplification of the true interaction of electrons and a crystalline lattice. For example, to better explain the types of bonding or the process of conduction in solids known as hopping, other models are more useful, such as adaptations of the Heitler-London molecular model to solids. However, the assumption that the electron moves in a periodic field caused by the periodicity of the lattice allows many important physical properties to be explained, especially those of semiconductors. The band theory of solids, as it is known, has been used profitably for many years and has only needed slight modifications to explain quite complicated phenomena.

The solutions of Schrödinger's equation

$$\nabla^2 \psi(\underline{r}) + \frac{8\pi^2 m}{h^2} (E - V) \psi(\underline{r}) = 0 \dots\dots\dots(3)$$

where the potential V is periodic with the periodicity of the lattice:

$$V(\underline{r}) \equiv V(\underline{r} + \underline{d}) \dots\dots\dots(4)$$

\underline{r} is the vector position of the electron,

\underline{d} is any vector of the form $l_1 \underline{a}_1 + l_2 \underline{a}_2 + l_3 \underline{a}_3$ where the l_i are the primitive lattice vectors and the \underline{a}_i are the

Bloch wave functions, given by Floquet's theorem as:

$$\psi_{\underline{k}}(\underline{r}) = \exp(i \cdot \underline{k} \cdot \underline{r}) u_{\underline{k}}(\underline{r}) \dots\dots\dots(5)$$

$\psi_{\underline{k}}(\underline{r})$ is periodic with the periodicity of the lattice and \underline{k} is a constant vector whose three components act as a set of quantum numbers and can take any real value. The vector $\frac{\hbar \underline{k}}{2\pi}$ is called the crystal momentum by analogy with the electron momentum $\frac{\hbar \underline{k}}{2\pi}$ in the free electron model of Sommerfeld. The energy E is an even periodic function of \underline{k} of period $\frac{2\pi}{\underline{a}}$. This allows the value of \underline{k} to be restricted to an interval of $\frac{2\pi}{\underline{a}}$, called the first Brillouin zone. This zone is the smallest volume of \underline{k} space, centred on the origin, which included all non-equivalent values of \underline{k} . Distances in \underline{k} space can be proved to be reciprocal to those in the crystal (14), so that the Brillouin zone is known in terms of the Bravais lattice of the crystal.

In the Brillouin zone E is a multi-valued function of \underline{k} . The successive values E_1, E_2 --- for a given \underline{k} correspond first to the inner core electrons, then finally to the valence and conduction

electrons. In a semiconductor one value, or more if degeneracy occurs, ~~corresponds~~ ^{corresponds} to the valence band, and the next value (or values in the degenerate case) to the conduction band. Higher values of E represent higher unoccupied bands. Thus a fourth quantum number, denoting the particular band, is required to fully describe a state in the reduced zone scheme. In the tight binding approximation this number is well-known s-band, p-band, etc., but in general they are the Γ numbers of a particular band (15).

The main problem of the band model is to determine the shape of the E_i curves in \underline{k} space in the Brillouin zone. In a semiconductor holes and electrons will be located usually at points where E is an extremum, so the problem is simplified in these cases to determining the shape of these extrema, and the properties of the semiconductor will be largely determined by the dispersion relations at such points. The set of E_i values for all \underline{k} within the Brillouin zone is one band of allowed energy levels. In one dimension the sets are always separated by forbidden energy values, as shown in Fig. 4. The forbidden energy values are known as energy gaps and are analogous to the energy gap derived from considerations of crystal chemistry and bonding. In three dimensions there are several possible types of band, determined by the symmetry of the crystal and overlapping commonly occurs. In general the energy is discontinuous at the edge of a Brillouin zone, but exceptions do occur and two bands may meet at points or over an area of the zone edge. The discontinuity always occurs for a non-degenerate band and then, for reasons of symmetry, the normal derivative $\frac{\partial E}{\partial k}$ is identically zero. Each non-degenerate band can accommodate two electrons, of opposite

spins, for each ~~fundamental~~ ^{atom} ~~cell~~ cell of the crystal.

Form of the Energy Bands for a Semiconductor.

The determination of the function $E(\underline{k})$ is an extremely difficult theoretical problem even for the simpler crystal structures and has been done in only a few cases for semiconductors (16), (17), (18). Fortunately for most semiconductors only the extremum values of $E(\underline{k})$ are required as it is only states near these that contribute to the properties concerned.

Now $E(\underline{k})$ is an even function of \underline{k} and hence, in the non-degenerate case, must only contain quadratic terms near $\underline{k} = 0$, as $\frac{\partial E}{\partial \underline{k}}$ at $\underline{k} = 0$ is identically zero. At $\underline{k} = 0$ a maximum or minimum may occur and if these are the lowest minimum and the highest maximum they will be of great importance. Hence the simplest of all band structures occurs when the lowest unfilled band has a minimum at the zone centre and is non-degenerate. $E(\underline{k})$ may then be expanded in terms of

$$E(\underline{k}) = E_0 + Ak_x^2 + Bk_y^2 + Ck_z^2 + \text{higher powers} \dots \dots \dots (6)$$

where A, B, C are positive constants. For an isotropic cubic crystal the Brillouin zone has also cubic symmetry, which means that $A=B=C$, and ~~fundamental~~ ^{near} the minimum only the quadratic terms are of importance. Taking the zero of energy at the bottom of the band, at $\underline{k} = 0$,

$$E = \frac{h^2}{8\pi^2 m^*} (\underline{k}^2) \dots \dots \dots (7)$$

This band is said to be parabolic and has spherical symmetry. The scalar m^* has the dimensions of mass, and as equation (7) is

identical to that for free electrons but with the electron mass in replaced by m^* , m^* is known as the effective mass.

Similarly a maximum at $\underline{k} = 0$ can be described for an isotropic cubic crystal by

$$E = -E_0 - \frac{h^2}{8\pi^2 m^{*2}} (\underline{k}^2) \dots\dots\dots(8)$$

Here the electrons behave like free particles but with a negative effective mass, which is analagous to the behaviour of holes, previously introduced from chemical considerations of bonding and energy gap.

The combination of these two bands as in Fig.5. gives the simplest possible configuration for the valence and conduction bands of a semiconductor. Unfortunately no actual semiconductor has been found with this band structure (19) but it is usual to work with this model until experimental results prove otherwise. In this model the energy bands are described as spherical, as the constant energy surfaces are spheres in \underline{k} space.

Maxima and minima may occur elsewhere in \underline{k} space, especially at the zone edges. Considerations of crystal symmetry then allow other extrema to be predicted. Expansions for E can be used similar to those of equations (7) and (8) but now m^* will generally vary with position in \underline{k} space and will thus be a second rank tensor. Constant energy surfaces will no longer be sperical in \underline{k} space. but ellipsoidal. Constant energy surfaces in \underline{k} space are shown for various extrema in Fig. 6. When degeneracy occurs the band structure is more complicated. If the degeneracy occurs at $\underline{k} = 0$ as in Fig.7.

then a simple expansion of E in terms of \underline{k} is impossible as E is now not single valued in \underline{k} and a more complex form of E must be used, the result being that the constant energy surfaces in \underline{k} space are distorted from spheres. Each degenerate band has its own effective mass, one being heavier than the other. Consideration of Equation (8) predicts that the heavier mass band will be the outer, the light mass band be the inner. If numerous extrema occur, the band structure is said to be multivalley and under these conditions the valence band may overlap the conduction band in energy although being separated from each other in \underline{k} space. Under these conditions some electrons from the valence band will always be in the conduction band and the material is termed a semimetal. Examples of these materials are HgTe and HgSe, HgTe being discussed later in chapter II.

Recent developments both in calculations on the band structure of materials and experimental techniques are given in references (20) and (21).

The Effective Mass

Due to the importance of the $E(\underline{k})$ curves in \underline{k} space and the generally complicated nature of these curves, the concept of the effective mass m^* , introduced in equation (7), has become increasingly important in band theory. Deviations from the ideal parabolic band model are usually now described as variations of m^* along the curve, not as variations of the band structure itself (22).

The effect of introducing an effective mass is that of re-normalisation of the free electron model. If a physical quality Q (specific heat, density of carriers) is given for free electrons

by $Q = f(m)$, and the corresponding equation for the real solid is observed as Q^* , then an effective mass tensor can be defined such that $Q^* = f(m^*)$. The usefulness of this concept depends entirely on whether the various defined effective masses (the specific heat effective mass, the density of states effective mass...) are identical. This has been found to be true to a surprising degree, so the effect of the perturbing periodic field can be replaced by an effective mass tensor, whose elements may be determined from the unperturbed band structure. In fact the idea of an effective mass can be obtained from the entire many electron wave function without recourse to the one particle model (23). In semiconductor physics an electron or hole is a very complicated disturbance, yet for many situations they can be completely described by an effective mass and charge.

It can be proved (24) that for the general case, the effective mass tensor is given by:

$$\left(\frac{1}{m^*}\right)_{ij} = \frac{4\pi^2}{h^2} \frac{d^2 E_x}{dk_i dk_j} \dots\dots\dots (9)$$

By a suitable choice of axes the tensor may be diagonalised so that the non-diagonal terms vanish, when only three principle effective masses are needed to specify the motion of the electron

$$\frac{1}{m_i^*} = \frac{4\pi^2}{h^2} \frac{\partial^2 E_x}{\partial k_i^2} \quad i = x, y, z \dots\dots\dots (10)$$

In the case of spherical energy bands, the three components of the effective mass become equal, so in this case

$$\frac{1}{m^*} = \frac{4\pi^2}{h^2} \frac{\partial^2 E_x}{\partial k^2} \dots\dots\dots (11)$$

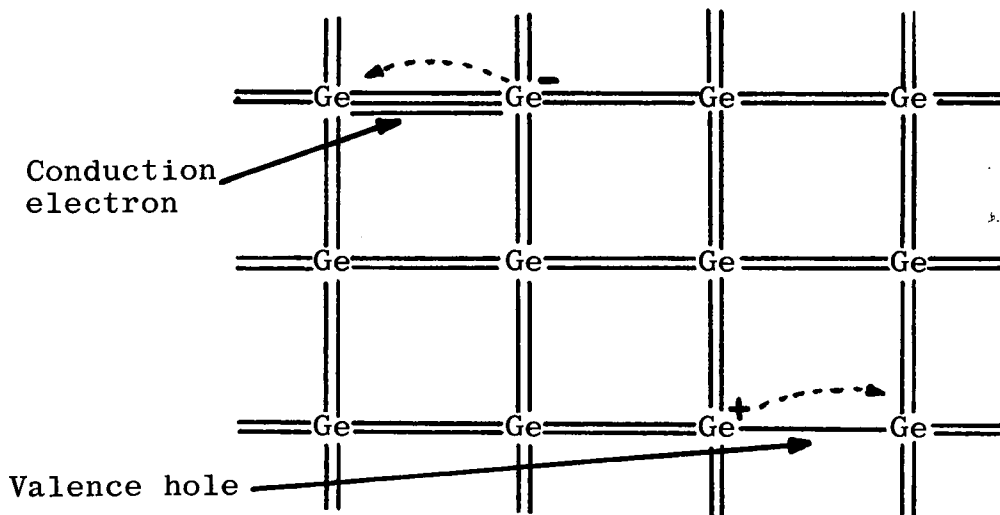


Fig. 2. Formation of hole-electron pair.

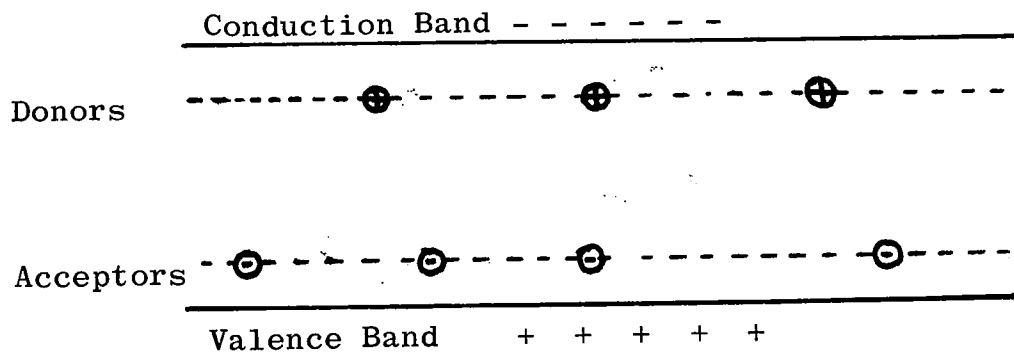
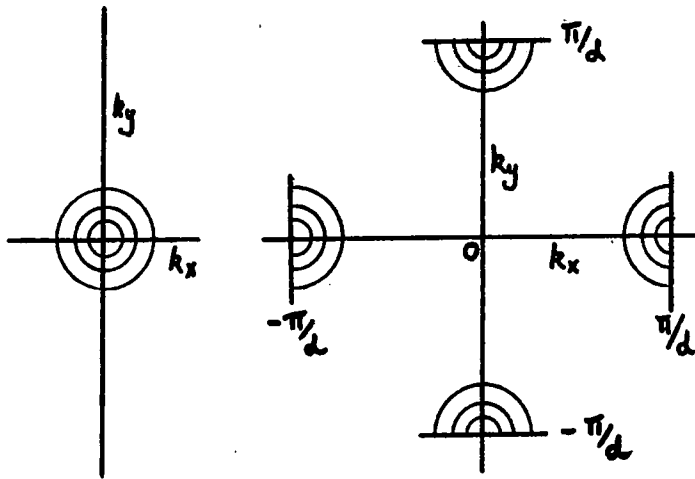
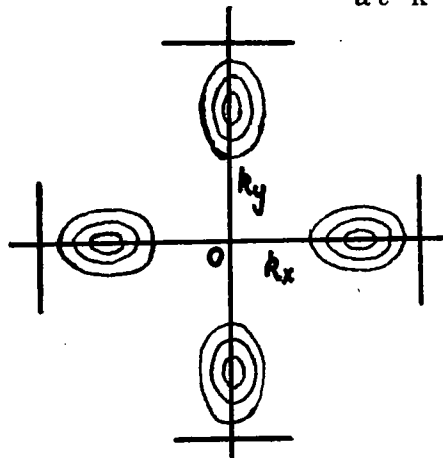


Fig. 3. Impurity Energy Levels in a Semiconductor.



Spherical surfaces
at $k = 0$.

Ellipsoidal surfaces
at $k = \pi/d$, etc.



Ellipsoidal surfaces at $k = k_0$
 $k_0 (< \pi/d)$, etc.

Fig. 6. Constant-energy surfaces shown as intersections
with the (k_x, k_y) plane.

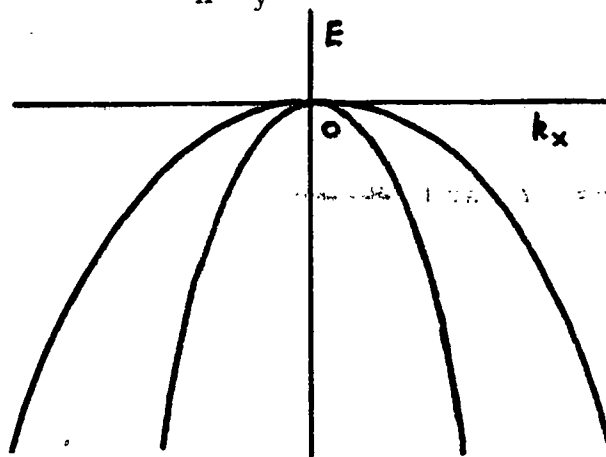


Fig. 7. Degenerate condition at $k = 0$ for k_x direction.

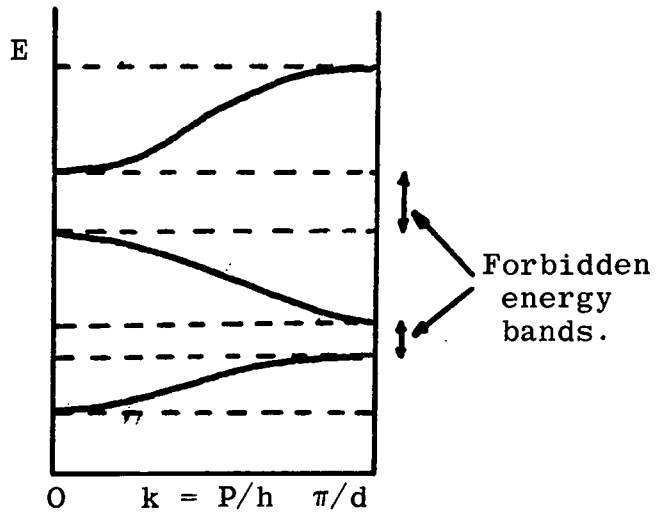


Fig.4. Reduced representation of E as a function of k .

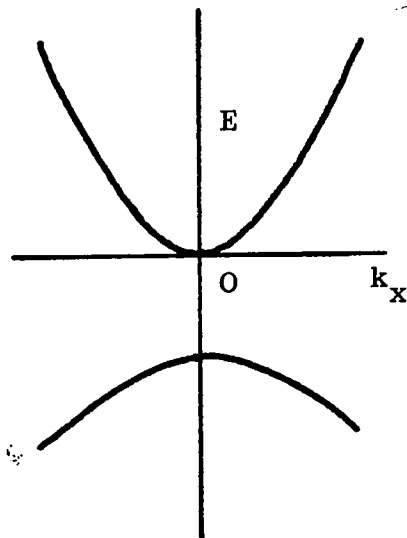


Fig.5. 'Spherical' energy bands at the centre of the Brillouin zone.

This equation implies that at the top of an energy band m^* is negative, as the second derivative of $E(k)$ will then be

P. 15

However, it is convenient to consider mass as positive, and as it is the transfer of energy in the conduction processes which is important, the holes at the top of the valence band are considered to have positive mass and positive charge.

conduction.

As previously mentioned there are various different effective masses, arising from different contexts. These are not all exactly identical and care must be taken to indicate which effective mass is being used. Two of these effective masses are of importance in conduction processes. The density of states effective mass, for ellipsoidal constant energy surfaces is defined as (25),

$$M_d^3 = M_1 M_2 M_3 \dots\dots\dots (12)$$

Where M_1, M_2, M_3 are the diagonal components of the effective mass tensor. The other components of the tensor are all zero as the principal axes of the tensor coincide, in this case, with the geometrical axes of the ellipsoid. $M_1, M_2,$ and M_3 can be thought of as the values of the scalar effective mass in the directions of the mutually perpendicular axes of the ellipsoid.

The conductivity effective mass M_c is defined by (26):

$$\frac{1}{M_c} = \frac{1}{3} \left(\frac{1}{M_1} + \frac{1}{M_2} + \frac{1}{M_3} \right) \dots\dots\dots (13)$$

and is usually used in connection with a relaxation time τ :

$$\mu_c = \frac{e\tau}{m_c} \dots\dots\dots(14)$$

where μ_c , the conductivity mobility, is defined by

$$\sigma = ne \mu_c \dots\dots\dots(15)$$

The effective mass as given from cyclotron resonance measurements for ellipsoidal constant energy surfaces is defined by (27)

$$W = W_0 = \frac{eB}{m_f}$$

$$\text{where } \frac{1}{m_f} \equiv \left(\frac{\eta^2}{m_2 m_3} + \frac{\xi^2}{m_3 m_1} + \frac{\zeta^2}{m_1 m_2} \right)^{1/2} \dots\dots\dots(16)$$

η, ξ, ζ are the direction cosines of the magnetic field B with the axes of the ellipsoidal and w_0 is the sharp resonance frequency for right hand circular polarisation. Equation (16) reduces to the simple form:

$$W_0 = \frac{eB}{M_d}$$

in the case of spherically symmetrical energy surfaces and parabolic bands. This effective mass is of great importance as it is directly given by measurement of the resonance frequency and magnetic induction. By far the most accurate determination of the effective mass tensor and the form of the band structure is thus given by this technique. However, it has only been successfully applied to a few semiconductors, such as Ge, Si, and InSb. Cyclotron resonance is observed at microwave frequencies for very pure samples of these semiconductors and this the band structures of Ge and Si near the extreme have been completely determined. To overcome the short relaxation time due to impurity scattering in less pure materials, and the magneto-plasma effect due to high carrier densities, very high magnetic

fields must be used even to observe the resonance frequency in the far infra-red region. These measurements have been made on a variety of materials but with less precision than with Ge and Si. In particular, alloys of HgTe with other II and VI compounds have been measured, which are discussed in Chapter 2. A full account of the technique of cyclotron resonance is given by Lax and Mavroides in reference (28).

The effective mass may also be determined from considerations of the Hall effect or the Seebeck effect, and the intrinsic carrier density (29). The theory used is invariably that for simple energy bands assuming the effective mass to be a scalar. It can also be obtained from studies of the magneto-resistance effect.

Intrinsic Semiconduction

Assuming the presence of an energy gap, it is possible to calculate the number of electrons excited into the conduction band from the valence band. The problem requires the use of Fermi-Dirac statistics which is only valid for particles, such as electrons, which obey the Pauli exclusion principle.

The probability P(E) that a non-degenerate energy level E will be occupied by an electron is given, from Fermi-Dirac statistics, by

$$P(E) = \frac{1}{\exp(E-E_f/kT)+1} \dots\dots\dots(17)$$

where

$$f(x) = \frac{1}{e^x + 1} \dots\dots\dots(18)$$

is known as the Fermi-Dirac distribution function, and E_F , known as the Fermi level, is that energy level with the probability of $1/2$

of occupancy. For large positive values of x the Fermi function approximates to e^{-x} and the probability $P(E)$ approaches the classical statistical mechanical value, in which the Pauli exclusion principle is not used:

$$P(E) = A \exp(-E/kT) \dots\dots\dots (19)$$

in which A is a normalising constant.

Consider only a simple spherical energy band semiconductor, having a direct energy gap of width E_g and no impurities in the gap, and take the zero of energy as the lowest level of the conduction band. If $N_c(E)dE$ is the density of allowed states in the conduction band between energy levels E and $E + dE$, then the number of electrons $n_i(E)dE$ in the conduction band between E and $E + dE$ is given by

$$n_i(E) dE = 2N_c(E).P(E)dE \dots\dots\dots (20)$$

The factor 2 accounts for the spin degeneracy of each level. Two electrons, of opposite spins, may occupy each level. The total number of electrons in the conduction band is therefore

$$n_i = 2 \int_0^{E_t} N_c(E). P(E) dE \dots\dots\dots (21)$$

where E_t is the energy of the top of the conduction band.

The function $N_c(E)$ is easily evaluated for the simple energy band structure under consideration (30), and is given by

$$N_c(E)dE = \frac{2\pi (2me)^{3/2}}{h^3} E^{1/2} dE \dots\dots\dots (22)$$

which is valid only for small values of E , and where M_e is the scalar density of states electron effective mass.

The classical approximation may be used for the Fermi probability

function, provided $E - E_f \gg kT$. With this provision, equation (22) may be used with all E in equation (21) as only small values of E will contribute greatly to the integral. For the same reason the upper limit of the integral can be extended to ∞ . So with these approximations and assumptions, equation (21) becomes

$$n_i = \frac{4\pi (2m_e)^{3/2} (kT)^{3/2} \exp(E_f/kT)}{h^3} \int_0^\infty x^{1/2} e^{-x} dx \dots \dots \dots (23)$$

where $x = E/kT$

on integration

$$n_i = N_c \exp E_f/kT \dots \dots \dots (24)$$

where

$$N_c = 2 \left(\frac{2\pi m_e kT}{h^2} \right)^{3/2} \dots \dots \dots (25)$$

A similar calculation for the number of holes in the valence band, the top of which has an energy $-E_g$, gives

$$p_i = N_v \exp \left(- (E_f + E_g)/kT \right) \dots \dots \dots (26)$$

where

$$N_v = 2 \left(\frac{2\pi m_h kT}{h^2} \right)^{3/2} \dots \dots \dots (27)$$

m_h being the scalar density of states hole effective mass.

As the number of electrons in the conduction band must be equal to the number of holes in the valence band, as they are created and destroyed in pairs, equating equations (24) and (26) gives a value of the Fermi level as

$$E_f = \frac{-E_g}{2} + \frac{3kT}{4} \cdot \ln \left(\frac{m_h}{m_e} \right) \dots \dots \dots (28)$$

If $m_h = m_e$ the Fermi level lies exactly halfway in the energy

gap, and for most semiconductors, where m_h does not equate m_e , the deviation is quite small. The deviation is towards the lighter mass band and becomes larger as the temperature increases. Insertion of this value of E_f , and the numerical constants, in equations (24) and (26) gives

$$n_i = p_i = 4.82 \cdot 10^{15} T^{3/2} \left(\frac{m_e m_h}{m_0^2} \right)^{3/4} \exp(-E_g/2kT) \text{ cm}^{-3} \dots\dots (29)$$

m_0 being the free electron mass. This equation may be used, with care, to determine the number of intrinsic carriers at a given temperature, but unless the effective masses are known, only an estimate can be deduced.

When the approximations made in integrating equation (21) are no longer valid, then n_i may be written in the form

$$n_i = 4\pi (2m_e kT/h^2)^{3/2} F_{1/2}(E_f/kT) \dots\dots\dots (30)$$

where the function $F_n(x)$, known as the Fermi Integral function, is defined by

$$F_n(x) = \int_0^\infty \frac{y^n dy}{\exp(y-x) + 1} \dots\dots\dots (31)$$

Similarly: $p_i = 4\pi (2m_h kT/h^2)^{3/2} F_{1/2}(-E_f + E_g/kT) \dots\dots\dots (32)$

and the Fermi energy E_f is given by the equation

$$m_e^{3/2} F_{1/2}(E_f/kT) = m_h^{3/2} F_{1/2}(-E_f + E_g/kT) \dots\dots\dots (33)$$

which has generally to be solved by numerical methods. Ehrenberg has proposed an approximation for $F_n(x)$ which is valid up to about $E_f = 2kT$ (31). Above this numerical calculation must be used.

Semiconductors with more complicated band structures can also be analysed (32) by this method, but only by introducing further approximations, or by introducing new parameters, such as a density of states effective mass tensor m_d , to take into account the non-spherical nature of the band structure. Even so, such approaches are valuable, as exact solutions are invariably cumbersome and tedious.

Impurity Semiconduction

When impurities are introduced into a semiconductor the effect of some of the impurities may be represented on the energy level diagram as extra allowed states within the energy gap, as only a small amount of energy is required to ionise these impurities fully. For small impurity concentrations the extra allowed states are discrete lines at either the ionisation energy above the valence band, for acceptors, or at the ionisation energy below the conduction band, for donors, as in Fig. (8). For large concentrations the wave

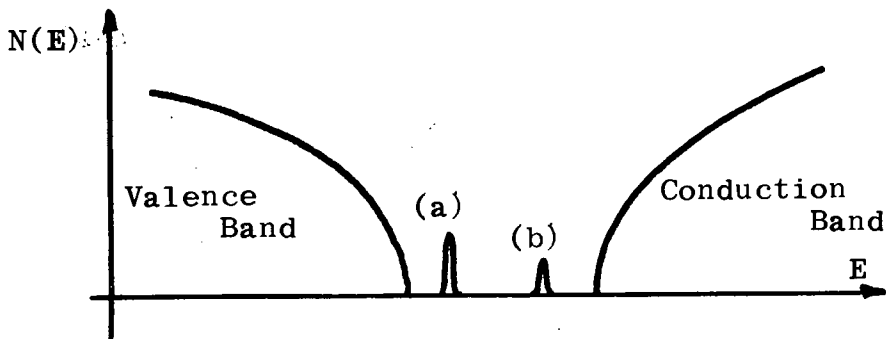


Fig. 8. Density of States for an Impure Semiconductor.

- (a) Acceptor Level
- (b) Donor Level

functions associated with the impurity atoms overlap and the discrete level broadens into a band, known as the impurity band. Then conduction is possible within this band as well as within the conduction and valence bands.

Provided the impurity concentration is not large, so that the

electrons and holes within the material are not degenerate, the concentration of electron, n , in the conduction band is still given by the equation (24),

$$n = N_c \exp. (E_f/kT) \dots\dots\dots(34)$$

Similarly $p = N_v \exp. -(E_f + E_g)/kT \dots\dots\dots(35)$

and the product $np = N_c N_v \exp. (-E_g/kT) = n_i^2 \dots\dots\dots(36)$

is independent of the impurity concentration and the Fermi level and is still equal to the square of the intrinsic concentration. As the number of electrons in the conduction band is now no longer equal to the number of holes in the valence band, the Fermi level E_f is no longer given by equating equations (24) and (26) as in equation (28), or its equivalent.

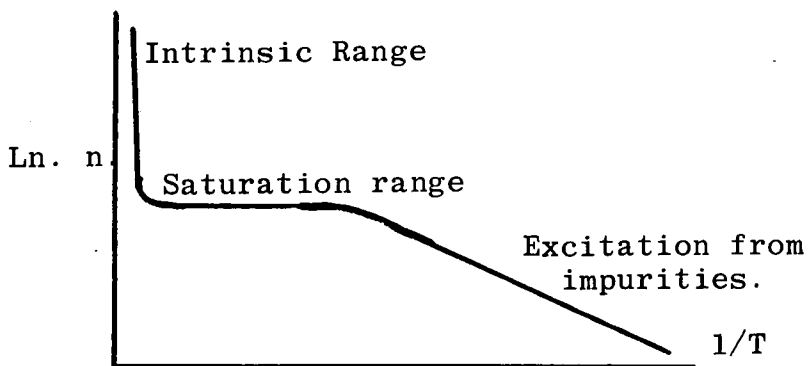
For non-degeneracy, the Fermi level E_f must be greater than kT below the conduction band. As N_c at room temperature is about $2.5 \cdot 10^{19} \text{ cm}^{-3}$ with $m_e = m_h = m_0$, when $n \ll 10^{19} \text{ cm}^{-3}$, E_f is $\gg kT$ below the conduction band, from equation (34). This value of n can thus be taken as a criterion of the onset of degeneracy, but naturally a smaller value of effective mass for a carrier lowers this value of n somewhat.

Numerous situations arise due to the impurity centres, the analysis of which is far too complex and lengthy to describe. This task is done in references (33) and (34) which deal with ~~the~~ impurity semiconductors at some length. It is instructive, however, to consider the simple case of an impurity concentration, N_d , at an energy E_d below the conduction band. If $E_d \ll E_g$, these donors will

ionise into the conduction band, as the temperature is raised from absolute zero, according to the equation

$$n = B \exp (-E_d/2kT) \dots\dots\dots (37)$$

where B involves N_c and N_d . At some higher temperature the donor electrons become fully ionised, and, provided the intrinsic electron concentration is still small compared to N_d , then the total number of carriers will remain constant as the temperature is increased further. Then, at some higher temperature, hole-electron pairs will begin to be created in considerable numbers, and again the total number of carriers will increase. This process is shown in Fig. 9. The slope of the line, after correcting for the temperature variation of N_c , at low temperatures is $E_d/2kT$ and in the intrinsic range is $E_g/2kT$. A similar process can be described for p-type material with only acceptor impurities present. A value for the donor or acceptor excitation energy may be obtained using this approach, though great care must be exercised, as this method is only valid when one impurity is present. (35).



Variation of Carrier Density n with Temperature.

Fig. 9.

Due to technical reasons, it is extremely difficult to prepare a semiconductor containing only one type of impurity and so both donors and acceptors are likely to be present. Consider a semiconductor with a concentration N_A of acceptor levels and N_D of donor levels, with $N_A < N_D$, and having the acceptor levels located just above the valence band such that $kT \approx E_d$ and $kT \ll E_g$. The probability of an electron being excited either from the acceptor levels or from the valence band to the donor levels or the conduction band is very small. But at absolute zero the acceptor levels would be occupied by electrons from the donor levels and so at temperatures just sufficient to excite electrons from the donor levels to the conduction band the number of electrons available must only be

$$n = N_D - N_A \dots\dots\dots (38)$$

Such a material is said to be compensated as the available number of conduction electrons is no longer equal to the number of impurity centres. For such material the position of the Fermi level changes with the difference between the donor and acceptor concentrations. This variation is shown in Fig. 10, for one particular temperature. The degree of compensation will also effect the value of the slope of the line obtained when $\ln n$ is plotted against $1/T$. For only one impurity it has been shown to be $E_d/2kT$, but when the material is compensated, this value is now E_d/kT (36).

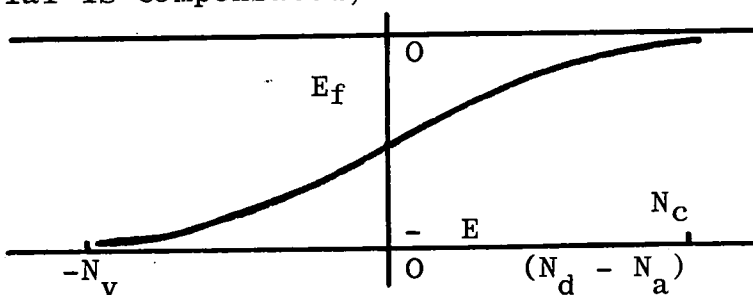


Fig. 10.

Naturally care must be taken to determine which value is applicable.
General Equations for the Transport Properties in any Magnetic Field

When a small perturbing field, such as an electric or a magnetic field, is applied to a semiconductor the probability of an electron occupying an allowed state will no longer be given by equation (17),

$$P(E) = \frac{1}{\exp(E-E_F/kT) + 1} \dots\dots\dots(39)$$

as this equation assumes an average electron velocity of zero, which no longer holds. A steady state will be set up, where the perturbing force is balanced by the interactions of the electrons with the lattice, and can be represented by a probability function $P_1(E)$, which for small perturbations will differ only slightly from $P(E)$. When the field is removed $P_1(E)$ will relax to $P(E)$ at a rate which is given by the equation

$$\frac{\partial P_1(E)}{\partial t} = -\frac{P_1(E) - P(E)}{\tau} \dots\dots\dots(40)$$

where τ is a relaxation time characteristic of the system. The precise validity of equation (40) is a very complex question, but it appears that it is justified in most cases, if the energy emitted or absorbed by the interacting electron is small compared to its initial energy (37).

The rate of change of the function $P(E)$ associated with the effects of a combined electric, thermal, and magnetic field can be written

$$\left(\frac{\partial P_1(E)}{\partial t}\right)_{dnft} = -\frac{\partial P(E)}{\partial V} \cdot \frac{\partial V}{\partial t} \dots\dots\dots(41)$$

where V is the velocity of the electrons due to the combined field.

In the steady state this rate of change is balanced by a restoring force, caused by the interactions of the electrons with the crystal lattice and other imperfections, so that

$$\left(\frac{\partial P(E)}{\partial t}\right)_{\text{drift}} + \left(\frac{\partial P(E)}{\partial t}\right)_{\text{interactions}} \equiv 0 \dots\dots\dots (42)$$

which is known as the Boltzman equation. In the absence of the field equation (41) would vanish, so:

$$\left(\frac{\partial P(E)}{\partial t}\right)_{\text{interactions}} = -\frac{P_1(E) - P(E)}{\tau} \dots\dots\dots (43)$$

Now, as the field is only a small perturbation, its effect may be written as the sum of the individual field effects. Hence, in vector form:

$$\frac{\partial P(E)}{\partial \mathbf{v}} \cdot \frac{\partial \mathbf{v}}{\partial t} = -\left(\frac{e}{m^*} \mathbf{E} + \frac{e}{m^*} \mathbf{v} \times \mathbf{B}\right) \nabla_{\mathbf{v}} P(E) + \mathbf{v} \cdot \nabla_{\mathbf{r}} P(E) \dots\dots (44) (44)$$

where the first term on the right hand side is that due to the electric and magnetic fields and the second term is that due to a general thermal gradient. Thus, from equations (44), (42) and (43),

$$\frac{P_1(E) - P(E)}{\tau} = -\frac{e}{m^*} \left(\mathbf{E} + \mathbf{v} \times \mathbf{B}\right) \nabla_{\mathbf{v}} P(E) + \mathbf{v} \cdot \nabla_{\mathbf{r}} P(E) \dots\dots (45)$$

Consider a function $c(E)$. To obtain a solution of (45) $P_1(E)$ may be expanded as a Taylor series in $P(E)$, but for small perturbations only the first two terms are important. The form is:

$$P_1(E) \approx P(E) - \mathbf{v} \cdot \mathbf{c}(E) \frac{\partial P}{\partial E} \dots\dots\dots (46)$$

since $P_1(E)$ will depend on both energy and velocity. With the

assumption that $P_1(E) - P(E)$ is small, the right hand side of (45) can be approximated by the following equations

$$\begin{aligned} \underline{v} \times \underline{B} \cdot \nabla_v P_1(E) &= -\underline{v} \cdot (\underline{B} \times \underline{c}(E)) \frac{\partial P}{\partial E} \\ \underline{E} \nabla_v \cdot P_1(E) &\approx m^* \underline{v} \cdot \underline{E} \frac{\partial P}{\partial E} \\ \underline{v} \nabla_r P_1(E) &\approx \underline{v} \nabla_r \left(\frac{E - E_F}{kT} \right) kT \frac{\partial P}{\partial E} \end{aligned} \quad \left. \vphantom{\begin{aligned} \underline{v} \times \underline{B} \cdot \nabla_v P_1(E) \\ \underline{E} \nabla_v \cdot P_1(E) \\ \underline{v} \nabla_r P_1(E) \end{aligned}} \right\} \dots (47)$$

On substituting equations (47) in (46)

$$-e \underline{E} \cdot \underline{v} + kT \underline{v} \nabla_r \left(\frac{E - E_F}{kT} \right) + \frac{e}{m^*} \underline{v} \cdot (\underline{B} \times \underline{c}(E)) = \underline{v} \cdot \underline{c}(E) \frac{1}{\tau} \dots (48)$$

Assuming that all electron and thermal fields are in the x,y plane and the magnetic field only in the z-direction, as commonly found in experimental work, then the perturbing force will act only in the x,y plane and thus only x and y components of $\underline{c}(E)$ need be considered. Resolution of equation (48) into its x and y components gives two equations, which when solved for c_x and c_y give

$$c_x = \frac{\beta - \alpha \gamma}{1 + \alpha^2} \quad c_y = \frac{\gamma + \alpha \beta}{1 + \alpha^2} \dots (49)$$

where α, β, γ are coefficients related to the individual field components. α is given by

$$\alpha \equiv \frac{e \tau}{m^*} B_z \dots (50)$$

Now an electron of energy E makes a contribution $\underline{v}_x E$ to the thermal current \underline{W} and $-\underline{v}_x e$ to the electric current. Integrating

to give the total number of electrons results in

$$\left. \begin{aligned} j_i &= -e \int_0^\infty v_i^2 c_i \frac{\partial P}{\partial E} N_c(E) dE \\ W_i &= \int_0^\infty E v_i^2 c_i \frac{\partial P}{\partial E} N_c(E) dE \end{aligned} \right\} i = x, y \dots \dots \dots (51)$$

When the expressions for $C(E)$ are substituted in (51) and rearranged, it is found that each current is expressed in terms of four variables, the electric field components and the thermal gradient components.

The relationships involve integrals of the form

$$\left. \begin{aligned} K_i &= \int_0^\infty \frac{E^i \tau}{1 + \alpha^2} \frac{\partial P}{\partial E} N_c(E) dE \\ H_i &= \int_0^\infty \frac{\alpha E^i \tau}{1 + \alpha^2} \frac{\partial P}{\partial E} N_c(E) dE \end{aligned} \right\} i = 1, 2, 3 \dots \dots \dots (52)$$

where α is given by the equation (50).

When α is small, that is, in a weak magnetic field, equations

(52) reduce to

$$\left. \begin{aligned} K_i &= \frac{-2}{\sqrt{\pi}} \omega n (kT)^{s+i-1} \Gamma(s + 3/2 + i) \\ H_i &= \frac{-2e B_z}{\sqrt{\pi} m^*} n \omega^2 (kT)^{2s+i-1} \Gamma(2s + 3/2 + i) \end{aligned} \right\} \dots \dots \dots (53)$$

in evaluating which, $P(E)$ has assumed the classical limiting value $P(E) = \exp - (E - E_F)/kT$, valid only for $E_F \ll -kT$ below the conduction band, and where the relaxation time τ has been expressed as a function of energy only

$$\tau = \omega E^s \dots \dots \dots (54)$$

Where ω and s are constants to be determined experimentally.

This assumption for ϵ implies that the material has spherical energy bands and is isotropic. The actual form of ϵ is complex and much analysis has been spent on evaluating ϵ for various systems.

When α approaches unity, that analysis breaks down, as then the radius of curvature of the electron trajectory is comparable to its mean free path. Under these conditions only a quantum mechanical analysis is valid, which becomes extremely complex (38). This behaviour manifests itself experimentally as the de Haas - von Alphen effect and oscillatory magnetoresistance.

Equations (51) are better written, with the electric currents and the thermal gradients as the independent variables, and with some changes of the variables. W is replaced by $w = W + j \theta$ the total energy flux when the electric and thermal fields are present. Also a term $K_L \nabla_r T$ is added to the expression for w for the energy conducted by the lattice. The electric current j is replaced by i , where $j = -ei$. Hence equations (51) now

become (39):

$$\left. \begin{aligned} \frac{\partial V^*}{\partial x} &= A_{11} i_x + A_{12} i_y - A_{13} \frac{\partial}{\partial x} \left(\frac{1}{kT} \right) - A_{14} \frac{\partial}{\partial y} \left(\frac{1}{kT} \right) \\ \frac{\partial V^*}{\partial y} &= -A_{12} i_x + A_{11} i_y + A_{14} \frac{\partial}{\partial x} \left(\frac{1}{kT} \right) - A_{13} \frac{\partial}{\partial y} \left(\frac{1}{kT} \right) \dots\dots\dots (55) \\ -w_x &= A_{13} i_x + A_{14} i_y + A_{33} \frac{\partial}{\partial x} \left(\frac{1}{kT} \right) + A_{34} \frac{\partial}{\partial y} \left(\frac{1}{kT} \right) \\ -w_y &= -A_{14} i_x + A_{13} i_y - A_{34} \frac{\partial}{\partial x} \left(\frac{1}{kT} \right) + A_{33} \frac{\partial}{\partial y} \left(\frac{1}{kT} \right) \end{aligned} \right\}$$

where $V^* = \frac{E_F - e\psi}{kT}$ is the reduced electrochemical potential,

θ being the electrostatic potential of the electrons, and where the coefficients A are given in terms of the integrals K_i and H_i :

$$A_{11} = \frac{3m^*}{2kT} \left\{ \frac{K_1}{K_1^2 + H_1^2} \right\}$$

$$A_{12} = \frac{3m^*}{2kT} \left\{ \frac{H_1}{K_1^2 + H_1^2} \right\}$$

$$A_{13} = - \left\{ \frac{K_1 K_2 + H_1 H_2}{K_1^2 + H_1^2} \right\} - e \theta.$$

$$A_{14} = \frac{K_1 H_2 - H_1 K_2}{K_1^2 + H_1^2}$$

$$A_{33} = \frac{2kT}{3m^*} \left\{ K_3 + \frac{K_1 H_2^2 - 2 H_1 H_2 K_2 - K_1 K_2^2}{K_1^2 + H_1^2} \right\} - kT^2 K_L$$

$$A_{34} = \frac{2kT}{3m^*} \left\{ H_3 - \frac{H_1 H_2^2 + 2K_1 K_2 H_2 - H_1 K_2^2}{K_1^2 + H_1^2} \right\}$$

Having obtained equations (55) and the expressions for the coefficients A, it is possible to write down a general expression for any effect. The treatment can be extended to the case of hole conduction, by changing the sign of e and of the electrochemical potential V^* . The expressions thus obtained are identical to those for electrons, but with the signs changed accordingly.

The analysis may also include the case of mixed, or multiband conduction, if it is assumed that for conduction processes, there are no interband interactions between the carriers. It is then

possible to write down a set of equations (55) for each carrier, in addition to a set representing the actual behaviour of the material. The coefficients for each carrier define the properties the material would have if conduction was due only to that carrier. The coefficients A can be inverted and expressed in terms of experimental coefficients and this means that the coefficients of the mixed conductor can be expressed as combinations of the contributions from the individual bands.

Consider the case of two-band conductors, with electrons in band 1 and holes in band 2. The combination is made by applying three rules.

1) The electrochemical potential V^* of the material is given in terms of V_1^* of the electrons and V_2^* of the holes by

$$V^* = V_1^* = - V_2^*$$

2) The electric and thermal currents are the sum of the individual carrier currents.

$$j_x = j_{x_1} + j_{x_2} = -e i_{x_1} + e i_{x_2}$$

$$W_x = W_{x_1} + W_{x_2}$$

3) The coefficients A of the individual bands are replaced by experimental coefficients, derived from the originals by a reciprocal summation.

It is seen that the process is analogous to the analysis of parallel circuits.

When this is done, general expressions can be calculated for

all the experimental coefficients, valid for any magnetic field, in terms of the contributions from the individual bonds. These general formula, and their weak magnetic field simplifications, are given under their respective headings, and their values are taken from reference (40).

Electrical Conductivity

The electrical conductivity of a material is defined by the equation

$$\sigma = \frac{j}{E} \quad , \quad \nabla \cdot T \equiv 0 \quad \dots\dots\dots (56)$$

For one dimension this reduces to

$$\sigma = \frac{j_x}{E_x} \quad , \quad \frac{\partial T}{\partial x} \equiv 0$$

so from equations (55),

$$\sigma = \frac{j_x}{e} = \frac{-e i}{kT \cdot A_{ii} \cdot i} = -\frac{e^2}{kT} A_{11}$$

Thus

$$\sigma = -\frac{2e^2}{3m^*} \left(\frac{K_1^2 + H_1^2}{K_1} \right) \quad \dots\dots\dots (57)$$

Assuming α^2 can be neglected, that is, in weak magnetic fields, this becomes

$$\sigma = -\frac{2e^2}{3m^*} K_1$$

Using the value of K_1 in equation (53), and mindful of its validity,

σ becomes

$$\sigma = \frac{4 ne^2}{3m^* \sqrt{\pi}} w(kT) S \Gamma (s + 5/2) \quad \dots\dots\dots (58)$$

From equation (15) σ can be expressed in terms of a conductivity mobility μ_c ,

$$\sigma = ne\mu_c$$

$$\text{so } \mu_c = \frac{4e}{3m^* \sqrt{\pi}} w(kT)^{5/2} \Gamma(s + 5/2) \dots\dots\dots (59)$$

from equations (15) and (58).

For two carriers, the expression for the conductivity, valid for arbitrary magnetic fields, is given by

$$\sigma = \frac{(\sigma_1 + \sigma_2)^2 + B^2 \sigma_1^2 \sigma_2^2 (R_1 + R_2)^2}{\sigma_1 (1 + B^2 R_1^2 \sigma_1^2) + \sigma_2 (1 + B^2 R_2^2 \sigma_2^2)} \dots\dots\dots (60)$$

which reduces to

$$\sigma = \sigma_1 + \sigma_2 \dots\dots\dots (61)$$

for weak magnetic fields, where σ_i are given by equation (58)

From equation (15), for this case,

$$\sigma = ne\mu_1 + pe\mu_2 \dots\dots\dots (62)$$

The Hall Effect

When a magnetic field is set up perpendicular to the direction of the current flow in a material, an electric field is produced in mutually perpendicular direction. This is the Hall field and the effect is known as the Hall effect. The isothermal Hall constant R is defined by the equation

$$R = \frac{E}{B \times j}, \nabla_r T \equiv 0 \dots\dots\dots (63)$$

which for one dimension, reduces to

$$R = \frac{E_y}{B_z j_x}, \nabla_r T \equiv 0 \text{ and } j_y = 0 \dots\dots\dots (64)$$

Using equations (55) in equation (64),

$$R = \frac{kT}{e} \frac{\delta V^*}{\delta y} = \frac{-kT}{e} \frac{A_{12} i_x}{B_z e i_x} = \frac{-kT}{e^2} A_{12}$$

So
$$R = \frac{3m^*}{2e^2 B_z} \frac{H_1}{K_1^2 + H_1^2}$$

Again assuming that a^2 can be neglected and using equations (53) for K_1 and H_1 , this becomes

$$R = \frac{3m^*}{2e^2 B_z} \frac{H_1}{K_1^2} = \frac{3\sqrt{\pi}}{4} \frac{1}{ne} \cdot \frac{\Gamma(s + 5/2)}{\Gamma^2(s + 5/2)} \dots\dots\dots (65)$$

The Hall mobility μ_H is defined by $R \sigma = \mu_H$ and is given by

$$\mu_H = \frac{e}{m^*} w (kT)^{s'} \frac{\Gamma(2s + 5/2)}{\Gamma(s + 5/2)} \dots\dots\dots (66)$$

from equations (65) and (58). The ratio $\frac{\mu_H}{\mu_c}$ is a quantity of great importance in semiconductors and is given, from equations (66) and (59),

by
$$\frac{\mu_H}{\mu_c} = \frac{4}{3\sqrt{\pi}} \frac{\Gamma(2s + 5/2)}{\Gamma^2(s + 5/2)} \dots\dots\dots (67)$$

From equation (65), R can be expressed by

$$R = \frac{r}{ne} \quad \text{where } r \text{ is a constant which, for most}$$

materials, never departs far from unity. From equations (65) and (67),

$$r = \frac{9\pi}{16} \cdot \frac{\mu_H}{\mu_c} \dots\dots\dots (68)$$

For $s = -\frac{1}{2}$, classical lattice scattering, $r = \frac{3\pi}{8}$, and for $s = \frac{3}{2}$, ionised impurity scattering, $r = \frac{315\pi}{512}$, and for all cases which have been investigated r does not vary much from unity, and putting it equal to unity will not materially effect the value of the number of carriers obtained from equation (65). This equation gives a direct measurement, then, of the number and type of carrier.

For mixed conduction, the Hall constant is given by

$$R = \frac{R_1 \sigma_1^2 + R_2 \sigma_2^2 + B^2 R_1 R_2 \sigma_1^2 \sigma_2^2 (R_1 + R_2)}{(\sigma_1 + \sigma_2)^2 + B^2 \sigma_1^2 \sigma_2^2 (R_1 + R_2)^2} \dots\dots\dots (69)$$

valid for arbitrary magnetic fields, which reduces to

$$R = \frac{R_1 \sigma_1^2 + R_2 \sigma_2^2}{(\sigma_1 + \sigma_2)^2} \dots\dots\dots (70)$$

for weak magnetic fields. Putting $R_1 = \frac{-r}{ne}$ and

$$R_2 = \frac{r}{pe}, \quad \sigma_1 = ne\mu, \quad \sigma_2 = pe\mu_2, \quad \text{and } b = \frac{\mu_1}{\mu_2}$$

equation (70) now becomes

$$R = \frac{-r}{e} \frac{nb^2 - p}{(nb + p)^2} \dots\dots\dots (71)$$

and when b, the mobility ratio, is large,

$$R = \frac{-r}{e} \cdot \frac{1}{n}, \dots\dots\dots (72)$$

equivalent to the extrinsic induction case of equation (65). The intrinsic case is given when $n = p$ in equation (71), so

$$R = \frac{-r}{n_1 e} \cdot \frac{b - 1}{b + 1} \dots\dots\dots (73)$$

If the value of n_1 from equation (29) is substituted in equation (73), it is seen that

$$RT^{3/2} = D \cdot \exp (E_g/kT) \dots\dots\dots (74)$$

and provided b does not vary greatly, D is a constant. From the slope of a graph of $\ln RT^{3/2}$ against $\frac{1}{T}$, the value of the energy gap may be obtained.

The Seebeck Effect

The Seebeck coefficient Θ , also known as the thermoelectric power, is defined by

$$\Theta = \frac{\mathbf{jE}}{\nabla_r T}, \quad \mathbf{j} \equiv 0 \quad \dots\dots\dots (75)$$

which reduces, for one dimension, to

$$\Theta = \frac{E_x}{\frac{\delta T}{\delta x}}; \quad j_x = j_y = \frac{\delta T}{\delta y} = 0 \quad \dots\dots (76)$$

From equations (55), equation (76) becomes, as $E = \frac{\partial V}{\partial x} = \frac{kT}{e} \frac{\partial V^*}{\partial x}$,

$$\Theta = \left(\frac{\frac{kT}{e} \cdot \frac{\partial V^*}{\partial x}}{\frac{\delta T}{\delta x}} \right) + \frac{k}{e} \cdot V^* \cdot \frac{\delta T}{\delta x} = \frac{\frac{-kT}{e} A_{13} \frac{\partial}{\partial x} \left(\frac{1}{kT} \right)}{\frac{\delta T}{\delta x}} + \frac{k V^*}{e} = \frac{k}{e} \left(\frac{A_{13}}{kT} + V^* \right)$$

So $\Theta = -\frac{k}{e} \left(\frac{K_1 K_2 + H_1 H_2}{K_1^2 + H_1^2} - \frac{E_F}{kT} \right)$ as $V^* = \frac{E_F}{kT} - e\psi$

When α^2 is small, $H_1 H_2$ and H_1^2 are negligible, and using equations (53) for K_2 and K_1 , this becomes

$$\Theta = -\frac{k}{e} \left((s + 5/2) - \frac{E_F}{kT} \right)$$

$$\Theta = \frac{-k}{e} \left[(s + 5/2) - \frac{E_F}{kT} \right] \quad \dots\dots\dots (77)$$

and when $s = -1/2$, classical lattice scattering, this becomes the well known expression

$$\Theta = -86.5 \left(2 - \frac{E_F}{kT} \right) \mu V/^{\circ}K \quad \dots\dots\dots (78)$$

after numerical values have been substituted.

For mixed conduction, the Seebeck coefficient is given by

$$\theta = \frac{\theta_1 [\sigma_1 (\sigma_1 + \sigma_2) + \sigma_1^2 \sigma_2^2 R_1 (R_1 + R_2) B] + \theta_2 [\sigma_2 (\sigma_1 + \sigma_2) + \sigma_1^2 \sigma_2^2 R_2 (R_1 + R_2) B] - \sigma_1 \sigma_2 (Q_1 - Q_2) (R_1 - R_2) B^2}{(\sigma_1 + \sigma_2)^2 + B^2 \sigma_1^2 \sigma_2^2 (R_1 + R_2)^2} \dots \dots \dots (79)$$

valid for all magnetic field strengths, and where Q_1 and Q_2 are the respective Nernst coefficients of the two carriers, given by

$$Q = \frac{wk}{m^*} \cdot s(kT)^s \cdot \frac{\Gamma(2s + 5/2)}{\Gamma(s + 5/2)} \dots \dots \dots (80)$$

$$= s \cdot \frac{k}{e} \cdot \mu_H \dots \dots \dots (81)$$

For weak magnetic fields, equation (79) reduces to the much simpler expression,

$$\theta = \frac{\theta_1 \sigma_1 + \theta_2 \sigma_2}{\sigma_1 + \sigma_2} \dots \dots \dots (82)$$

On substituting equation (77) in this expression for θ , it becomes

$$\theta = - \frac{k}{e} \left[\frac{nb \left(s + \frac{5}{2} - \frac{E^*}{kT} \right) + p \left(s + \frac{5}{2} + \frac{(E_g - E^*)}{kT} \right)}{nb + p} \right] \dots \dots \dots (83)$$

From equation (78) the Fermi level may be calculated, and using equation (36) for the extrinsic carrier density, and the Hall coefficient, an approximate value of the effective mass may be obtained.

From equation (83) it can be seen that, for p-type material, θ will change sign when approximately $p = nb$, and from differentiating equation (71) for R , it is seen that this value of p gives the maximum value of the Hall effect.

The Seebeck coefficient for semiconductors is usually much

larger than that for metals, as can be seen from examination of equation (78) and its equivalent for a metal, so little error is introduced by measuring the Seebeck coefficient of a semiconductor against, for example, the copper leads of a copper-constantan thermocouple, as

$$\begin{aligned} \theta_{\text{meas.}} &= \theta_s - \theta_{\text{cu}} \\ &\approx \theta_s \quad \text{as} \quad \theta_{\text{cu}} \ll \theta_s \end{aligned}$$

Magnetoconductivity

In deriving the above expressions for the conductivity Hall coefficient and Seebeck coefficient, it was assumed that

$\alpha = \frac{e \tau}{m^*} \cdot B_z \ll 1$, and if this restriction is removed all these effects become dependent on the magnetic field strength.

The most important of these is the magnetoconductivity effect, the variation of the conductivity with applied field. Detailed studies of this effect have been made for numerous materials attempting to determine the band structure of the material, but as this effect is extremely dependent on the behaviour of the relaxation time τ , high quality materials are required to avoid spurious results.

Two cases need be considered. The low field case, where B is so low that α^2 and higher power can be neglected and the high field case where $\alpha \rightarrow \infty$. From equation (57).

$$\sigma = \frac{-2e^2}{3m^*} \left(\frac{K_1^2 + H_1^2}{K_1} \right) \dots \dots \dots (84)$$

and using the binomial expansion for K_1 in equation (51)

$$K_1 \approx \int_0^{\infty} (1 - \alpha^2) E \tau \frac{\partial P}{\partial E} \cdot N_c(E) dE$$

$$= K_1 \text{ approx.} - \int_0^{\infty} \alpha^2 E \tau \frac{\partial P}{\partial E} \cdot N_c(E) dE$$

and $K_1 \text{ approx.}$ and $H_1 \text{ approx}$ are given by equations (53). The second term of K_1 can be evaluated using the same assumptions involved in evaluating equations (53). Then

$$\int_0^{\infty} \alpha^2 E \tau \frac{\partial P}{\partial E} \cdot N_c(E) dE = \frac{-2}{\sqrt{\pi}} \frac{e^2 B_z^2}{M^{*2}} w^3 n (kT)^{3s} \Gamma(3s + 5/2)$$

Using equations (53) for $K_1 \text{ approx}$ and $H_1 \text{ approx}$ and introducing σ_0 , the zero magnetic field conductivity, and the zero field Hall mobility, $R_0 \sigma_0 = \mu_H$, equation (84) becomes:

$$\sigma = \sigma_0 \left[1 - \mu_H^2 B_z^2 \left(\frac{\Gamma(s + 5/2) \Gamma(3s + 5/2)}{\Gamma^2(2s + 5/2)} - 1 \right) \right] \dots \dots \dots (85)$$

and for classic lattice scattering, $s = -\frac{1}{2}$,

$$\sigma = \sigma_0 \left[1 - \mu_H^2 B_z^2 \left(\frac{8}{\pi} - 2 \right) \right]$$

$$\text{So } \frac{\sigma - \sigma_0}{\sigma_0} = \mu_H^2 \cdot B_z^2 \cdot \left(\frac{8}{\pi} - 2 \right) \dots \dots \dots (86)$$

and this will vary as B_z^2 at a rate of about unity times the Hall mobility squared.

Now when $\alpha \rightarrow \infty$, the integrals K_1 and H_1 are approximated to by

$$K_1 = \int_0^{\infty} \alpha^{-2} E \tau \frac{\partial P}{\partial E} \cdot N_c(E) dE$$

$$H_1 = \int_0^{\infty} \alpha^{-1} E \tau \frac{\partial P}{\partial E} \cdot N_c(E) dE$$

and evaluating these gives

$$K_1 = \frac{-2}{\sqrt{\pi}} \frac{m^{*2}}{e^2 B_z^2} \frac{n}{w} \cdot (kT)^{-s} \Gamma(5/2 - s) \dots \dots \dots (87)$$

$$H_1 = -\frac{3}{2} \cdot \frac{m^*}{e B_z} \cdot n$$

In the high field limit equation (84) for σ reduces to

$$\sigma = \frac{-2e^2}{3m^*} \cdot \frac{H_1^2}{K_1}$$

so substituting equations (87) for K_1 and H_1 gives

$$\sigma = \frac{9\pi}{16} \times \frac{\sigma_0}{\Gamma(5/2 - s)\Gamma(5/2 + s)} \quad \dots\dots\dots(88)$$

and when $s = -\frac{1}{2}$, this is

$$\sigma = \frac{9\pi}{32} \sigma_0 \quad \dots\dots\dots(89)$$

So σ should tend to a saturated value, a fact which is not usually observed, although deviations from the parabolic low field case are often encountered. The fact that equation (88) is not confirmed experimentally is not surprising, considering the numerous approximations involved in deriving it. Inhomogeneities in the material and quantum effects due to large magnetic fields also tend to invalidate it.

For the above analysis, no magnetoconductivity should be found when the magnetic field is parallel to the electric field, that is, there should be no longitudinal magnetoconductivity. Experimentally it is found that there is always some longitudinal magnetoconductivity and to explain this much more complex analysis is needed, taking into account the anisotropy of a solid in a magnetic field, in which the relaxation time is now a tensor. Substances are known which, though isotropic in structure, become markedly anisotropic in a magnetic field. However, for an isotropic solid with spherical band structure, no marked longitudinal magnetoconductivity should be encountered.

For multiband conduction, it can be shown (41) that the transverse magnetoconductivity does not vanish even if conditions are such that the magnetoconductivity of each band vanishes. For small magnetic field strengths this variation is proportional to B^2 , and it tends to saturate for very large fields as in the single band case considered previously.

The Hall Effect with Induction

Using analysis similar to that used for the variation of conductivity with induction, it can be shown that the low field Hall constant is independent of the magnetic field and that the high field limiting case is given by

$$R = -\frac{1}{ne}$$

which is independent of the scattering mechanism, and hence of the relaxation time. The Hall coefficient thus only varies slowly with the magnetic field, and for the case of $s = -\frac{1}{2}$, classical lattice scattering,

$$\frac{\mu_{H\infty}}{\mu_{H_0}} = \frac{8}{3\pi}$$

From the exact expression for the Hall constant in a mixed conductor it will be seen that, even if R_1 , R_2 , σ_1 and σ_2 are all independent of B , their resultant effect will depend on B . For a p-type material, just below the temperature corresponding to the onset of intrinsic conduction, there will be a relationship;

$$\sigma_1^2 R_1 + \sigma_2^2 R_2 = 0 \quad \dots\dots\dots(90)$$

Putting the usual expressions for R and σ in equation (90) gives

$$nb^2 = p$$

which, from equation (71) makes the Hall coefficient zero.. Hence a large dependence of the Hall coefficient on the magnetic field strength would be expected around the temperature at which it changes sign. This change will obviously depend on the value of the product $R\sigma = \mu_H$ from examination of equation (69), and it is experimentally found that the largest variations occur in materials with very large Hall mobilities.

For a material such as InSb the experimental agreement with equation (69) is very good and values of n_i , μ_{H_1} and μ_{H_2} have been obtained in good agreement with more directly measured values. Disagreement between this theory and observed results led to the discovery of the lighter mass valence band in germanium (42).

Magnetoseebeck Effect

Using analysis similar to that used for the low and high field, cases of the magnetoconductivity it can be shown, after tedious mathematics, that the magnetoseebeck effect behaves similarly to the magnetoconductivity. At low fields it varies parabolically with magnetic field strength and for high fields it tends to a saturated value. At extremely high fields the coefficient again begins to rise, due to quantum effects. This behaviour has been observed in InSb by Amirkhanov (43).

For the two carrier case, similar to the Hall coefficient, it can be shown that there will be a large variation of Seebeck coefficient with induction at the temperature at which θ is changing sign, even though conditions are such that the variation of Seebeck coefficient within each individual band, if it were conducting alone, would be small.

Puri and Geballe (44) have pointed out the advantages to be gained from magnetoseebeck studies rather than magnetoconductivity studies. These stem from the behaviour of the "unwanted" transverse electric fields created when Θ and σ are measured in a magnetic field. When Θ is measured, the Nernst field classically approaches zero as B increases, whereas when σ is measured the Hall field tends to infinity with B. Any disturbances of the Nernst field, due to experimental procedure, say, will produce only minor errors, but a similar disturbance of the Hall field can produce disastrous effects.

The thermomagnetic effects in general are extremely sensitive to the charge-carrier scattering mechanisms and can provide a means of studying such phenomena. Extensive treatments of these effects will be found in reference (45) and the theory of the effects in reference (46).

Inhomogeneities

It is well known that any disturbance of the Hall or Nernst fields, caused by such things as contacts, two carrier recombination effects, or inhomogeneities in the measured sample, can seriously influence the galvanomagnetic voltages, although in practice disturbances of the Hall field are more serious than disturbances in the Nernst field. The subject of inhomogeneities in samples is a large one and complex to analyse, and fuller details are given in reference (47), which is a review article on the subject.

When gross inhomogeneities exist, distortion of the current vectors takes place and each separate geometry must be considered in detail. Only the case of an exponential carrier density variation along the direction of the current flow will be considered as this

case can lead to the phenomenon of negative magnetoconductivity under certain conditions. It can be shown, under these conditions, that for a long rectangular sample of width w and thickness t , that the current density far from the boundaries of the sample is given by (48)

$$J_x = \frac{I}{wt} \frac{\gamma/2}{\sinh \gamma/2} \cdot \exp\left(\frac{-\gamma y}{w}\right); \quad J_y = J_z = 0 \quad \dots\dots\dots(91)$$

in which I is the total current and $\gamma \equiv Kw\beta$, where $K = \frac{1}{n} \frac{dn}{dx}$ and β is the Hall angle defined by

$$\beta = RB\sigma$$

It is seen that the effect of the magnetic field under these conditions is to move the current towards one side of the sample. For large magnetic fields or large Hall angles, this distortion can be severe, even for small concentration gradients. This effect is shown in Fig 11, for various values of γ and it will readily be

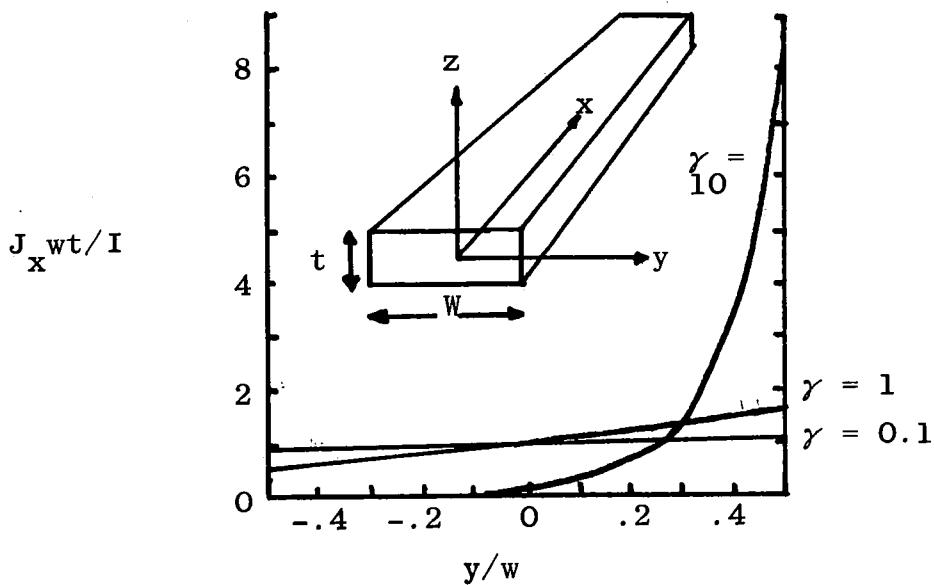


Fig.11. Effect of transverse magnetic field on longitudinal current density in the presence of a longitudinal gradient in carrier density.

appreciated that for contacts located along one side of the sample, negative magnetoconductivities are encountered. Also, reversal of

the magnetic field will not, except for contacts located at the centre, give an identical value of the magnetoconductivity. After an average over both directions of the magnetic field, the voltage developed across the contacts is given by

$$\frac{(V_1 - V_2)_B}{(V_1 - V_2)_0} = \frac{\rho_B}{\rho_0} \frac{\delta/2}{\sinh \delta/2} \cosh\left(\frac{\delta y}{w}\right) \dots\dots\dots(92)$$

The magnetic field dependence of the inhomogeneity factor thus depends on the location of the contacts. At the centre of the sample ($y = 0$) the factor is $(\delta/2 / \sinh \delta/2)$ so that the magnetoconductivity is reduced and can readily become negative. For contacts at the edges of the sample ($y = \pm \frac{w}{2}$) the inhomogeneity factor for large δ will vary as $\delta/2$ that is, linearly with magnetic field. For $\delta \ll 1$ and for weak magnetic fields, equation (92) becomes

$$\left[\frac{\Delta e}{\rho_0 (\mu_H B)^2} \right]_{\text{eff.}} = \frac{\Delta e}{\rho_0 (\mu_H B)^2} + \frac{1}{2} (Kw)^2 \left[\left(\frac{y}{w} \right)^2 - \frac{1}{12} \right] \dots\dots\dots(93)$$

The second term on the right hand side, the inhomogeneity factor, is plotted in Fig. 12, and it is seen that this is negative over a

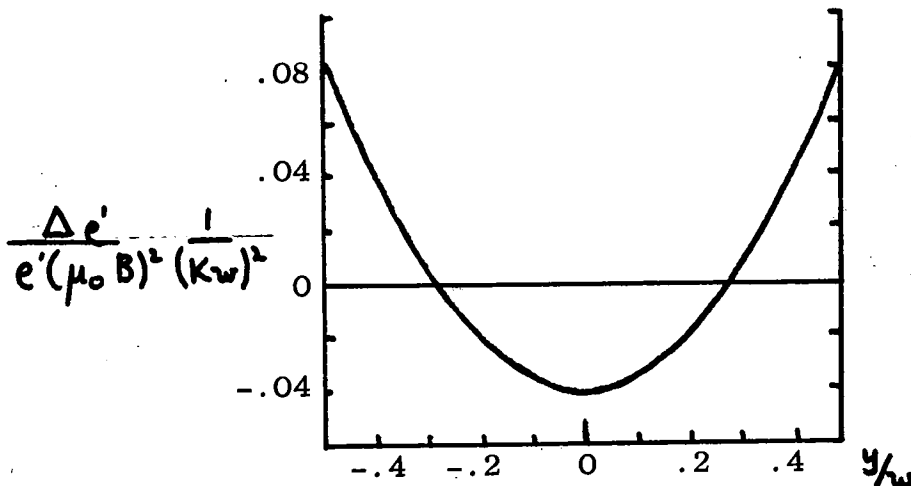


Fig.12. Inhomogeneity contribution to the weak field transverse magnetoresistance as a function of the y-coordinate of the probe positions.

large part of the sample width. If the actual magnetoresistance is small, then the first term is effectively zero and negative transverse magnetoconductivity can occur, even in the limit of zero magnetic field.

Similar results to that of the magnetoconductivity can be expected for the magnetoseebeck effect, although the actual variations should be relatively smaller.

Scattering Mechanisms in Semiconductors

A number of different mechanisms have been proposed for the scattering of the charge carriers in solids, and even under the conditions where the process can be represented by a relaxation time (49) the analysis is complicated, and the transport integrals have only been evaluated for certain specialised cases. Blatt (50) gives an extensive review of this theory and a good summary of the essential details is to be found in reference (51).

According to the Bloch theory of solids, the mean free path of the carriers in a perfect lattice is limited only by the dimensions of the crystal and hence scattering must be caused by departures from this perfect lattice. These departures may be divided into two classes, vibrations of the lattice and imperfections in the lattice structure. There are also several mechanisms which couple these deviations to the carriers.

Usually the relaxation time τ is considered to be a function of energy only and thus can be described by an equation of the form

$$\tau = \omega E^s$$

where ω is a constant and s is the scattering parameter. The

conductivity mobility is then given by (52)

$$\mu_c = -\frac{e}{m^*} \langle \tau \rangle_{F-D} \dots\dots\dots (94)$$

where

$$\langle q \rangle_{F-D} \equiv \frac{\int_0^\infty q(E) E^{3/2} \frac{\partial P}{\partial E} dE}{\int_0^\infty E^{3/2} \frac{\partial P}{\partial E} dE} \dots\dots\dots (95)$$

So $\langle \tau \rangle_{F-D}$ is an average over the Fermi-Dirac function. The Hall mobility is given similarly by

$$\mu_H = \frac{e}{m^*} \frac{\langle \tau^2 \rangle_{F-D}}{\langle \tau \rangle_{F-D}} \dots\dots\dots (96)$$

and as $\mu_H = r \mu_c$, then

$$r = \langle \tau^2 \rangle_{F-D} \dots\dots\dots (97)$$

To evaluate these integral expressions it is necessary to know the value of s and w , and to make approximations to the form of the Fermi-Dirac function. For non-degenerate semiconductors this function reduces to the classical probability function and then equation (95) is integrable,

Only two forms of the scattering mechanisms are of prime importance in non-degenerate semiconductors at temperatures away from the absolute zero. These are lattice scattering and ionised impurity scattering as these two deviations from perfect periodicity are always present to some extent in all semiconductors. Two other types of scattering will also be mentioned, scattering by dislocations and alloy scattering as these have relevance to an alloy system.

Lattice Scattering

The vibrations of the atoms forming the lattice of a crystal can be described as lattice waves and depending on the energy exchanged in collisions, these waves will be of the acoustic type or the optical type. Depending on whether the direction of vibration of the atoms is parallel or perpendicular to the direction of propagation of the wave, these types can either be in the longitudinal or in the transverse modes. There are two independent transverse modes. These waves are considered as quantised and each quantum is a phonon. In multivalley semiconductors there are two ways of scattering after a collision, either intervalley or intravalley. Most theories only consider scattering by one phonon but several authors (53) (54) have invoked multiphonon scattering to explain the large temperature dependence of the Hall mobility of some semiconductors.

For low energy scattering the acoustic branch predominates and analyses of the problem all give a value of $\frac{1}{2}$ for s , r equal to $3\pi/8$ and a Hall mobility proportional to $T^{-3/2}$. Also w is given, from deformation potential theory as

$$w = \frac{h^4 \rho u_l^2}{16\sqrt{2} \pi^3 E_1^2 m^{*3/2} (kT)^{3/2}} \dots\dots\dots(98)$$

where ρ is the density of the solid, u_l is the velocity of the longitudinal sound waves and E_1 , essentially constant with temperature, is the change in the band edge energy per unit dilation.

This type of scattering is naturally predominant in extremely pure material and at higher temperatures in less pure ones. It is also generally assumed when no other information is known about the

scattering process. For higher energies the optical branch becomes more dominant and then $s = \frac{1}{2}$ and w is given by

$$w = \frac{h^2 V_a M \omega_l^2}{16\pi^3 e^2 (2m^*)^2 e^{*2} kT} \dots\dots (99)$$

where $e^{*2} = (\epsilon_\infty^{-1} + \epsilon_0^{-1}) V_a M \omega_l^2 / 4\pi$.

in which V_a is the volume of the unit cell, M is the reduced mass of the cell,

$$M^{-1} = \sum M_i^{-1}, M_i$$

the masses of the ions in the cell, and ω_l is the frequency of the longitudinal optical mode.

Ionised Impurity Scattering

When the impurity atoms become ionised, the charged ions remaining in the lattice act as a scattering centre for the carriers. This form of scattering is predominant in impure semiconductors or ones which have been doped. It is found that then the relaxation time can be described by an equation (55)

$$\tau = \frac{K^2 (2m^*)^{1/2} (kT)^{3/2}}{\pi e^4 N_1 g(n^*, T, \frac{E}{kT})} \cdot \frac{E^{3/2}}{(kT)^{3/2}} \dots\dots (100)$$

where $g(n^*, T, \frac{E}{kT})$ is a slowly varying function which has been evaluated theoretically from many approaches. K is the dielectric constant, N_1 is the total density of ionised impurities and n^* depends on the degree of compensation in the semiconductor. Thus s is now equal to $3/2$ and τ can be shown to be equal to $\frac{315\pi}{312} = 1.93$, and the Hall mobility now varies as $T^{3/2}$.

Neutral impurities have been shown to have little effect on the temperature dependence of the mobility, though naturally they will lower the absolute value of the mobility.

When several scattering processes act simultaneously it is usually assumed that the effective relaxation time can be obtained from the separate relaxation times for each scattering process by reciprocal addition

$$(\tau^{-1})_{\text{eff}} = \sum_i (\tau_i^{-1}) \quad \dots\dots\dots(101)$$

This method can also be used for the mobility if each relaxation time has the same energy dependence.

Dislocation Scattering

Dislocations can cause scattering by two different mechanisms. The first is caused by the change in the lattice at the dislocation, and is only important at low temperatures in semiconductors with high dislocation densities. Then the mobility will vary linearly with the temperature.

The second mechanism treats the dislocation as an acceptor centre, as the dislocation in a semiconductor is effectively a charge centre. If the distance between the charged regions is much longer than the mean free path of the carriers, the carriers will tend to avoid these regions, thus increasing the resistance. If, however, the distance between the regions is comparable to the mean free paths, the dislocations act as a scattering centre, and the net effect is to reduce even further the mean free path of the carriers. Both these mechanisms have been considered in detail by Read (56).

Alloy Scattering

In an alloy of two semiconducting compounds or elements, the carriers can be scattered by the random fluctuations in the composition of the material. As the energy of the band edges is a function of composition this edge will vary from place to place in the alloy, producing an effect similar to that produced by the vibrations of the lattice in lattice scattering. Hence the energy dependence of the relaxation time should be the same as in acoustic lattice scattering with $s = -\frac{1}{2}$, but now the relaxation time will be independent of temperature as the amplitude of the band edge fluctuation is caused, not by the temperature as in lattice scattering, but by fluctuations in the alloy composition. Thus the mobility should only vary as $T^{-\frac{1}{2}}$. Nordheim (57) has given the relaxation time for this process as

$$\tau = \frac{h^4}{4\pi^2 (2m^*)^{3/2} uv \beta (1 - \beta)} E^{1/2} \dots\dots\dots (102)$$

where u is the square of the scattering matrix element for the difference of potentials averaged over the scattering angles, V is the atomic volume, and β is the mole fraction of minority component in the alloy.

Chapter 2

Previous Studies on the Materials.

Introduction

In the first part of this chapter previous studies of the compound mercury telluride (HgTe) are reviewed. HgTe has been considerably investigated by many workers, mainly due to interest shown in its very high Hall mobility and mobility ratio. The results have all been analysed assuming a band structure of a semi-metal type. Recent work has shown that the compound is particularly sensitive to its previous heat treatment.

The second part deals with the other constituent of the alloy system under investigation in this thesis, the defect compound indium sesquitelluride, (In_2Te_3). Much less is known about this material as suitable single crystals have not been obtained, although some properties of its ordered and disordered phases are known.

The chapter ends with a full discussion of previous studies of the HgTe - In_2Te_3 alloy system.

The Mercury-Tellurium Binary Alloy System

A detailed study of this system has not been carried out, but a clear picture of the principal features has been obtained by Hansen and Andenko (58) and Delves and Lewis (59). Analysis of the tellurium rich part of the system reported in reference (1) shows that the only compound is HgTe, which is sharply defined, and that there is a eutectic at 88 atomic per cent tellurium at

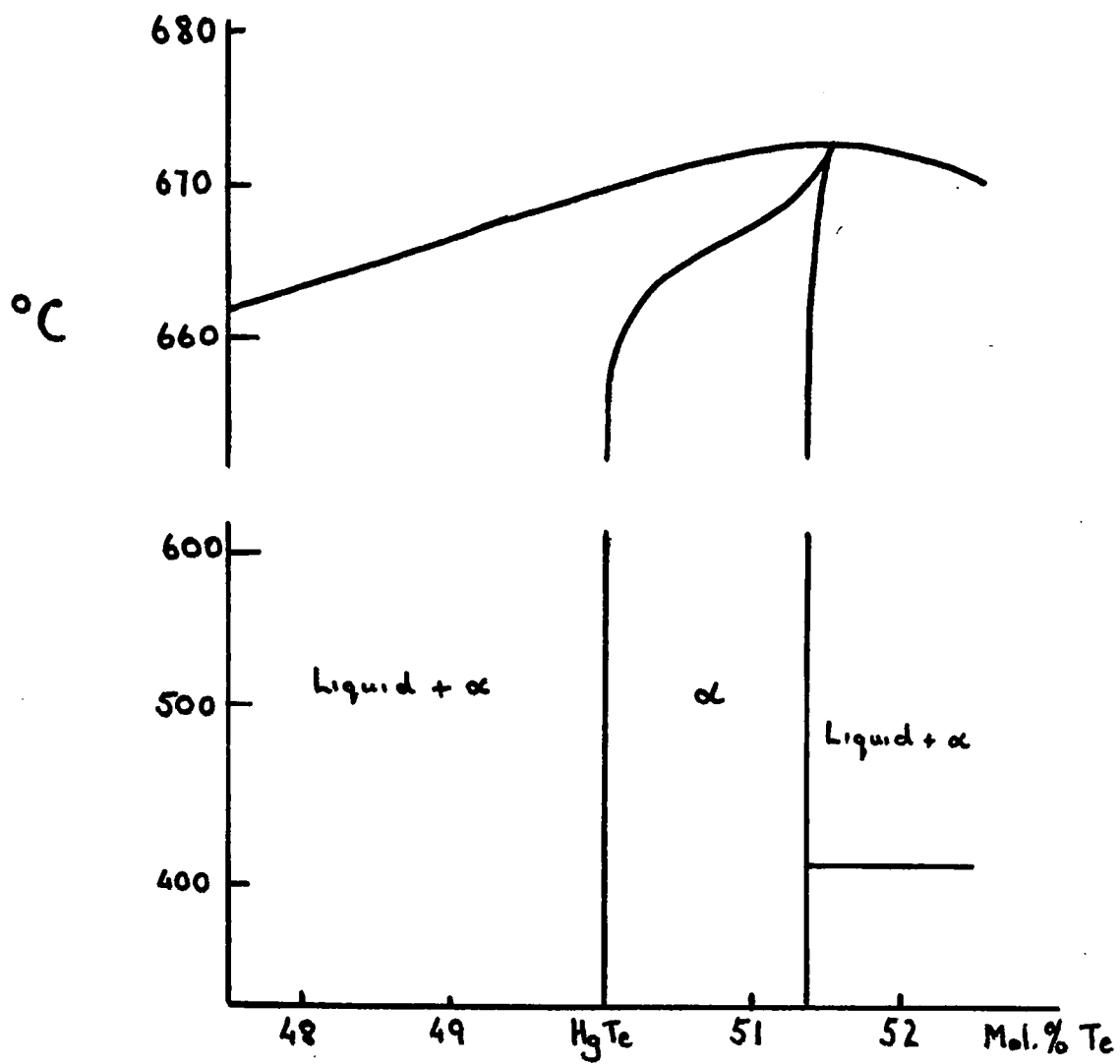


Fig. 13. Proposed phase diagram in the region of HgTe (after Delves)

a temperature of $409 \pm 2^\circ\text{C}$ the melting point of tellurium being 435°C . Delves and Lewis agree with these findings and have proposed a phase diagram in the region of HgTe, which is reproduced in Fig.(13). Using the techniques of differential thermal analysis and vapour phase analysis they found the melting point of HgTe to be $670 \pm 1^\circ\text{C}$, not 600°C as previously reported by Lawson et al. (60), a solid solubility of Hg in HgTe of considerably less than 2 atomic per cent, but a considerable solubility of Te in HgTe of up to 2.5 atomic per cent. A maximum in the liquidus occurs on the Te rich side between 2.5 and 4 atomic per cent, although they admit that their samples may have been up to at least 2 atomic per cent deficient in Hg near the melting point.

All samples of HgTe are now synthesised in the laboratory, as the natural form, Coloradoite, occurs only in small impure deposits. In common with many other II - VI compounds the structure is cubic with a zincblende (sphalerite) type lattice, class $\bar{4}3m$. Krucheanu et al. (61) have investigated a high pressure modification of HgTe which is of the cinnabar type lattice, class 32, unlike other II -VI compounds which modify to the wurzite-type structure class 6 mm. Kuchanu and Nistov (62) have managed to cleave HgTe both at 100°K and room temperature in the $[110]$ direction and report that the bond is identical to other II - VI compounds. The lattice parameter is generally observed to lie between 6.459 and 6.462 \AA (59) (60), although Hansen and Andenko report the rather low value of $6.429 \pm 6 \text{ \AA}$ (58).

The Preparation and Electrical Properties of HgTe

Although this compound has been studied by numerous workers in a number of countries, a comprehensive investigation of its properties has not yet been carried out. Various reasons may be put forward to account for this, but it is mainly due to the fact that until recently, exact control over the stoichiometry of samples was impossible, for lack of data, and that the effects on the electrical properties of various anneals were not fully understood or appreciated, both of which led to results being non-reproducible and inconsistent. Also, as HgTe has an extremely small energy gap, more advanced techniques than those used on other materials needed to be employed before any useful information could be obtained about the band structure. It is significant that it is only in the last few years that sensible results on this compound have been forthcoming, although it has been studied by various workers for nearly a decade.

The earliest studies (63, 64, 65, 66) of the properties of HgTe were carried out in Russia on sintered or pressed samples and were only sufficient to indicate that conduction was by electrons whose mobility was fairly high and that an energy-gap of between 0.025 and 0.08 eV would account for the variation of Hall coefficient and conductivity with temperature.

This work was then taken up by Harman and Logan (67) and Black, Ku, and Minden (68) in the United States, both of whom obtained a value of approximately 0.02 eV for the energy gap. In 1958 Carlson (69) extended the measurements of the Hall coefficient and conductivity down to liquid hydrogen temperatures and also repeated some work

on doped specimens. The samples were ground from polycrystalline ingots formed from stoichiometric quantities of elements fused by the two furnace technique. They were not annealed for any length of time and the presence of any free mercury inside the capsule was not reported. The variation of the Hall coefficient with temperature indicated that undoped samples were p-type and that copper acted as an acceptor and zinc as a donor. Room temperature electron mobilities of nearly $10,000 \text{ cm}^2/\text{V-sec}$ were obtained and the calculated values at 20°K were similar. The mobility ratio at the lower temperature was estimated at between 40 and 100, and the Seebeck coefficient was observed to follow the normal p-type variation from $210 \mu\text{V}/^\circ\text{K}$, at 50°K to $150 \mu\text{V}/^\circ\text{K}$ at 300°K . Below room temperature the Hall coefficient was shown to vary linearly with magnetic field strength, whilst at very low temperatures, for one sample, the Hall coefficient was found to change sign for high magnetic fields. A complicated band structure involving a light and heavy hole mass band, together with an extremely light electron mass band, was tentatively proposed to account for these variations. Lagrenoudie (70) working independently in France reported similar results to some of those found by Carlson, whilst Bell (71) examined the crystalline perfection of this compound and some other single crystals by X-ray diffraction.

Black et al. (72) were the first workers to prepare large single crystal ingots of HgTe, using the Bridgeman method. The variation of Hall coefficient and conductivity with temperature and the magnetoresistance were measured and it was concluded that

the material was intrinsic above 250°K and had an electron mass ratio of about 0.04 and an energy gap of 0.02 eV. The value of $16,000\text{cm}^2/\text{V}\cdot\text{sec}$ is a little low for the mobility of single crystal material compared with later results, as is the mobility ratio of only 10.

By zone refining some carefully prepared material Lawson et al. (60) were able to produce both p and n - type HgTe. Analysis of measurements on a p-type sample gave a mobility ratio of 70 and an intrinsic carrier density of $6.4 \cdot 10^{17}/\text{c.c.}$ at 174°K , and values at other temperatures were predicted. Analysis of the Hall coefficient variations at 77°K gave a value of the intrinsic carrier density of that temperature which was in good agreement with the previously predicted value. The electron mobility varied between $19,000\text{cm}^2/\text{V}\cdot\text{sec}$ at 300°K and $23,400\text{cm}^2/\text{V}\cdot\text{sec}$ at 77°K and an energy gap of about 0.01eV was deduced for the material. Single crystal specimens of HgTe exhibiting similar properties were also produced by Herman et al. (73). Mobilities varying from 17,000 to 25,000 $\text{cm}^2/\text{V}\cdot\text{sec}$ between 300°K and 143°K were obtained, and a mobility ratio of 100 was deduced for the material, with an energy gap of about 0.02 eV; a lower value of 0.01 eV, which was also obtained from the data, was considered of doubtful validity.

High electron mobilities were recorded by Rodot and Triboulet (74) on material which had been annealed in controlled mercury vapour pressures, work which had been foreshadowed by experiments previously carried out by Harmen et al. (73). Ingots made by

the normal method and zone refined to remove foreign impurities were further annealed for 7 days at the same temperature, one group at 200°C, the other at 300°C, but under various pressures of the mercury vapour. High pressures were found to produce n-type samples, low pressures p-type. In an intermediate pressure range, which was broader for the lower temperature group, samples were produced which were intrinsic down to at least 77°K. None of the material prepared in this way showed any appreciable variation of Hall coefficient with magnetic induction as had been observed by previous workers.

This work was continued by H. Rodot (75) who obtained the experimental vapour pressure of mercury - temperature of sample - extrinsic carrier concentration diagram, the (P_{Hg}, T, x) diagram, from similar experiments to those performed by Rodot and Triboulet. The results were interpreted by assuming one type of structural defect at temperatures below 350°C, probably a Frenkel defect, and, indicated by a discontinuity in the (P_{Hg}, T, x) diagram for intrinsic material at 350°C, a second type of defect, most probably an anti-structure, at higher temperatures. The thermodynamical constants associated with the Frenkel defects were deduced, which permitted a theoretical (P_{Hg}, T, x) diagram to be prepared, which was in excellent agreement with the experimental one for n-type samples. From studies on the p-type samples, a mobility ratio of 65 at 77°K was deduced and the intrinsic carrier concentration between 20°K and 350°K was determined. The Hall coefficient variation with magnetic induction was now found to depend on the temperature at which the sample had been annealed. For low temperature anneals no variation was found for magnetic field

strengths of up to 5000 Gauss. For the temperature range 225°C - 350°C the Hall coefficient depended strongly on the magnetic induction, but for a sample annealed at 400°C, no variation was found. Above 400°C the variations in the Hall coefficient again appeared very strongly. It was thought that the variations were due to inhomogeneities in the material, the lower region of variation being caused by the compound decomposing, giving microprecipitates of tellurium the higher region being due to anti-structure defects. The lower region of field independence is that of stoichiometric and homogenous material whilst the region around 400°C is due to an equilibrium between the microprecipitates of tellurium dissolving in the anti-structure defects, which only begin to appear above 350°C. This equilibrium leads to a quasi-homogenous material, and hence a field independence of the Hall coefficient. Quilliet et al (76) have also suggested that these precipitations could be the cause of the Hall coefficient variations, and work by Giriat (77) on annealing HgTe in vacuum indicates that this hypothesis is correct.

The technique of annealing in mercury vapour was extended by Giriat (77). For a given vapour pressure, controlled by the temperature, an optimum time of anneal was found which produced the highest mobility. Materials prepared in this way were intrinsic down to 77°K and the highest mobility recorded at this temperature was 77,000 cm²/V-sec. However, the Hall coefficient below room temperature was found to be considerably dependent on the magnetic induction, which is not surprising, in view of the work of H. Rodot, as the temperature of the anneal was either 250°C or 300°C., the temperature range in which microprecipitates of tellurium begin to appear.

It is surprising, nevertheless, that such high electron mobilities should have been measured on these samples. Giriat considered that the anneal in mercury vapour took place in two stages. In the first reaction the micro precipitates, most probably of tellurium, contained in the unannealed material, are dissolved and in the second reaction mercury vapour enters the material ultimately making it stoichiometric, at which point the material will have maximum mobility. If the anneal is continued beyond this point excess mercury will enter the material and non-stoichiometry will again result, with a consequent reduction in the value of the mobility. The need to introduce mercury into the unannealed HgTe is borne out by reference to the phase diagram of Delves and Lewis Fig. (13), page 53. As the compound that is grown from the melt probably contains excess tellurium it will be necessary to increase the mercury content to achieve stoichiometry. All later workers have noticed the presence of some free mercury inside the ampoules after reaction has taken place, indicating that the ingot is rich in tellurium. On the other hand, the work of Rodot and Triboulet (74) and Giriat (77) indicates that the solid solubility of mercury in HgTe is not negligible, as stated by Delves and Lewis.

The latest work on HgTe has been carried out by workers in Russia and Poland, Kot and Maronchuk (78) have investigated the variation of the electrical properties of thin layers of HgTe with the thickness of the layers, and Ivanov - Omskii et al (79) have studied the electrical properties of single crystals of p-type HgTe, whilst some galvanomagnetic and thermomagnetic work has been carried out by Tovstyuk et al. (80).

Tovstyuk et al, from measurements of the variation of the Hall effect with magnetic induction at several different temperatures, and measurements of the Nernst effect, conclude that these properties were best explained by assuming the presence of an extra heavy hole mass band, that is, a three carrier situation. However, no quantitative results were given. Ivanov-Omskii et al, from considerations of the variation of the Hall coefficient with magnetic induction at 4.2°K concluded that the position of the Fermi level did not vary with temperature over a considerable temperature range. The measurements were analysed using a non-parabolic band structure similar to that proposed for HgTe by Strauss et al. (81).

Similar results to Ivanov-Omskii et al. were reported by Dziuba and Zakrzewski (82) from measurements on material which was found to be intrinsic over the temperature range 20°K - 400°K. From analysis of their results, again using equations describing a non-parabolic band structure (83), (84), they concluded that the position of the Fermi level in this temperature range remained constant, and as a consequence, from measurements of the Seebeck coefficient, the value of the scattering parameter in this temperature range was also constant. The dominant scattering mechanisms at high and low temperatures were then deduced.

Dziuba, by a method of multiple distillation in vacuum, has managed to produce high purity HgTe (85). This material has an electron concentration of $3.5 \cdot 10^{15} \text{ cm}^{-3}$ at 4.2°K and is intrinsic for temperatures above 20°K. Various annealing techniques were employed with results similar to that obtained by Giriat (77). The maximum mobility measured was $170,000 \text{ cm}^2/\text{V-sec}$ at 20°K.

Dziuba has also studied the effect on the electrical properties of doping HgTe with IIIrd Group atoms (86). Results are given for boron, aluminium gallium, indium (both annealed and unannealed) and tallium.

The Band Structure of HgTe

Investigations into the band structure of HgTe have been mainly in conjunction with study of the alloy systems HgTe-CdTe and HgTe-HgSe.

Some work on the latter system has been carried out by Rodot (87, 88). From measurements of the longitudinal and transverse magnetoresistance the longitudinal effect being virtually zero for HgTe, it was concluded that the conduction band for HgTe is of the standard isotropic form, that of HgSe being a system of ellipsoids centred on the direction [100].

Harman et al have deduced a band structure for HgTe, based on the properties of HgTe when alloyed with CdTe and HgSe. In the first paper (73) it was shown from detailed analysis of the Hall coefficient measurements on HgSe and an equimolar alloy of HgSe and HgTe that they are both semi metals, with an overlap in energy of 0.07 eV between the valence and conduction bands rather than semiconductors having a conventional two band energy structure. In later papers (89) (90) on the properties of HgTe-CdTe alloys, a wide range of experimental evidence was analysed which showed conclusively that HgTe and low Cd content alloys were also semimetals. The transition to a true semiconductor occurred at about 20 molar% CdTe in HgTe. The intrinsic carrier concentration at 4.2°K was estimated from Hall coefficient and conductivity measurements on both p and n-type samples

and was found to be $2.10^{16}/\text{c.c.}$ This high value can only be explained by assuming an overlap in energy between the conduction and the valence bands, as the intrinsic carrier concentration for zero energy gap, with reasonable values of effective masses, would be only about $10^{12}/\text{c.c.}$ at 4.2°K . The Hall coefficient at 300°K and 77°K were plotted against those at 4.2°K and the results compared with theoretical curves obtained by assuming high values for the intrinsic carrier concentrations. The good agreement confirmed the assumption of an overlap in energy structure.

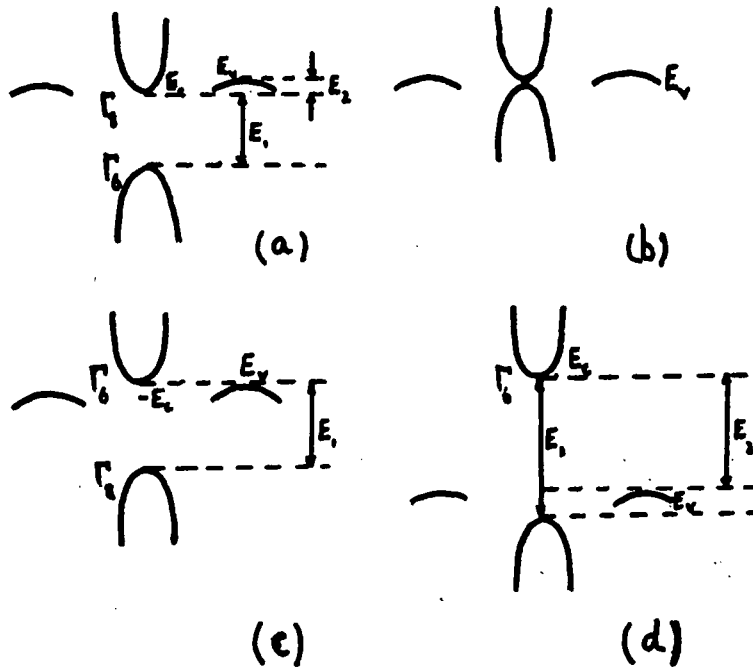
Magneto reflection measurements carried out on low Cd content alloys in magnetic inductions of up to 70,000 Gauss, showed both cyclotron resonance and interband transitions. The measurements were interpreted on the basis of a non-parabolic conduction band and a semimetal band structure, similar to the band model proposed by Kane (91) for InSb. Good agreement between theory and experiment was obtained by adopting a value of 0.006 eV for the direct energy gap and an electron effective mass ratio, at the bottom of the conduction band, of 4.10^{-4} .

In a further paper, Harman et al (92) have adopted the grey-tin band model of Groves and Paul (93) for HgTe and HgTe-CdTe alloys, and extended it to include the overlap of the valence and conduction bands found in these materials. Their schematic diagram for such a band model is reproduced in Fig. (14) and a summary of the salient band parameters is given below:

$$E_1 \equiv E_{r_6(r_1)} - E_{r_8(r_{15})}; \quad E_2 \equiv E_V - E_{r_8(r_{15})}; \quad E_t \equiv E_C - E_V$$

E_1 (eV)	E_t (eV)	E_2 (eV)	Me^*/Mo
-0.140 ± 0.050	-0.020 ± 0.010	$+0.020 \pm 0.010$	0.02
(a, b, c)	(d)	(d)	(a, b)

- a) From infra-red measurements (81) (94) (95).
- b) Used conduction band $E(\underline{k})$ derived from $\underline{k.p}$ approach as in reference (91), where $P = 7.5 \pm 1 \cdot 10^{-8} \text{ eV-cm}$.
- c) From plot of energy gap versus composition for the alloy system HgTe-CdTe (96).
- d) From plot of R vs. $\frac{1}{T}$ measurements. (97).



Band structure of Cd_xHg_{1-x}Te alloys (after Harman)

- a) HgTe, $x=0$
- b) Cd_{.17}Hg_{.83}Te, $x = .17$
- c) $x > .17$
- d) $x \gg .17$

Fig. 14.

Scattering Mechanisms in HgTe

M. and H. Rodot (87, 88) have determined the dominant scattering mechanisms in HgTe, both at high and low temperatures, from measurements of the magneto thermoelectric effect δQ with temperature. At low temperatures the sign of δQ is positive, indicating ionised impurity scattering, but at room temperatures it has changed sign to negative, showing that scattering at that temperature must be by acoustic phonons. From the dependence of the mobility on the temperature Girit (77) also deduced that these were the two dominant scattering mechanisms in the temperature range considered.

However, Dziuba and Zakrzewski (82) have recently reported that, in intrinsic material which they have measured, the scattering of electrons by holes in the most probable mechanism at low temperatures and by optical phonons at higher temperatures. They deduced these results from the fact that the scattering parameter for their material was constant over the temperature range considered. It follows from this fact that the scattering mechanism can only be a combination of the two mechanisms mentioned. Acoustic mode phonon scattering predicted a value of mobility two orders of magnitude higher than that ever measured, and only the two mechanisms quoted gave values of the position of Fermi level which were equal and independent of the temperature, both necessary conditions which had been deduced from the measurements. Work by Ivanov-Omskii et al (79) confirms that this condition is valid.

Over the temperature range 20°K to 100°K Dziuba and Zakrzewski found the electronmobility to vary as $T^{-\frac{1}{2}}$, similar to Tsidilkovski

(66), but Harman et al (97) found the dependence to be closer to T^{-1} .

Other Properties of HgTe

Most work on HgTe has been directly concerned with either its electrical properties or its band structure, but a few workers have concentrated on other aspects of its properties.

Blair and Smith (98) have reported that the resistivity of HgTe changed abruptly by a factor of 10^4 under a pressure of about $15,000 \text{ kg/cm}^2$. It was an essentially reversible effect and the pressure at which the reverse transition occurred was around $12,000 \text{ kg/cm}^2$. This is almost certainly a result of the pressure induced change in structure found by Kruczeanu et al (61). The structure changes under pressure from the zincblende type lattice to a cinnabar type, class 32. A similar effect has been noticed in HgSe by Kafakas et al (99) for which the high pressure structure was retained at low temperatures under atmospheric pressure, enabling X-ray analysis of the structure to be made. This phase was shown to be of the cinnabar type, best represented by a highly distorted NaCl structure in which the mercury atoms only form two bonds, as in the mercury halides, instead of the normal four as in the zincblende structure.

Photoelectric emission has been investigated by Sorokin (100) and by Ivanov-Omskii et al (79) the latter on HgTe-CdTe alloys. The spectral curve was found to possess a smooth threshold at 4.0 eV which was followed by a steep rise to 4.8 eV and it had a maximum at 6.0 eV . The photoelectric emission was considered high for material of this type and the energy distribution was characterised

by two groups of electrons, one of which was not very pronounced. Examination of the measurements rendered a value of 4eV for an electron affinity and 0.45 eV for the energy gap.

Photoconductivity has been studied by Braithwaite (101), Ivanov-Omskii et al. (79) and Kruse et al (102), the latter also measuring the thermal Nernst effect. The long wavelength threshold for photoconductivity in a thin film of the HgTe at 77^oK was found to be 3.1 microns, about 0.4 eV. These measurements were made before any firm ideas on the band structure had been formulated but it would seem that the photoeffects are due to electron transitions between the lower valence band and the lowest unfilled levels in the conduction band, with a minimum energy change of 0.4eV.

Lawson et al (60) found that samples of HgTe were opaque to radiation out to 38 microns, about 0.033 eV, the limit of their apparatus. Transmission through annealed p-type samples has been observed by Quilliet (103) in the range 3 to 15 microns. A value of 0.01 eV was deduced for the direct energy gap, as in the range measured the square of the absorption coefficient was proportional to the energy of the incident radiation, indicating direct transitions. This value is in good agreement with the energy gap obtained from electrical work, provided the Fermi level is not far above the conduction band minima, as should be the case in p-type samples which have been annealed in mercury vapour. The energy gap as obtained from the absorption edge would be the sum of the Fermi level and the true energy gap. Most workers have found that work in the far infra-red is difficult to do, and any effects may be further masked by free carrier absorption although an energy gap has been determined

by Harman and Strauss (89) for HgSe by this method.

The absorption spectra of thin films of HgTe and other II - VI compounds have been measured by Cardona and Harbeke (104). The L absorption edge and its spin orbit splitting were easily seen and Cardona and Greenaway (105) have also studied the fundamental reflectivity of HgTe and its application to the band structure.

Some mechanical properties of HgTe have been studied by Krüchanu and Nistov (62) and they succeeded in cleaving an ingot in the $[110]$ direction both at 100°K and at 300°K . Mavroides and Kolesar (106), using ultrasonic pulse techniques have determined the room temperature elastic constants of HgTe and from them have deduced the fundamental lattice absorption frequency and the Debye characteristic temperature.

Carlson (69), Ioffe and Ioffe (107), Rodot (108), and Spencer (109) have all studied the thermal conductivity of HgTe. They are in good agreement on the value of the phonon contribution to the thermal conductivity, but only Carlson reports that the thermal conductivity varies reciprocally with temperature in the usual manner.

Summary of the Properties of HgTe

The melting point of HgTe is given by Delves and Lewis as $670 \pm 1^{\circ}\text{C}$, (59), the rather low figure of 600°C quoted by Lawson et al (60) being obviously in error. In the following summary of the properties of HgTe the figures refer to the source of the quoted values.

Property	Value or Nature	Source and Comments
Lattice	zinblende (sphalerite)	(110) High pressure modification to the cinnabar type (61)
Space group classification	$\bar{4}3m$	(111) High pressure modification to class 32 (61)
Lattice Constant (\AA)	6.461 (average value)	(59)(60) a low value of $6.429 \pm 6\text{\AA}$ reported by (58)
Density (gms/c.c.)	8.12	(82)
Energy Gap (eV)	$E_1 = -0.140 \pm 0.050$ $E_t = -0.020 \pm 0.010$ $E_2 = +0.020 \pm 0.010$	Semi-metal type band-structure with non-parabolic conduction band, (92) see also section on band structure p.61.

Electron Mobility cm^2/Vsec

300°K	77°K	20°K	4.2°K	Reference
19,000	23,000	-	-	(60)
22,000	31,000	18,000	-	(74)
23,000	73,000	-	-	(77)
25,000	70,000	140,000	60,000	(82)
22,000	68,000	120,000	25,000	(82)
-	-	-	15,000	(81) estimated

Mobility Ratio μ_b

300°K	174°K	77°K	4.2°K	Reference
-	70	-	-	(60)
50	-	50	100	(81) estimated
-	-	65	-	(75)
-	-	> 500	-	(77)

Effective Mass Ratios for Electrons M_c^*/M_o

300°K	200°K	150°K	100°K	Reference
0.04	-	-	-	(72)
-	-	.012	-	(112)
0.031	0.027	-	0.007	(88)
0.020	-	-	-	(82)

M_c^*/M_o at bottom of conduction band $1.7 \cdot 10^{-3}$ (75); 4×10^{-4} (81)

M_h^*/M_o in the valence band 0.6 (75).

Intrinsic Carrier Concentration ($\times 10^{17}/cc$).

300°K	116°K	77°K	44.5°K	4.2°K	Reference
6.8	2.3	-	0.46	-	(60)
5	-	1	-	0.2	(81)
3.5	0.8	0.35	-	-	(77)
4.2	0.84	0.52	0.21	.006 (est)	(82)

Thermal Conductivity $mW/cm^{\circ}K$

Quantity	300°K	77°K	Reference and Comments
K total	27	270	varies as $1/T$ (69)
K phonon	19	-	(107)
K phonon	21	-	(108)
K phonon	19	-	(109)
K total	24	-	(109)

In the summary of the properties of HgTe, the values quoted are thought to be representative of those found in the complete literature of HgTe, bearing in mind the degree of perfection of the materials used. Although the early values of mobility were at maximum only around $10,000 \text{ cm}^2/V\text{-sec}$, due to continuous improvements in the production of stoichiometric and homogeneous single crystals, the latest values of

mobility are now well above 100,000 cm²/V-sec at their maximum. The properties naturally depend not only on the lattice defects but also on the distance of the Fermi level above the conduction band, which is a function of the foreign impurity concentration.

The Indium-Tellurium Binary Alloy System

As with the mercury-tellurium alloy system a detailed study has not been carried out, but a clear outline of the phase diagram of the system is given by Hanson and Andenko (113). Only the compositions in the region of In₂Te₃ were investigated by Holmes et al (114) who modified the phase diagram of Hansen and Andenko to include the polymorphism of In₂Te₃ and the peritectic compound In₄Te₇. The revised diagram is shown in Fig (15). The principle compounds in

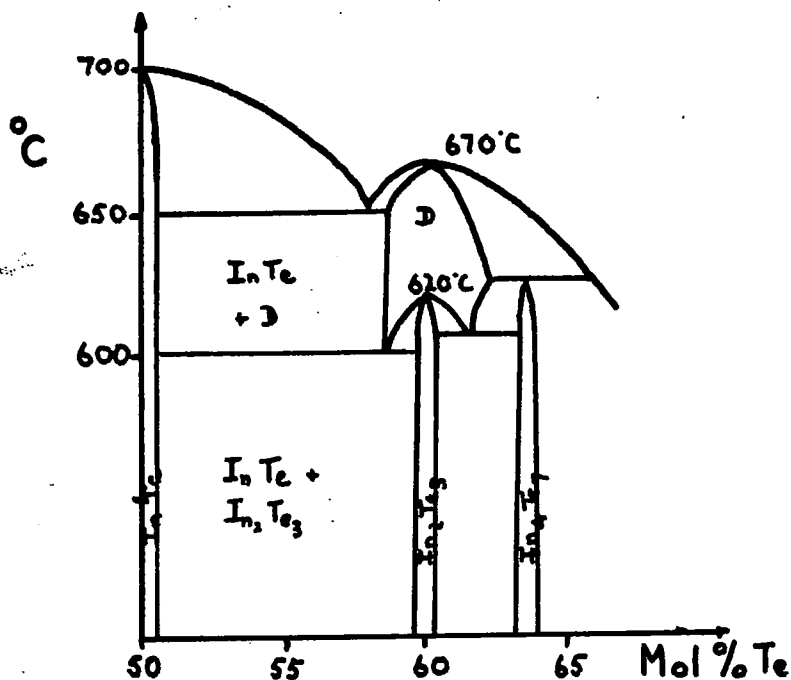


Fig. 15. Proposed phase diagram in the region of In₂Te₃ (after Holmes et al.)

this region are InTe , In_2Te_3 , In_2Te , In_2Te_5 , and In_4Te_7 , of which the last three are formed peritectically. There is a eutectic at 90 atomic per cent tellurium at a temperature of 427°C . The compound In_2Te_3 has two forms, a disordered phase existing above $615 \pm 10^\circ\text{C}$, and a low temperature ordered phase.

The Compound In_2Te_3

Ingots of this material have been prepared from very pure stoichiometric amounts of the elements by the technique of directional freezing, Woolley and Pamplin (115); by zone refining in a background temperature of 600°C , Holmes et al (114); and by very slow cooling from the melt. Zaslavskii and Sergeeva (116), Zhuze et al (117). In all cases good single crystals were not obtained and the crystal grains were only a few mm in size, though Zaslavskii and Sergeeva (116) have managed to extract thin flakes of up to 16 mm^2 in area for optical and photoelectrical work on the compound.

By using infra-red microscopy, Holmes et al (114) have observed three types of inhomogeneity in their material. The opaque regions, corresponding to grain boundaries, have been shown by X-ray diffraction to consist exclusively of InTe . It also seems likely that the other two inhomogeneities, small random blobs and opaque needles, are also InTe , as Te is more likely to be lost by evaporation than In from In_2Te_3 , so that compositions between In_2Te_3 and InTe are more probable in the resulting ingot than compositions on the other side of In_2Te_3 . The opaque needles dissolve above 600°C and it is thought that there is wider range of solid solution in the higher temperature phase. Their work agrees well with that of Zaslavskii and Sergeeva (116)

except on a few points, one of which is the disorder-order transition temperature range. Holmes et al give a much narrower range than the Russians, who quote a temperature range of 620° - 520°C . However, all workers agree that the order-disorder transition temperature range is quite small, and is complete by 620°C . The process is also completely reversible provided that the initial stoichiometry is exact. The work of Holmes et al throws considerable doubt on the validity of any measurements performed on material which has not been examined for a second phase by infra-red microscopy.

The structure of In_2Te_3

Woolley et al (118) have discussed the structure of both phases of In_2Te_3 on the basis of X-ray powder photographs alone. They found that the structure could be either defect zincblende or for the low temperature phase, defect antiferite on which is superimposed a pattern of ordering of the vacancies, Gasson et al (119) in a later paper support the view that the low temperature phase is a fluorite type structure.

Zaslavskii and Sergeeva (116) have interpreted Laue photographs of single crystals in the assumption of a zincblende structure. They found that the high temperature phase was of the zincblende type with a random distribution of vacancies on the tetrahedral sites of the cationic sublattice. The low temperature phase was found to be a face centered cubic structure with a unit cell of $a = 18.5\text{\AA}$ and a space group classification of $F\bar{4}3m$. It was based on a nine layer cubic packing with three patterns of ordering. A three fold increase in the lattice parameter takes place on alternation of two occupied and one vacant tetrahedra and vice versa. Thus

the lattice parameter of the hightemperature phase should be approximately $a = 6.166\text{\AA}$.

Hahn and Klinger (120) are reported (121) to have measured the high temperature phase lattice parameter as $a = 6.146\text{\AA}$, in good agreement with the Russian prediction. However Holmes et al (114) and Inuzuki and Sugaike (122) have expressed some doubt as to the validity of the space group classification and the latter have proposed an ordered unit cell of rather larger dimensions than $a = 18.5\text{\AA}$.

Optical and Photoelectrical Properties of In_2Te_3

Petrusevitch and Sergeeva (123) in investigating the infra-red transmission properties of In_2Te_3 discovered that the radiation was scattered strongly by their samples, more so by the high temperature disordered phase than by the ordered phase. When this strong scattering was allowed for, a sharp absorption edge was obtained although high absorption experiments were not carried out. It would seem that this scattering accounts for the poor absorption curves obtained by other workers and the rather large differences in the values obtained for the energy gap. These values vary according to whether they were based on measuring the absorption coefficient at the edge of the main absorption band, or on the use of curves of the spectral distribution of photoconductivity, both of which would be erroneous to different degrees if the scattering of the radiation was ignored. The cause of the large scattering was not explained but in view of the work of Holmes et al (114) it may well be due to the presence of small precipitates of InTe in the In_2Te_3 . The measurements were interpreted

using the formula for indirect transitions and the values of the energy gap obtained were 1.026 eV for the ordered material and 1.022 eV for the disordered.

Woolley et al (124) obtained values of 1.16 eV and 1.10 eV for the energy gap of the ordered and disordered material. The energy gap was defined as that energy at which the absorption coefficient had changed by 300 cm^{-1} from the background value. However, the half-maxima points in the photoconductivity curves of Petrusevitch and Sergeeva give values of 0.94 eV and 0.92 eV for the energy gap of ordered and disordered material respectively, but these low values must be due largely to the strong scattering observed.

Electrical Properties of In_2Te_3

Good agreement is not to be expected between the several sets of electrical measurements which have been reported in the literature as in each case the material was polycrystalline and also the work was completed before Holmes et al. reported on the effects of inhomogeneities on the properties of In_2Te_3 . There is a need for large single crystals of this interesting compound to be grown. Most workers also assumed that their material was stoichiometric which in view of the work of Holmes et al. is unlikely. The combination of low mobility and low carrier density in intrinsic material makes measurements of the bulk properties below 300°C difficult and any results very questionable. High temperature measurements are also of doubtful validity due to changes in the surface layer of samples and due to redissolution of precipitates which takes place in this temperature range as reported by Holmes et al.

Woolley and Pamplin (115) together with earlier workers, have observed singularities in the conductivity and Hall effect curves in the region of 470°C. This effect was not encountered by Zhuze et al. (117) who explained previous results as being affected by irreversible changes in the material under investigation, due to inappropriate annealing times and procedures. They observed that, when conducting surface layers were removed, the activation energy was constant up to the melting point, being $1.12 \pm .05$ eV, which agrees well with the value of the optical energy gap obtained by Petrusevitch and Sergeeva.

Variations of the Hall mobility with temperature, reported by Woolley and Pamplin for ordered material were not found by Zhuze et al., but both reports agree on room temperature values of 14 and 50 cm²/V-sec for the mobility of the disordered and ordered phases respectively. The mobility was found to be constant over a wide temperature range which suggests that scattering is predominantly caused by the electrically neutral cationic vacancies. These vacancies also cause the mobility to be smaller than that found in the neighbouring isoelectric binary compounds which have a perfect structure. N-type material has been prepared by Zhuze et al. using bismuth and p-type using iodine and in these cases the mobility was found to increase rapidly with temperature. However other atoms (Mg, Cd, Cu, Hg, Sb, Sn, Zn, and Ge) in quantities up to one atomic per cent were found to cause no impurity conduction. Zhuze et al have also managed to obtain a value for the mobility ratio of about four, from considerations of the variation of Seebeck coefficient with temperature. They also quote an electron effective

mass ratio of 0.7 and a hole effective mass ratio of 1.2. They emphasise however that the method used was extremely approximate.

Ioffe (125), (126) and (127) has pointed out that, with materials having mobilities as small as these found in the disordered phase of In_2Te_3 , conduction processes should theoretically be explained in terms of a hopping process rather than in terms of the usual semiconductor model which has been used by all workers on In_2Te_3 so far.

Chizhevskaya and Glazov (128) have studied the indium-tellurium system in the temperature range 500 and 1000°C by means of the variations in electrical conductivity and viscosity with the temperature and alloy composition. They report that the conductivity of solid In_2Te_3 increases exponentially up to the melting point, in agreement with Zhuze et al., giving a value of activation energy of about 1 eV. Immediately above the melting point the conductivity increases sharply but begins to level off about 60°C above the melting point and finally saturating at about 400°C above the melting point. They believe the sudden increase in conductivity at the melting point is due to a rearrangement of structural elements in the melt, on the principal of close packing. They also found that the liquid phase of In_2Te_3 was an extremely stable compound, not becoming dissociated until high temperatures were reached, the solid covalent bonding scheme being retained above the melting point.

Sergeeva and Shelykh (129) have worked on the influence of omnidirectional pressure on the conductivity of In_2Te_3 . They report that there is no effect observed on n-type samples, but

a threefold increase in conductivity occurs for p-type samples. In the intrinsic case there is a definite minimum in the conductivity-pressure curve at about 3000 kg/cm^2 after which there is a continuous rise in conductivity up to the maximum pressure employed, 7000 kg/cm^2 .

Thermal Conductivity of In_2Te_3

As with the electron mobility, the thermal conductivity of In_2Te_3 is very much lower than that found in perfect zincblende compounds in the same isoelectric series. Zaslavskii et al (130) have measured the lattice thermal conductivity of cast and compressed In_2Te_3 after subjection to various heat treatments. They found that the abnormally low heat conductivity of $6.8 \text{ mW/cm}^\circ\text{C}$ is characteristic of the disordered phase and that the value is independent of temperature in that region. The value steadily increases with increasing ordering in the structure and finally reaches a room temperature value of $11.2 \text{ mW/cm}^\circ\text{C}$ rising considerably at lower temperatures. They conclude that the low value in the disordered phase is due to phonon scattering on the random vacancies in the indium sublattice, the scattering being reduced as the ordering increases.

They also found that coarse crystalline specimens had a higher heat conductivity than fine crystalline specimens in the ordered phase in the temperature range $200 - 400^\circ\text{C}$. It was not possible to explain this result in terms of normal heat conduction processes and so it was proposed that the extra heat was being conducted by electromagnetic radiation, similar to processes which Smirnov and his associates had discovered in Te and Ge. Petrushevitch et al (131) later verified this hypothesis by experimental work

on the compound.

The Effects of Ordering in In_2Te_3

Although only a few workers have investigated the properties of In_2Te_3 and despite the difficulties involved in obtaining reliable and valid measurements, it is clear that the ordering of the vacancies in the crystal structure has considerable effects on the properties. Besides a structural change, both the thermal conductivity and electron mobility are increased in the ordered material. The increase in the number of carriers and the widening of the energy gap in the ordered phase are indicative of changes in the band structure, whilst thermal conductivity work suggests that different scattering mechanisms exist for the phonons in the two phases.

Summary of the Properties of In_2Te_3

The high temperature phase has been designated by β , and the low temperature ordered phase will be designated by α . The figures refer to the source of the quoted values.

The transition temperature range of the ordered to disordered phase is given as $600 - 620^\circ\text{C}$ by both Zaslavskii and Sergeeva (116) and Holmes et al (114) whilst (116) quotes a value of $620 - 520^\circ\text{C}$ for the reverse transition, against a value of 620 to about 600°C of (114). The melting point is given as 667°C by (113) and 670°C by (114).

Property	β -disordered phase	α -ordered phase	Source and Comment
Lattice	cubic face centred, zincblende with random vacancies on the In sub lattice	cubic face centred	(117)
		cubic face centred with ordered superlattice formed from the vacancies	(116)
Space Group classification	$\bar{4}3m$	$F\bar{4}3m$	(116) but doubted by (114) and (122)
Lattice Constant \AA	6.160	18.5	(116)
	6.146	-	(120)
	-	18.4	(122)
No. of cation vac.	$5.5-10^{21}$ random	$5.5-10^{21}$ - ordered into a superlattice	(117)
Density at 20°C grm/c.c.	5.73	5.79	(117)
Energy Gap eV. at 300°K	1.02	1.026	(123) from absorption coefficient
	0.92	0.94	(123) from photocond. band edge-low value due to large scatter
	1.10	1.16	(124) from optical band-edge
	1.09 -	1.14 $1.12 \pm .05$	(132) optical at 0°K (117)
Electron Mobility $\text{cm}^2/\text{V-sec}$	14	50	(115)
	14	50	(117)
Mobility Ratio	~ 4	~ 4	(117) very approx.
Effective Mass Ratio	-- --	$m_e^* = 0.7 m_0$ $m_h^* = 1.12 m_0$	(117) very approximate.

Property	β -disordered phase	α -ordered phase	Source
Intrinsic Carrier Conc.			
334°K	-	$7.68 \cdot 10^{11}$	(117)
417°K	-	$4.10 \cdot 10^{13}$	
556°K	-	$1.60 \cdot 10^{15}$	
Thermal Cond. $\text{mW/cm}^2\text{K}$	6.8	11.2	(130)
Scattering Mechanisms	Scattering by electrically neutral random cation vacancies	Scattering by electrically ordered neutral cation vacancies. Thermal conductivity is increased in range 200-400°C by electromagnetic radiation.	(130)

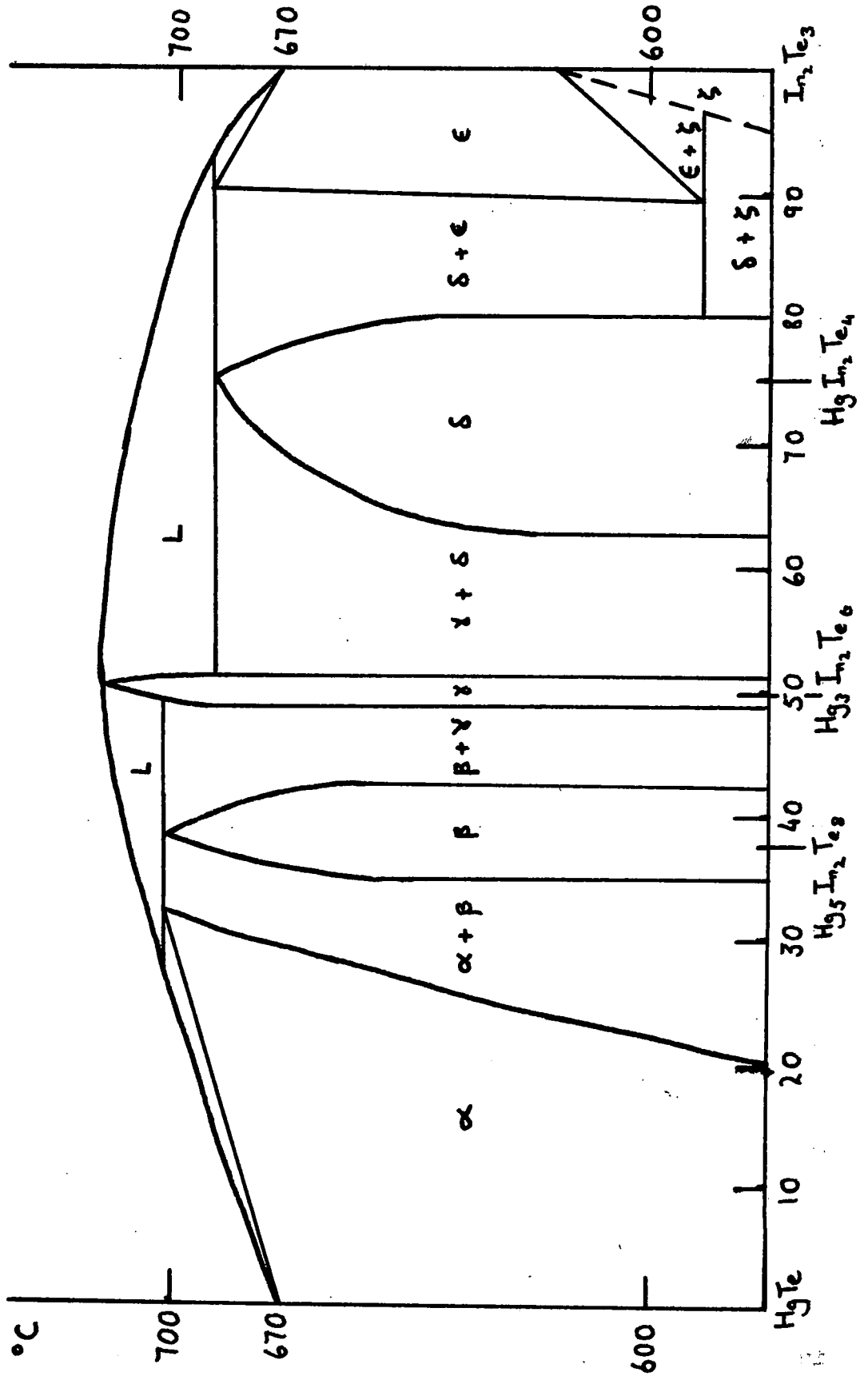
In the above summary of properties it must be remembered that in all cases polycrystalline samples were used, which were assumed to be single phase and stoichiometric. In the opinion of Holmes et al. (114) this is unlikely. The variation in the values obtained for the energy gap can be explained in terms of errors introduced by workers neglecting the large scatter of incident radiation found in this compound. All the electrical results must be treated as very tentative, as values were obtained from only a few polycrystalline samples, and no corroboration of them has been made.

The HgTe - In₂Te₃ Pseudo-Binary Alloy System

This system was first investigated by Woolley and Ray (133) who measured the lattice parameter and the limits of solid solution of various alloy compositions, mainly on the In₂Te₃ rich side of the system. They found that there were two regions one centred about 40 mol.%, the other at about 75 mol.% In₂Te₃, when an ordered structure is superimposed on the zincblende phase. In between, from about 50 to 60 mol %, there existed a two phase region. Pamplin (134), in his thesis, began investigations into the compound Hg₅In₂Te₈, at 37.5 mol % In₂Te₃, mainly into its structure, which was known to be highly ordered, and some measurements of its lattice parameters were made. These early investigations were confirmed by work on the system carried out by Spencer et al. (135) who also began some studies on the effects of ordering on the properties of the system, and the electrical properties of a number of compositions from HgTe to Hg₅In₂Te₈ were measured. Values of the lattice parameter, energy gap, Seebeck coefficient, conductivity, and Hall coefficient were obtained for this region from measurements made on polycrystalline samples, and the lower limit of the ordered region centred on 40 mol.% In₂Te₃ was found to be around 25 mol.% In₂Te₃, below which the alloys were disordered and had a similar structure to that of HgTe.

This work was continued by Spencer (136) in his doctoral thesis, detailed studies of the optical, electrical, and thermal properties of the system from HgTe to Hg₃In₂Te₆, 50 mol.% In₂Te₃, being made on polycrystalline samples. Although no differential

Fig. 16. Proposed phase diagram for HgTe-In₂Te₃ alloy system
(after Spencer)



thermal analysis was carried out on the system, from X-ray analysis and optical examination of annealed samples, for phases and homogeneity, etc., a tentative phase diagram for the system was proposed, which was in accordance with the observed measurements. This phase diagram is reproduced in Fig. (16) but it is stressed that the diagram, based largely on the CdTe - In_2Te_3 phase diagram proposed by Mason and Cook (137) is only tentative and needs confirmation, and possible alteration, following differential thermal analysis measurements.

Spencer found that the lattice parameter was linear with composition in the range 0 - 50 mol.% In_2Te_3 , but that the optical energy gap, obtained from measurements of the absorption edge, exhibited two plateaux, one centred at 25 mol.% the other at 45 mol.%, a sharp rise in energy occurring between these two plateaux at around 35 mol.% In_2Te_3 . Only in the low In_2Te_3 content alloys was a linear region obtained, up to about 20 mol. % In_2Te_3 .

The lattice thermal conductivity was found to drop sharply with increasing In_2Te_3 alloy content and by 15 mol.% In_2Te_3 had virtually fallen to the low value of In_2Te_3 . The electron mobility, which was around 20,000 $\text{cm}^2/\text{V}\text{-sec}$ for HgTe at room temperature, also dropped sharply and was only 2,000 $\text{cm}^2/\text{V}\text{-sec}$ at 15 mol.% In_2Te_3 . It was conclusively shown that the presence of only slight quantities of In_2Te_3 materially lowered the large mobility of HgTe, and no intermediate alloy composition was found where properties were better suited to thermoelectric applications than HgTe. However, the work was performed on polycrystalline samples, some of which were in a poor condition, so any conclusions on the system are of

necessity only tentative, requiring corroborative evidence deduced from much more reliable and reproducible results obtained from work carried out on single crystal samples.

CHAPTER 3

Apparatus and Experimental Techniques

Introduction

The first part of this chapter deals with the synthesis, preparation, and examination of the materials and the techniques used in preparing single crystal samples. The rest of the chapter deals with the experimental procedure used to determine the lattice parameter, the electrical conductivity, the Hall effect, the Seebeck coefficient, the magnetoresistivity and the magnetoseebeck coefficient of the materials.

Some of the techniques used in the preparation of the materials are described in greater detail in Lawson and Nicholson (138) and in the review book, the Art and Science of Growing Crystals (139), which also describes furnace construction and growing techniques. Measurement techniques for the galvanomagnetic and thermomagnetic properties of the materials are described in Methods of Experimental Physics (140) and The Hall Effect and related Phenomenon (34), which also describes various apparatus for these measurements. Cutting, grinding and polishing techniques are described in Methods of Experimental Physics (144) though not in too great a detail.

Furnace Technique

Three furnaces were used in preparing and annealing the materials. One was used to further purify the tellurium; the

second was used to grow the single crystal ingots, the third was used for annealing the cut samples.

All the furnaces utilised the same materials and techniques of manufacture. Impervious mullite was used for the central furnace tube, on which was wound 18 or 20 S.W.G. Kanthal A wire to the required number of turns per inch and length.

For the annealing furnace, a tube of 35 mm bore, 1 metre long, was used. The wire was wound at 10 t.p.i. at the ends, decreasing progressively to 4 t.p.i. over the central 20 cm. It was found that this procedure gave a uniform temperature over above 20 cms. of the tube.

The single crystal growing furnace was wound uniformly at 5 t.p.i. on a 26 mm tube and was centre tapped so that different voltages could be applied to the upper and lower halves, enabling a sharp temperature gradient to be set up along the tube.

The tellurium purifying furnace was made with a gradual temperature gradient down its tube, to separate out impurities (mainly oxides) in the tellurium. The windings decreased progressively from 10 t.p.i. at one end to 4 t.p.i. at the other.

Typical temperature profiles of these furnaces are shown in Fig. (17); page 86.

As the resistance of these furnaces was about 80 ohms, the power could be taken from the mains supply through a rotary regavolt of 6 amps capacity.

The outer casings of the furnaces were made from Sindanyo asbestos sheet and the insulation was of dexramite blocks with granular

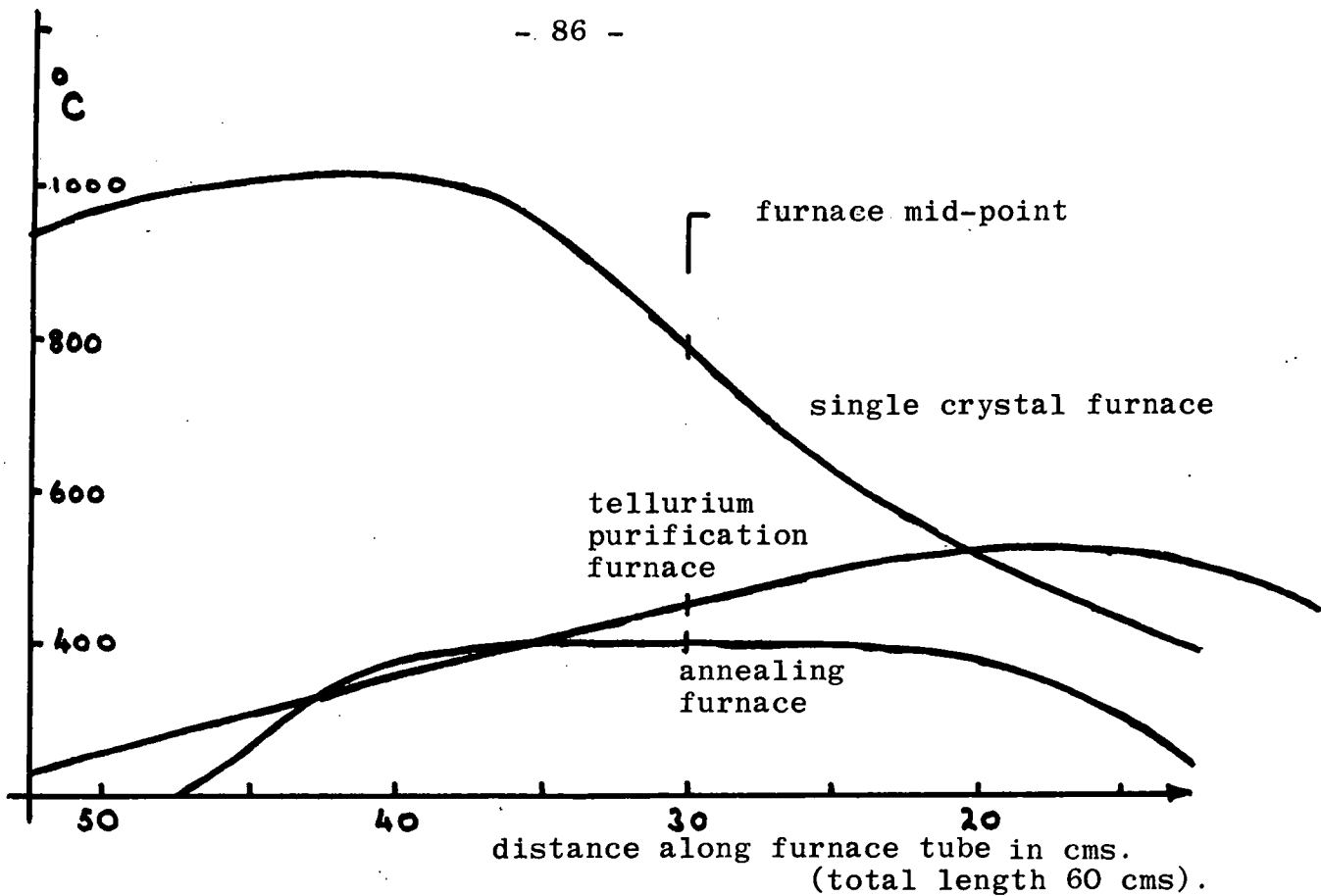


Fig. 17. Furnace temperature profiles.

vermiculite to pack the remaining spaces. These materials gave excellent insulation so that only about half a kilowatt was required to reach a furnace temperature of 800°C.

Each furnace was controlled by an anticipatory Transitrol instrument, made by Ether Ltd., from a 0/13% Pt-Rh thermocouple. This thermocouple, in its silica sheath, was placed on the outside of the furnace tube, and its exposed head was situated as close to the windings as possible. This method allowed the required temperature to be controlled to about 1°C, even better if a metal sheath was used inside the furnace, as in the annealing procedure.

Preparation of the Materials

In the preparation of semiconductors, the reduction of unwanted impurities to an insignificant level is of the prime importance. As all the samples were synthesised from the constituent elements, these elements were purified before synthesis took place.

In the earliest part of the work commercial tellurium was purified by successive distillations from a glass compartment at 450°C to a similar cooler one, under continuous vacuum, the process being repeated until the surface of the tellurium appeared bright and clean.

Later, tellurium which had been purified in Poland by the multiple pass zone technique was used. This also had a bright metallic sheen.

Finally, 99.9995 % pure tellurium was obtained from L. Light and Co., in lump form. This had a dull-grey coating of oxide formed on it, which was removed by melting the tellurium in a thoroughly cleaned silica tube of 7 mm diameter in the tellurium purifying furnace. It was left in the temperature gradient for at least 12 hours, at a temperature well above its melting point (460°C). It was then slowly cooled, using a motor to lower the indicated temperature of the controlling apparatus. The tellurium thus obtained was clean and bright over its middle section, with its ends discoloured, and of a convenient shape and size for weighing (7 mm diameter cylinders). Invariably large single crystals of tellurium were found, which cleaved easily.

This tellurium was kept in its silica tube until required and then only the clean central portion was used, this being cleaved or broken into short lengths.

Mercury was bought from L. Light and Co. in 500 gram ampoules, 99.9999% pure. This was used as bought, it having no perceptible impurities floating on its surface and no tendency to wet its container.

The Indium was also bought from L. Light and Co., in shot form, the most convenient for weighing, 99.9999% pure. Immediately on purchase it was etched in an HCl etch to remove the surface tarnish, then stored in small quantities, under vacuum, in glass phials. This indium then had a bright appearance, unlike the tarnished or blackened appearance of similar indium which had been left exposed to the atmosphere.

Preparation of the Charge

As none of the elements used reacted with quartz, crystals were formed in transparent silica ampoules. Furthermore this material is easily worked and can be obtained in a very pure form, and will withstand the necessary temperature and pressure.

Firstly, the silica tube, of 10 mm internal diameter and 30 cms long, was closed at one end to a fine point, to facilitate nucleation of a single crystallite, using an oxygen-coal gas flame. Then it was etched in hydrofluoric acid to remove any surface contamination (or hot concentrated nitric acid if it were relatively clean), to prevent the growing crystal from keying or nucleating to the sides of the tube. The tube was then washed thoroughly in distilled de-ionised water and dried under vacuum using the torch. Care

was taken to ensure that no rubber particles from the vacuum system entered the tube when releasing the vacuum, and a small drop of mercury was rolled around the tube to ensure that all impurities had been removed. Impurities showed themselves if the mercury wetted the surface or as smears on the surface of the mercury. If this was not the case, the mercury was removed and the tube immediately used to hold the weighed constituents of the crystal to be grown. If an unclean tube was used, a single crystal ingot was rarely formed, the ingot being usually heavily pitted on its surface. The smoother the surface the better the ingot, as a rule.

Stoichiometric amounts of the elements required for each composition of the alloy system were weighed to 0.5 milligram and introduced into the silica tube. Care was taken to eliminate tellurium dust to a minimum, as this caused the greatest single error in the weighings. The tellurium used had been previously purified and solidified into rods, of 7 mm diameter, which easily filled the silica ampoule, and did not create dust, as it easily cleaved for weighing into convenient sizes. The mercury was placed in the tube first, then the tellurium. The mercury was then carefully moved around the tube so that it floated away any small particles of tellurium away from the mouth of the tube. The indium was then introduced, in shot form.

A neck was then formed on the tube above the materials, which were protected from oxidisation and evaporation by wet tissue wrapped around the tube. The ampoule was then evacuated, for at

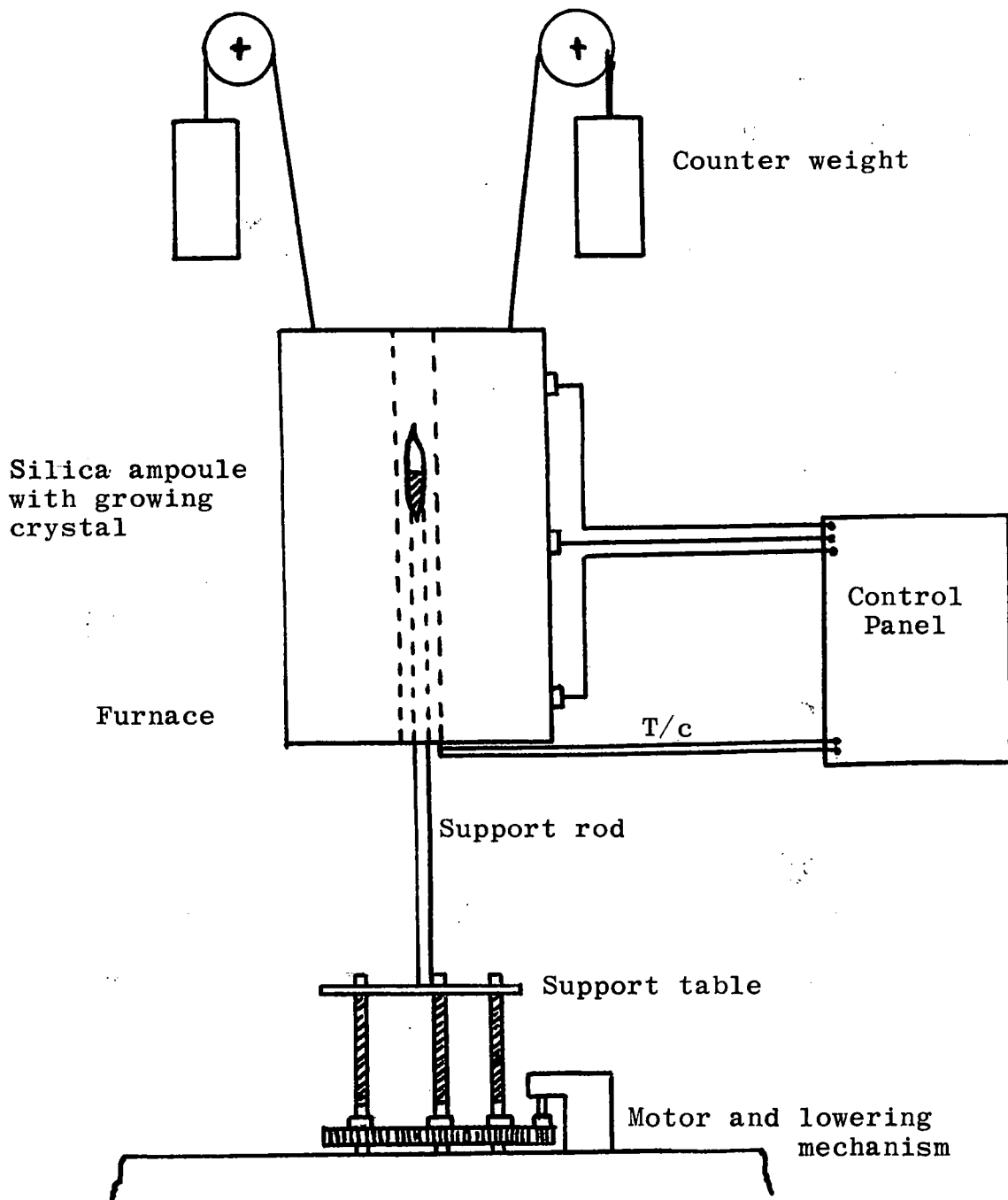


Fig. 18.
 The Single Crystal Growing Furnace.

least four hours, at a pressure of about one micron of mercury, using an oil diffusion pump coupled to a rotary backing pump. During this time the mercury in the ampoule was carefully boiled, to remove any occluded oxygen or air. The mercury was condensed using a wet tissue wrapped around the tube, and no mercury was lost through the neck. Finally, the neck of the ampoule was closed, care being taken to leave as thick a wall as possible.

The Single Crystal Growing Furnace

The single crystal growing furnace, shown in Figure (18) consisted essentially of the Stockbarger arrangement, (142), in which the molten charge is drawn through a temperature gradient. The furnace tube winding was centre-tapped and different voltages were applied to each half, via a rotary regavolt and rheostats. This provided the sharp temperature gradient. The temperature profile of the furnace was controlled by an anticipatory Transitol instrument, made by Ether Ltd., from a 0/13% Pt-Rh thermocouple. This was placed, in a silica sheath, on the outside of the furnace tube, and its exposed head was held as close to the centre tap of the windings (i.e. the mid-point of the temperature gradient) as possible. The temperature of this point was controlled to better than 2°C , so that the temperature profile inside the furnace was controlled to about 1°C .

The temperature profile used in growing the crystals is shown in Fig. (17), page (86).

The charge was placed on top of a metal rod, good thermal contact being made between the ampoule and the rod so that the isotherms within the furnace, including the charge, would remain

flat. If the solid liquid interface became concave, the resultant sideways cooling would cause spurious nucleation, giving a polycrystalline ingot as in Figure (19). The rod was moved downwards



Fig. 19. Polycrystalline ingot, effect of sideways cooling.

through the temperature gradient by a lead-screw mechanism worked by a small electric motor. This gave a lowering speed of 3.2 mm per hour with minimum vibration to the growing crystal.

The maximum melting point of the alloy system is about 680°C so the temperature of the charge was held at 700°C for at least 6 hours, to allow thorough mixing of the constituents by thermal agitation. This temperature was only attained after about 12 hours, as it was found that a rapid increase in temperature caused explosions, due in part to the high vapour pressure of mercury at these temperatures (50 atmos. at 700°C). This slow increase was obtained by using a cam to actuate the controlling mechanism. The cam was cut to give a linear increase in temperature of about $60^{\circ}\text{C}/\text{hour}$. After the charge had been fully lowered through the temperature gradient to the lower half of the furnace, the temperature of the furnace was lowered to room temperature using the same cam mechanism in reverse.

Good crystals, that is, ones appearing bright and clean all over, and not keyed to the silica ampoule, were invariably obtained. These crystals were of 10 mm diameter and about 10 - 15 cm long and usually

contained only a few single crystal domains, each being large enough to easily obtain a single crystal sample.

Cutting, Grinding, and Polishing of Samples

All the samples were cut on a standard rotary cut-off machine, rotating at 6,000 r.p.m., in a jet of soluble oil to prevent the material from decomposing due to overheating. Carborundum wheels 4" diameter and 0.010" thick were first used, but later it was found that a diamond wheel 0.030" thick was far better, giving a cleaner cut and far less chipping.

Ampoules were opened by cutting off both ends; the ingot could then be pushed out. Two types of sample were cut, oriented and non-oriented. For the latter, the ingot was mounted on a steel block with cement, the block being gripped in the rotatable chuck of the cut-off machine. Two planes at right angles were cut in it, one usually being parallel to the axis of the ingot.

For cutting oriented samples, the ingot was mounted on a small precision goniometer head, and the ingot was aligned to a known direction by means of the Laue X-ray technique. The datum planes for this direction were the faces of the mounting track of the X-ray generator. A similar track was mounted on the cut-off machine, with one of the datum faces parallel to the plane of the wheel, the other perpendicular to it. Thus by aligning the $[001]$ plane of the crystal parallel to a datum face it was possible to cut along this plane on the machine and accurately at right angles to it. Hence two datum faces of known orientation were cut in the ingot.

A clear plastic cement was used for the mounting of the ingots and cut samples on the steel blocks. This was easily soluble in

acetone, but had to be left for a day to set firmly on steel. Otherwise cracking of the ingot resulted, due to the cement giving under the strain of cutting. No other cement was found that was better suited to the needs of this particular job, although several others were tried.

Having obtained two faces at right angles the sample was then mounted in accurately machined steel jigs which allowed the other faces of a rectangular parallelepiped to be ground out. Later, the two original cut faces were also ground down. This resulted in a sample which was comparatively strain-free on its surface, as the final grinding was carried out on 6 micron lapping paste. The sample size was determined in terms of the recommended minimum dimensions (143) and was about 12 mm x 3 mm x 2 mm. Occasionally, especially with oriented samples, the length to width ratio was less than four, due to the limited length of the ingot the sample was cut from. Reduction in the other dimensions resulted in a fragile sample.

In each case, one surface of an ingot would be polished with 6 micron grade lapping paste until the crystal grains were apparent; each different orientation showing up in obliquely reflected lighting. Then the surface was polished with 2 micron grade lapping paste on a soft cloth until a fine uniform mirror finish was obtained.

This surface was examined under a microscope for defects and for two-phase regions. The defects were usually only scratches due to the lapping process, and more rarely holes. These holes may also be due to the lapping process, and not typical of the bulk of the material, as holes were rarely found on the surface of the uncut ingot. The presence of holes was indicative of the quality of an ingot, more holes being found with compositions which gave diffuse X-ray

powder photographs than with compositions which were sharp. Two phase regions, as reported by Spencer (144) were not found in any ingot examined, although the 30% and 40% compositions gave diffuse X-ray powder photographs and Laue photographs. This indicates that the phases, if phases they were, were intimately mingled giving the appearance of single phase material under microscopic examination. More probably, the diffuse lines were due to the onset of ordering in the alloy system (145).

X - ray Technique

X-ray powder photographs were taken of all ingots. Usually two photographs were taken of each ingot, from widely differing regions. The sharpness of the lines and any differences in the two photographs gave quantitative information on the homogeneity of the sample and its suitability for cutting into samples.

The photographs were taken using a Debye - Scherrer powder camera fitted to a Phillips X-ray Diffraction Generator, which provided CuK_α radiation through a Ni filter. Exposures of up to 50 hours were sometimes necessary to discern the higher angle lines, even with a very fast fine grain film, Ilford Industrial G. Small samples from the ingot were crushed in an agate mortar and pestle, and then mounted on fine glass fibres with collodian. Neither the glass nor the collodian gave rise to any lines, only background darkening especially at low angles. The overall size of the sample plus fibre was kept to a minimum to shorten the exposure time necessary.

The sharpness of the lines is influenced mainly by the homogeneity of the sample. The lattice parameters need vary only from one set of a

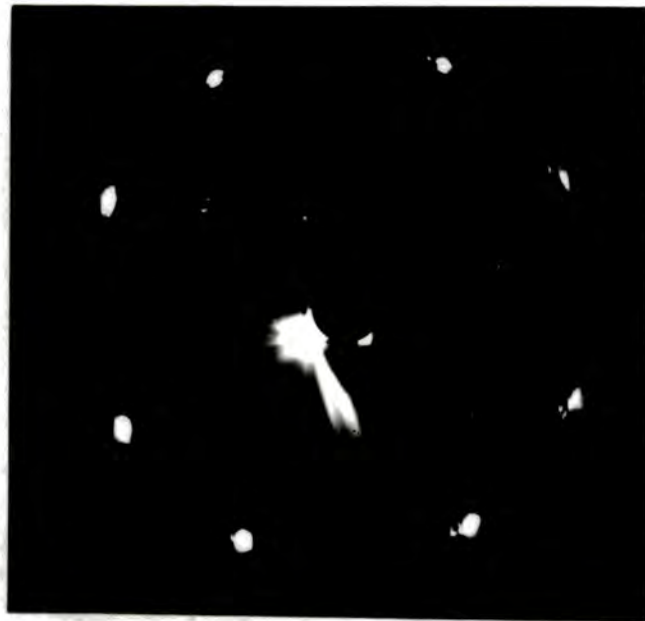


Fig. 20. Laue photograph of a strained single crystal
[001] direction

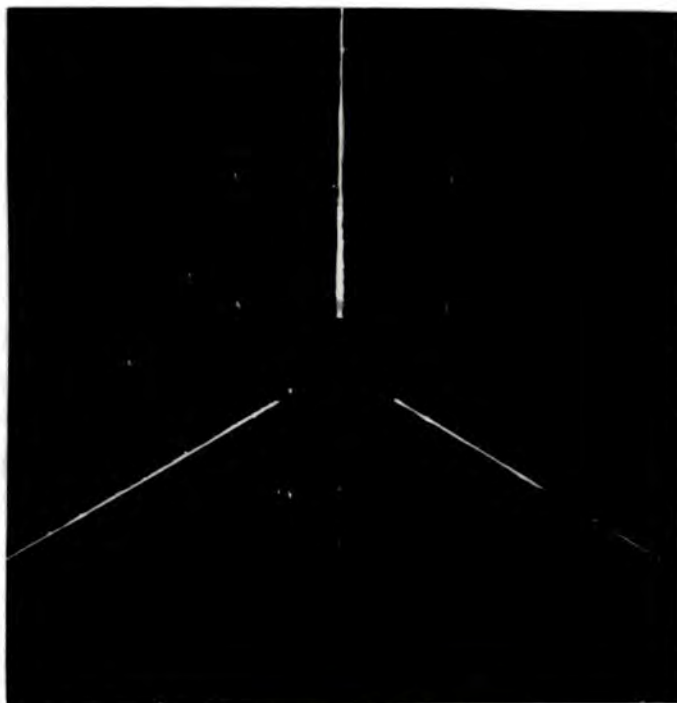


Fig. 21 Laue photograph of an unstrained single crystal
[111] direction

few hundred atoms to the next to give rise to diffuse lines at the higher angles. Gross inhomogeneities in the ingot, such as variations in composition, would lead to two different powder photographs. In the ingots grown none showed this gross effect, although the 30% and 40% compositions showed diffuse high angle lines. This was expected as these compositions are thought to be two phase in the sense that the ordering of the atoms in the crystals is not complete. Thus the low angle side of the photographs showed two distinct sets of lines, one the normal set, the other the superlattice ones, but these sets become progressively more diffuse towards the higher angle side. The 37.5% and 50% compositions showed complete ordering, with two distinct sets of lines present up to the highest angles with reasonably well resolved high angle doublets. The ordering found in the 50% composition is in direct disagreement with the results found by Spencer (146) and confirm the work of Woolley and Ray (133). Recently powder photographs of the 50% composition, taken by Spencer, have been found, which have the ordering lines present.

Laue back-reflection X-ray photographs were also taken of the later ingots. This was mainly to orientate an ingot prior to cutting a sample, but the method also gave information on the homogeneity of the ingots and any strain present in them. Strain caused blurring of the pattern on the photograph. A cut face would give a badly blurred pattern as in Fig. (20) indicating strain. By careful grinding with 6 micron lapping paste a better photograph was invariably obtained, Fig. (21), which rarely improved on annealing. Thus the

ingots as grown seem to be relatively strain free, surface strain being introduced by the cutting procedure. The strained region was apparently removed by the grinding procedure.

All the compositions gave a pattern of three-fold symmetry about an axis, Fig. (21). As four of these axes could be found, each at 90° to the other, the system must have cubic symmetry, as this system is the only one in which all groups of symmetry elements have four triad axes. When the ingot was oriented along a principal axis $[001]$ the photographs showed a four fold rotational symmetry, so the space group of these compositions must be either $\bar{4}3m$, 432 , or $m\bar{3}m$, (Hermann-Mauguin notation) (147). However, the Laue technique has one important limitation, for a pattern obtained from a non-centrosymmetrical class is indistinguishable from that obtained from a crystal belonging to the higher centrosymmetrical class, generated by the addition of a centre (147). Thus for each composition it was not possible to decide in which class, $\bar{4}3m$, 432 , or $m\bar{3}m$ each one should be placed. However, it is known that HgTe is in the class $\bar{4}3m$, the zincblende class (148), and it is reasonable to assume that the crystal structure does not change at least until the 50% composition is reached, as there is a linear relationship between lattice parameter and composition over this range.

Determination of the Lattice Parameter

The asymmetric method of mounting the film in the camera, due to Ievins and Straumenis, was used. This method eliminates calibration of the camera, since by measuring both high and low angle lines and as many resolved doublets (due to the 0.25%

difference in the two $\text{CuK}\alpha$ wavelengths) as possible, the positions corresponding to $\theta = 0^\circ$ and $\theta = 90^\circ$ can be found. After careful processing, the 25 mm x 355 mm film was attached to a Hilger and Watts vernier film measurer so that the positions of the lines could be measured to an accuracy of 0.05 mm.

The cubic lattice parameters were calculated according to the standard method. (149). As many high angle doublets as could be resolved were measured, and the value of the lattice parameter calculated for each. These results were plotted against the function $\frac{1}{2} \frac{\cos^2 \theta}{\sin \theta} + \frac{\cos^2 \theta}{\theta}$ (150) which corrects for absorption and divergence of the X-ray beam, and the value of the extrapolation to $\theta = 90^\circ$ was taken at the correct lattice parameter, a_0 . The accuracy depended mainly on the sharpness of resolution of the high angle doublets; for well defined doublets the error in a_0 was about 0.002\AA .

For the cubic system the lattice parameter a is calculated from the reflection angle θ using the Bragg equation

$$\sin^2 \theta = \frac{\lambda^2 N}{4a^2}$$

where λ is the wavelength of the radiation and N is defined from the Miller indices of the reflecting plane by the relation

$$N = h^2 + k^2 + l^2$$

Values of N are restricted for the zincblende structure, which is essentially face centred cubic, to values of h , k , l which are either all even or all odd. There are also the forbidden numbers $N = 7, 15, 23, 28 \dots$ as these numbers can not be expressed as a sum of three squares. Thus the photographs of the compositions

had a characteristic pattern, due to the superposition of two sets of lines, one being the diamond-type pattern, indexed

$N = 3, 8, 11, 16, 19, 24, 32 \dots$ and the other being the face centred cubic pattern

$N = 4, 12, 20, 36 \dots$ These latter lines are only faintly seen for zinblende materials. They were visible in HgTe, 7%, and 10% compositions, but not in the higher ones. The final value of N occurs for the highest value of θ less than 90° . Thus line 67 could be identified, with its associate doublet, in HgTe 7% and 10% compositions, but was indistinct in the higher compositions, and was not present in the 50% one. The calculation of the lattice parameters for these relied on the much lower angle of lines $N = 56, 59$, and so are not quite as accurate.

Sample Holders

Basically, two sample holders were designed, one for measuring the Hall effect, conductivity, and magnetoresistance; the other for measuring the Seebeck effect and magnetoseebeck effect. Variations of these two holders were devised for special applications such as longitudinal magnetoresistance measurements and low temperature magnetoseebeck measurements. All holders were used in the temperature range $77^\circ\text{K} - 500^\circ\text{K}$.

The holder used for the Hall effect etc. is shown in Fig (22), p.99. The base was machined from sindanyo, an excellent thermal and electrical insulator. The probes were made from phosphor-bronze wire, ground to fine points and located opposite each other. They were held in contact with the sample by phosphor-bronze springs, tensioned by screws. The current was led to the sample by copper blocks, one

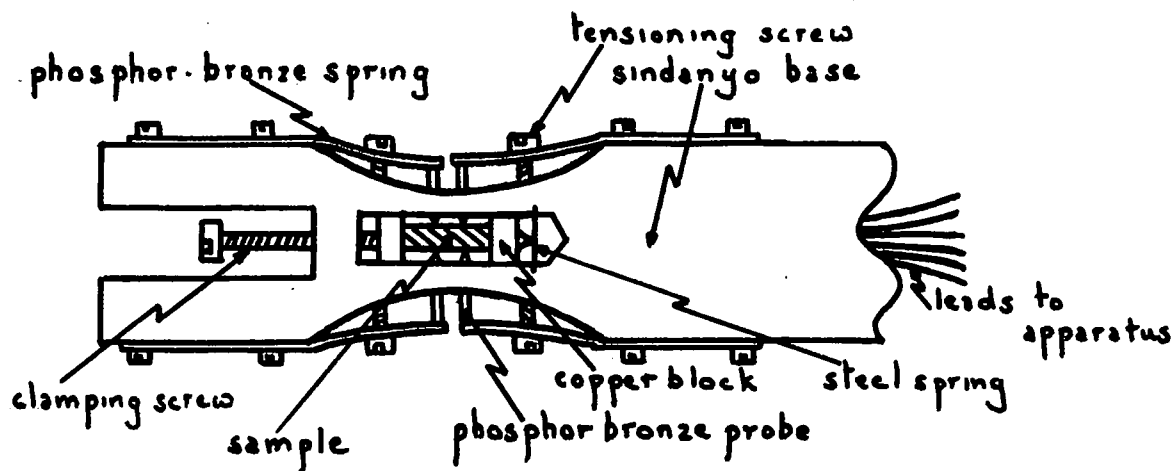


Fig. 22.

Hall Effect Sample Holder.

dims. width - 32 mms, depth - 15 mms, length - 90 mms.

of which pressed against a small steel spring, the other pressing against the sample by means of a further screw. To ensure uniform low resistance current contacts at the ends of the sample were coated with silver dispersed in a solvent, manufactured by Acheson Colloids Ltd. The total resistance across the sample was then of the order of a few ohms and the little trouble was experienced with bad contacts or non-ohmic effects due to contacts. A non-inductive heater was provided on the back of the holder which was capable of raising the temperature of the sample, when in a vacuum dewar, to about 500°K . Higher temperatures were not attempted as loss of mercury and oxydation of samples could be expected. Temperatures were measured by a copper-constantan thermocouple embedded in a thick copper block, which lay between the heater and the sample.

This basic design was modified so that the sample, instead of having its axis along the axis of the vacuum dewar, had its axis perpendicular to it. This enabled the longitudinal as well as the transverse magnetoresistance to be measured.

The overall dimensions of the sample, usually about 12 mm x 3 mm x 2 mm approx., were measured using a micrometer screw gauge, but after the sample had been placed in the holder the distances between probes, and distances of the probes from the current contacts were measured using a travelling microscope. Certain samples, due to brittleness, were smaller than the optimum size required for Hall effect measurements (151) correction factors had to be applied to take into account the shorting effect of the end contacts, both for the Hall effect (152) and the magnetoresistance effect (153).

The holder used for measuring the Seebeck effect and the magnetoseebeck effect is shown in Fig. (23). The base was machined

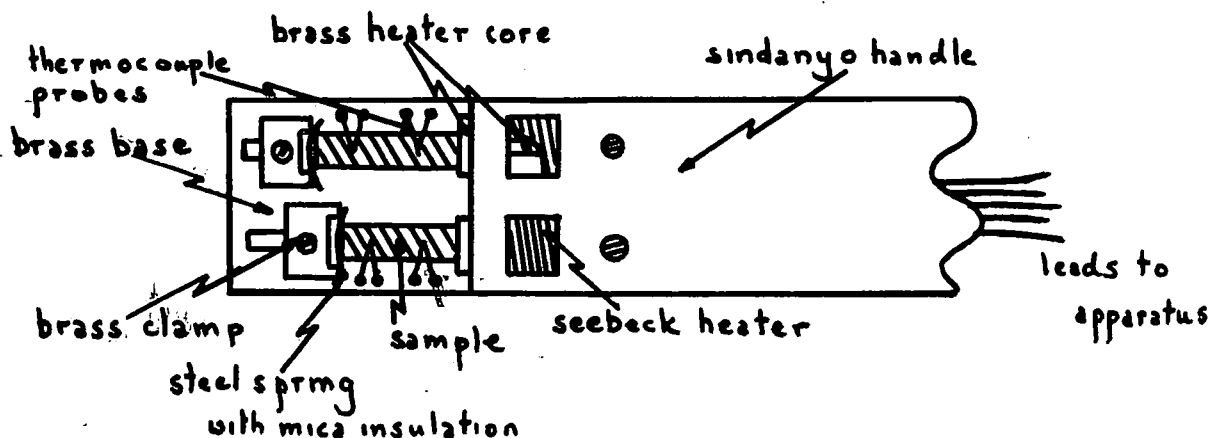


Fig. 23. Seebeck effect sample holder.

dims. width - 27 mms, depth - 15 mms,
length - 70 mms.

from brass, to which was screwed a small heater which provided the temperature gradient. The sample was placed against the end of the heater and was held in position by a flat steel spring, tensioned by means of an adjustable block, which was held by a further screw. The sample was insulated electrically from the base so that no current could flow through the sample due to the thermoelectric voltage. The brass block was attached to a sindanyo handle, to minimise heat-losses. Two matched copper-constantan thermocouples were used for measuring the temperature gradient and as voltage probes. These thermocouples were sprung on the surface of the sample and good thermal contact was ensured using small blobs of silver dispersed in solvent. Care was taken to keep these contacts small and to centralise each one on the sample. The copper lead in each case was used as a voltage probe. A cylindrical heater was provided which fitted around the holder and could raise the temperature to about 500°K when in a vacuum dewar.

The Seebeck holder was later modified to allow the low temperature magnetoseebeck effect to be measured. For this a steady low temperature of about 100°K was required and it was achieved by using the same design of holder but of slightly smaller dimensions and putting the whole into a slim copper tube, closed at its lower end. The ambient heater was formed on the outside of this tube. Totally immersed in liquid nitrogen and the seebeck heater on, steady temperatures varying from 95°K to 120°K could be obtained for various heater currents, that is, various temperature gradients. These varied from 1°K to 6°K per cm.



All these sample holders could be attached in turn to a brass rod which was journalled in two bearings, so that it could turn in the vertical plane. This allowed the sample holder to assume any desired angle in the vertical plane. The sample holders all fitted into the same vacuum dewar, the outside dimensions of which were just less than 2", and fitted between the magnet pole pieces.

The Magnet

The magnet was a medium sized electro magnet, which provided an induction of 6,250 Gauss at a pole gap of 5 cm. This was adequate to measure all the galvanomagnetic and thermomagnetic properties of each sample. It took a current of 11 amps. at 120 volts D.C. and it could be run for sufficient time to take all the measurements without any noticeable drop in induction. The current and hence the induction was varied by rheostats, and this relationship was measured with a calibrated search coil and a ballistic galvanometer to about 1% accuracy. The pole faces were 7 cm. in diameter and although levelled, there was a considerable increase in induction towards the edge of the pole-pieces. In the central area of the pole faces, where the sample was located, the induction was much more uniform, to less than 5% of the total induction.

Experimental Arrangement and Procedure

The leads from the Hall effect holder, in its dewar, were taken to a switch network, which allowed various probes to be connected in turn to a Philips D.C. microvoltmeter. This could measure voltages down to 15 μ V on its low impedance range, which

was 1 megohm, and down to 10 mV on its high range, 100 megohms. These input impedences were much higher than any sample impedance measured. The current for the sample was provided from a battery and kept constant by cascaded potentiometers using a milliammeter. The value of this current was checked by measuring the voltage developed across a 10 ohm standard resistance, which was in series with the sample. The temperature of the sample was measured by a potentiometer and galvanometer, with reference to an ice point. Readings of the Hall voltage and conductivity voltage were taken with the temperature of the holder increasing from 77°K to room temperature. As this took over three hours, little error was introduced due to non-isothermal conditions. The heater was then switched on, obtaining higher temperatures. The magnetoresistance was measured at 77°K whilst immersed in liquid nitrogen, and at 300°K. In these cases the holder was rotated so as to give the variation of the magnetoresistivity with angle of magnetic field.

The conductivity was calculated from the formula

$$\sigma = \frac{I}{V_c} \frac{l}{bd} \quad \text{mho-cm}^{-1} \quad \dots\dots (103)$$

where V_c is the mean of the voltages measured for forward and reverse current, I the current through the sample, l the distance between the probes, b the breadth of the sample, and d the depth.

The magnetoresistance was calculated from the change in conductivity with magnetic field

$$\rho = \frac{l}{\sigma} \quad \text{ohm-cm}$$
$$\Delta \rho = \frac{\rho_H - \rho_0}{\rho_0} = \frac{V_H - V_0}{V_0}$$

where ρ_H is the resistance in the magnetic field and ρ_0 is the zero field resistance, V_H , V_0 the respective voltages measured across the probes.

The reversal of the current was necessary to eliminate any thermoelectric voltages which might have developed across the sample. Provided the sample is homogeneous and the probes are in a region where the current density is uniform equation (103) should give the conductivity to a high degree of accuracy. The magnetoresistance is very sensitive to any non-uniformity or inhomogeneity in a sample (47) and the effects of the end contacts are not negligible on high mobility material. Corrections for this effect were applied when calculating the true magnetoresistance. (153).

Measurement of the Hall voltage necessitated reversing not only the current but also the magnetic field; the mean of the four voltages was taken as the Hall voltage. This was to eliminate all errors except those due to the Ettinghausen effect (154), which is quite small, and inhomogeneities etc. The out of balance voltage due to misalignment of the probes was usually much smaller than the Hall voltage, but for the 50% composition, due to its high resistivity, it was necessary to bias this voltage off using a potentiometer in one of the probe leads. Corrections to the Hall voltage, due to end-contact shorting (152), were applied if the sample geometry required it.

The Hall coefficient was calculated from the formula

$$R = \frac{d}{BI} \cdot V_H \times 10^8 \quad \text{cm}^3/\text{Coulomb}$$

B is the induction in Gauss.

The accuracy of the Hall coefficient depends mainly on the condition of the sample. For good samples the error would be about 5%, but for the high resistivity 50% composition the error would be about twice this, due to difficulties in reading the probe voltages. Fluctuations in the Hall voltage were materially reduced if good electrical contacts were made to the sample and errors were reduced accordingly.

For all these measurements standard precautions were taken. The linearity of conductivity voltage and sample current was checked over at least three decades of the current, from 10^{-3} A to 10^{-1} A. The conductivity voltage was measured on both sides of the sample, to ensure homogeneity of the sample. The Hall voltage was also measured at two points along the sample. Any change in the Hall coefficient meant either non-uniform current densities or inhomogeneous sample, giving variations in the carrier density. Each of these tests would corroborate evidence gleaned from the others and only samples which gave results such that uniformity of both sample and current density was indicated were used in the experiments. Gross errors can be introduced if non-uniform samples or current densities are used, especially in galvanomagnetic or thermomagnetic work (47).

The leads from the Seebeck holder were led into two potentiometers, which measured the output of the two copper-constantan thermocouples using sensitive galvanometers. The two copper leads were used as voltage probes, the voltage being measured by the Philips D.C. microvoltmeter which could measure down to $10 \mu\text{V}$ on its most sensitive scale with an input impedance of 1 megohm.

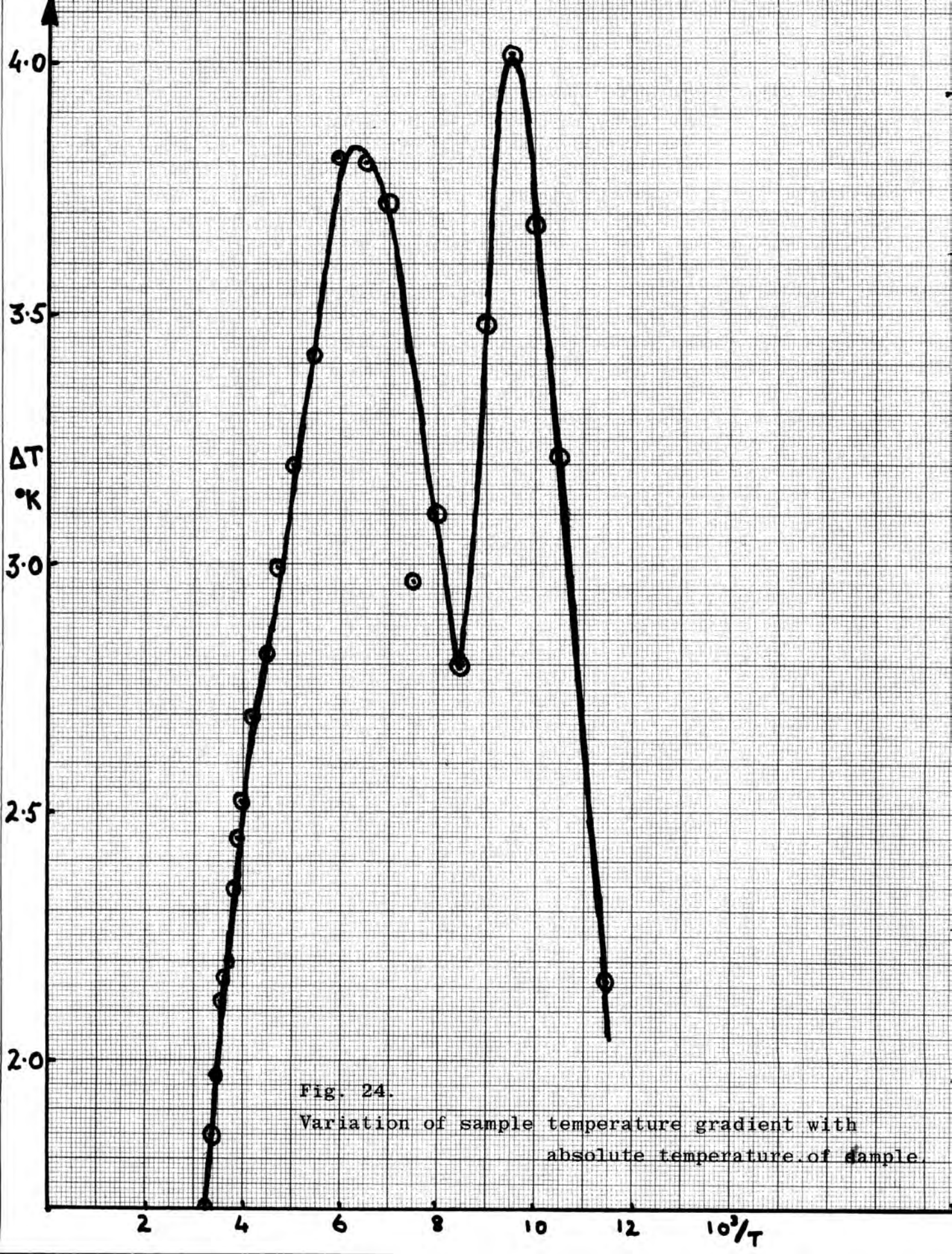


Fig. 24.

Variation of sample temperature gradient with absolute temperature of sample.

The holder, in its dewar between the poles of the magnet, was cooled to 77°K using liquid nitrogen and then allowed to rise to room temperatures when its ambient heater was switched on, to obtain temperatures up to 450°K. At set temperatures the temperatures of the hot and cold end of the sample were measured, the average being taken as the temperature of the sample, and the voltage developed also noted. A graph was drawn of the temperature difference plotted against the temperature as in Fig (24). A smooth curve was drawn through the points obtained, this curve being taken as the true locus of the temperature difference with temperature. Then the thermo - electric power was given by the formula

$$\theta = \frac{\Delta V}{\Delta T} \quad \mu V/^{\circ}K$$

where ΔV was the measured voltage developed across the sample and ΔT was the sample temperature difference from the plotted graph.

The error using this method is quite small for temperatures greater than 100°K, being about 5%, if care is taken to choose a suitable heater current, one which gives only a small temperature gradient along the sample. A check must always be taken of the linearity of the voltage with temperature gradient. A value of $\Delta T = 6^{\circ}K$ over a length of 8 - 10 mm was found to be the upper limit of linearity, and a value of $\Delta T \approx 1^{\circ}K$ the lower limit of temperature difference detected with sufficient accuracy. The value of the thermoelectric power thus obtained was always sufficiently large to ignore the effect of the thermoelectric power of the copper leads, about 1.5 $\mu V/^{\circ}K$.

The magnetosebeck effect was also measured in the same manner, but with the introduction of a transverse magnetic field. Then

$$\frac{\Delta\theta}{\theta} = \frac{\theta_H - \theta_0}{\theta_0} = \frac{\Delta V_H - \Delta V_0}{\Delta V_0} \quad (\Delta T, T \text{ constant})$$

where θ_H is the thermoelectric power in the magnetic field and θ_0 is the zero-field thermoelectric power. ΔV_H and ΔV_0 are the corresponding voltages generated in the sample.

Errors introduced in measuring the magnetosebeck effect due to the various other thermomagnetic effects are negligible with the size of magnetic fields used.

The greatest single error is caused by the probes shorting out the sample at the contact area and so distorting the carrier distribution in the sample. Care was taken to make the area of contact of the probes as small as possible and also to align the probes along the axis of the sample.

For measuring the magnetosebeck effect at low temperatures the sample was kept out of direct contact with the liquid nitrogen coolant in a copper sheath. By altering the current to the temperature gradient heater a stable equilibrium could be established at any temperature between 90°K and 120°K , limited by the need to maintain a reasonable thermal gradient down the sample. Care was needed to maintain the coolant level constant in the dewar, and measurements were taken in the usual manner.

CHAPTER 4

The Properties of Mercury Telluride

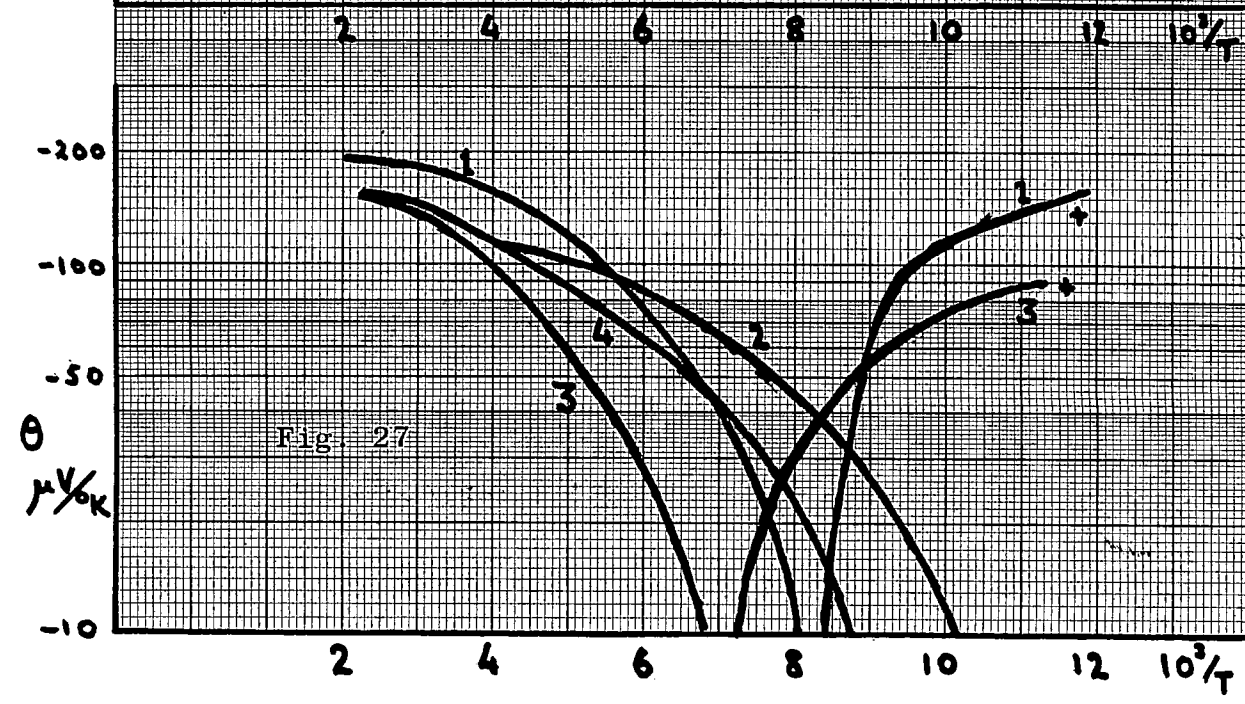
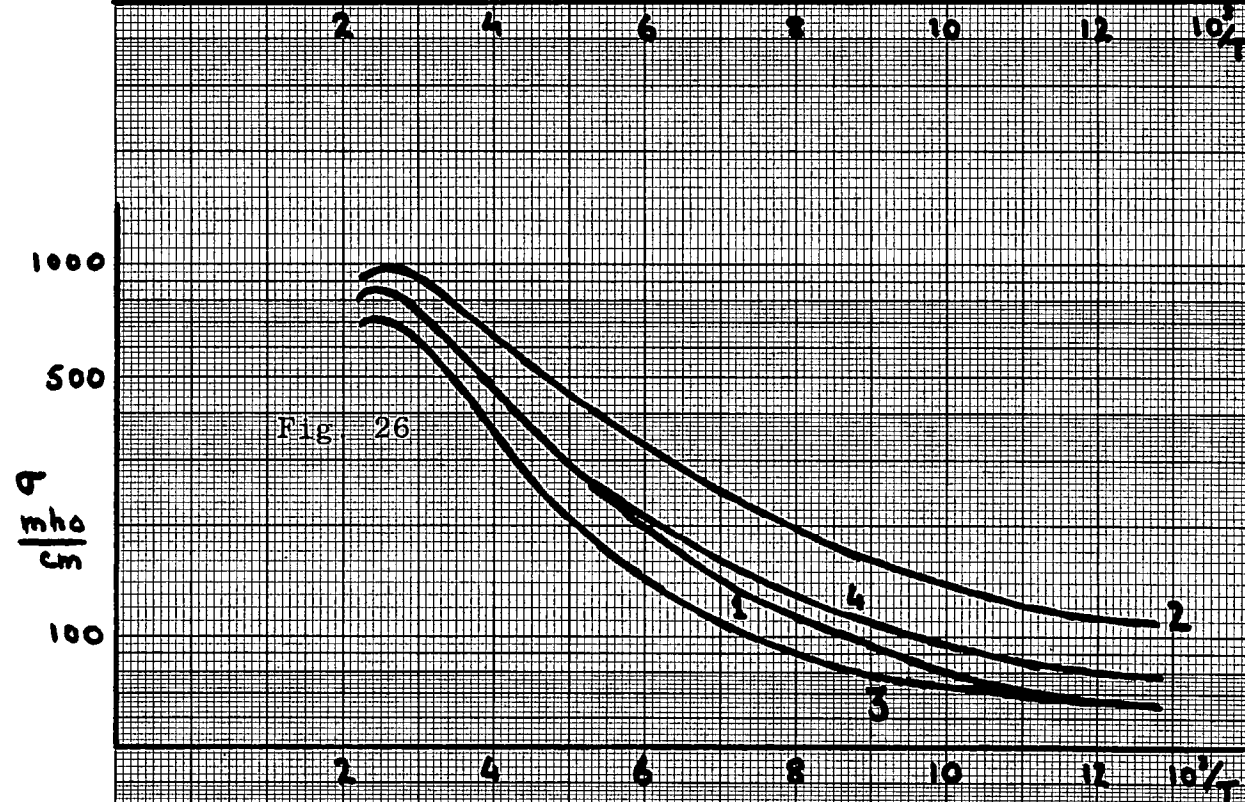
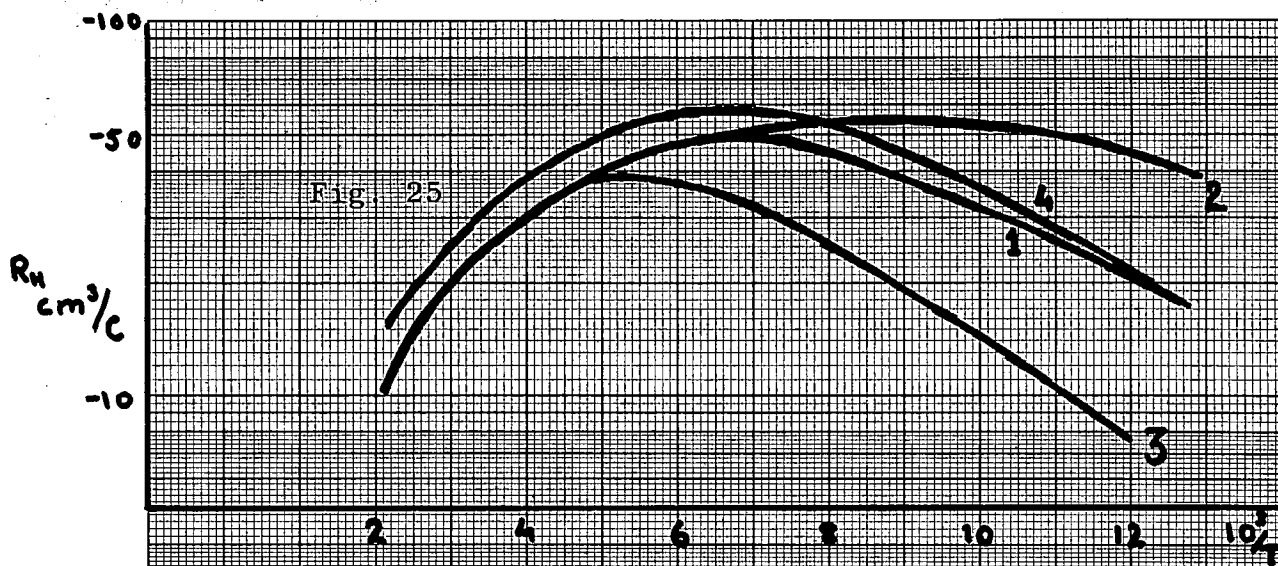
Introduction

This chapter is concerned with the work carried out on the compound mercury telluride. The first part deals with the measurement of the conductivity, Hall coefficient, and Seebeck coefficient, and related topics, together with the effects of these properties of various annealing treatments. The second part then turns to the galvanomagnetic and thermomagnetic measurements carried out on the compound.

There is a short discussion on the results in each section.

Four different samples of HgTe were investigated, prepared from four separate ingots of the material. The preparation and production of the samples has been described in detail in chapter 3. All the samples were single crystal and one was oriented so that its edges were parallel to the crystallographic direction $[001]$. As grown all the samples were extremely brittle and chipped easily, especially as pressure contacts were applied, and it was found that after a full programme of measurements on each sample only two were in a sufficiently good condition to be subjected to an annealing treatment followed by further measurements. One of these samples was sufficiently strong to undergo a second annealing treatment.

From visual and microscopic examination each sample appeared



to be homogeneous and of good quality, no cracks or pits being apparent on its surface. X-ray powder photographs verified this judgement as each sample yielded an exactly similar powder photograph with extremely well resolved lines. An accurate measurement of the lattice parameter of the HgTe was possible, as the high angle doublet lines were clearly resolved, and a value of 6.460 \AA was obtained for the unit cell edge.

Electrical Measurements on Unannealed Samples

The Hall coefficient R_H , the electrical conductivity σ , and the Seebeck coefficient θ were all measured in the temperature range 77°K to 455°K , the Hall coefficient being measured at a magnetic field strength of 6,000 gauss. The measurements on the unannealed samples are presented in Figs. (25), (26), and (27). It will be seen that the variation of R_H , σ and θ with temperature is essentially similar for each sample, especially at the higher temperatures and that the sign reversal of θ occurs in the neighbourhood of the corresponding Hall maximum, which is the normal behaviour for a p-type material with a large mobility ratio. At higher temperatures than those corresponding to the Hall maximum the material tends to become intrinsic, as $\ln(R_H T^{3/2})$ is becoming linear with $1/T$ in this region. Due to the large mobility ratio of this material, the effect of the holes on the electrical properties will be swamped by the electrons, and thus the product $R_H \sigma$ in this region can safely be taken to denote the electronic mobility of the material. However, at temperatures lower than those of the Hall maximum the effects of the hole current carriers become more noticeable, as the ratio of the hole carrier density to the electron carrier density is becoming

larger, and at 77°K the electrical properties must be described in terms of mixed conduction. Here the product of $R_H \sigma$ does not denote a mobility as neither carrier is predominant.

P. 110
The variation of the Hall coefficient R_H with temperature is shown in Fig. (25). The variations indicate that the majority carriers are holes but that the effect of the minority electrons is of importance even at 77°K, due to their much larger mobility. Thus R_H is negative over the temperature range investigated, but at 77°K it varies appreciably with magnetic field strength, tending to become more positive with increasing field. This is because the minority electrons have much larger mobilities, and the majority holes tend to take over the conduction processes.

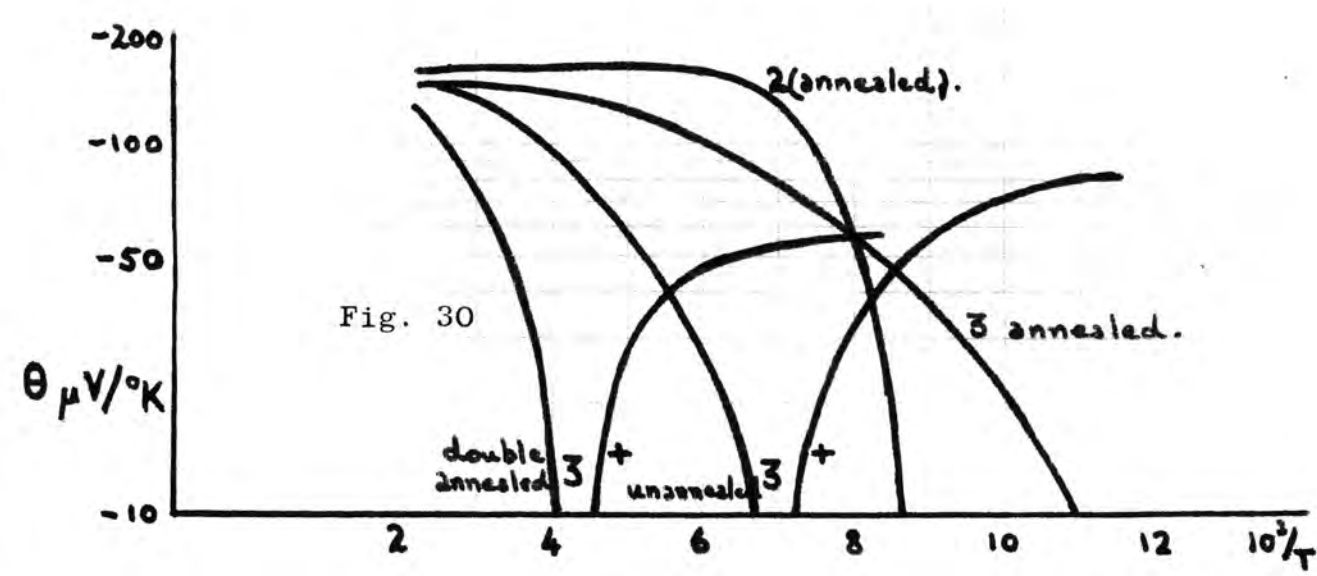
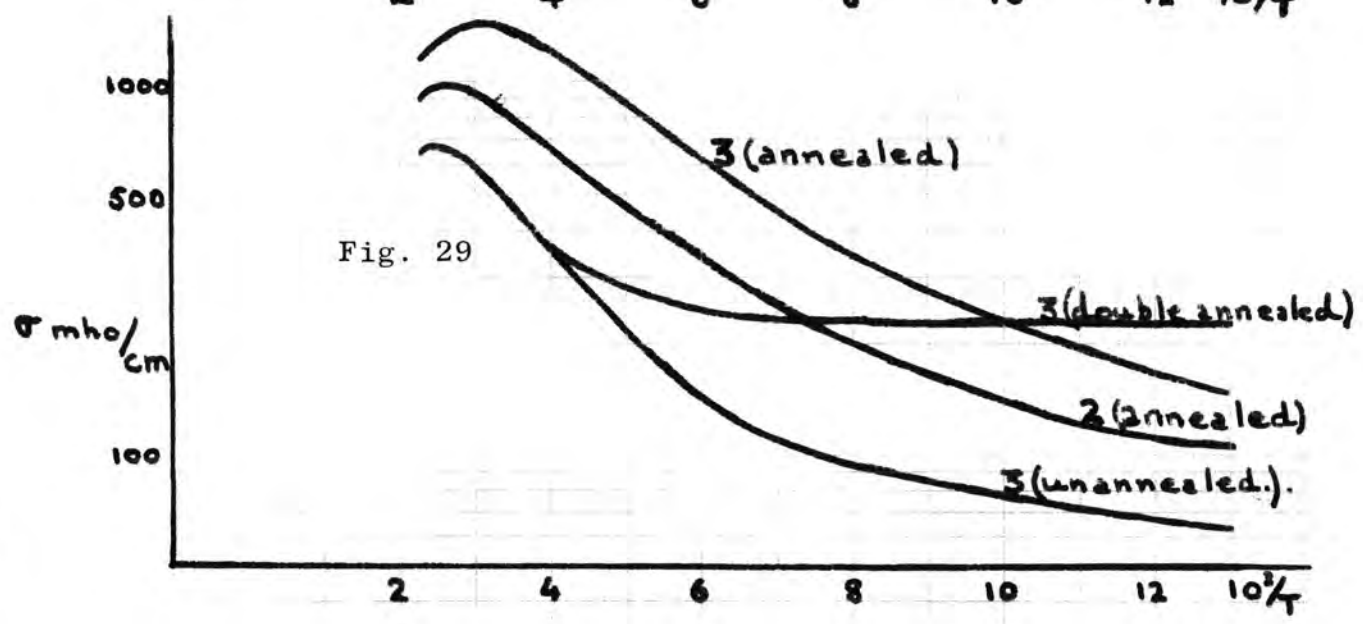
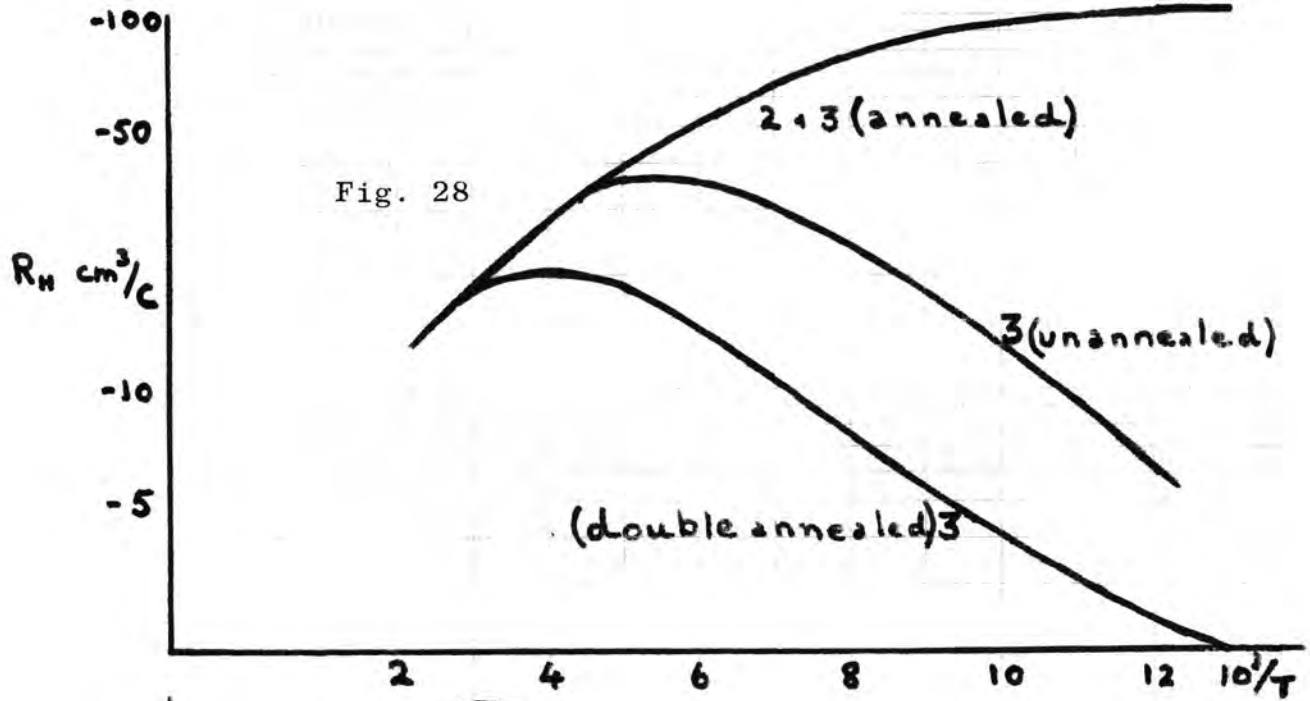
From Fig. (26), the conductivity has a low value of around 70 mho/cm at 77°K which rises steadily with increasing temperature to a maximum value of about 800 mho/cm near room temperature, after which it begins to fall due to the increase in scattering associated with these higher temperatures. The value of the Hall coefficient varied from sample to sample at 77°K, depending on the number of mercury defects occurring in the non-stoichiometric material. The nearer to stoichiometry the higher becomes the value of R_H at this temperature. Above 250°K, after passing through a maximum, the variation of the Hall coefficient with temperature became sensibly identical for every sample, the room temperature value of R_H being about $-22 \text{ cm}^3/\text{C-sec}$ corresponding to a carrier density of about $2.8 \cdot 10^{17}/\text{cm}^3$ which is close to the intrinsic values reported by Giriat (77) and Dziuba (85) at this temperature. The Seebeck coefficient

(Fig. 27), was always positive at 77°K, the value depending on the temperature at which it changed sign. The position of the sign reversal was always close to the associated Hall maximum as is to be expected in such p-type samples. Above room temperature the Seebeck coefficient was still rising, having reached values of around -150 $\mu\text{V}/^\circ\text{K}$, but in some samples it was showing signs of saturating at higher temperatures. In each case the product $R_H \sigma$ reached its maximum value close to room temperature, above which point it can be assumed to be equal to the electric mobility of the sample. At higher temperatures it had begun to fall, in some cases quite steeply.

The room temperature (300°K) properties of the unannealed samples are given in table 1. Due to the stoichiometry of each sample being different and to two-carrier effects, the values of 77°K are not representative of the material and hence are not listed.

Sample	θ	σ	R_H	$R_H \sigma \approx \mu_e$	n
	$\mu\text{V}/^\circ\text{K}$	mho/cm	cm^2/C	$\text{cm}^2/\text{V-sec}$	per c.c.
1	-175	600	-24.0	15,000	$2.6 \cdot 10^{17}$
2	-135	810	-21.5	18,000	$2.9 \cdot 10^{17}$
3	-120	500	-23.0	12,000	$2.7 \cdot 10^{17}$
4	-135	640	-29.5	19,000	$2.1 \cdot 10^{17}$

Table 1. Room temperature electrical properties of HgTe.



Electrical Measurements on Annealed Samples

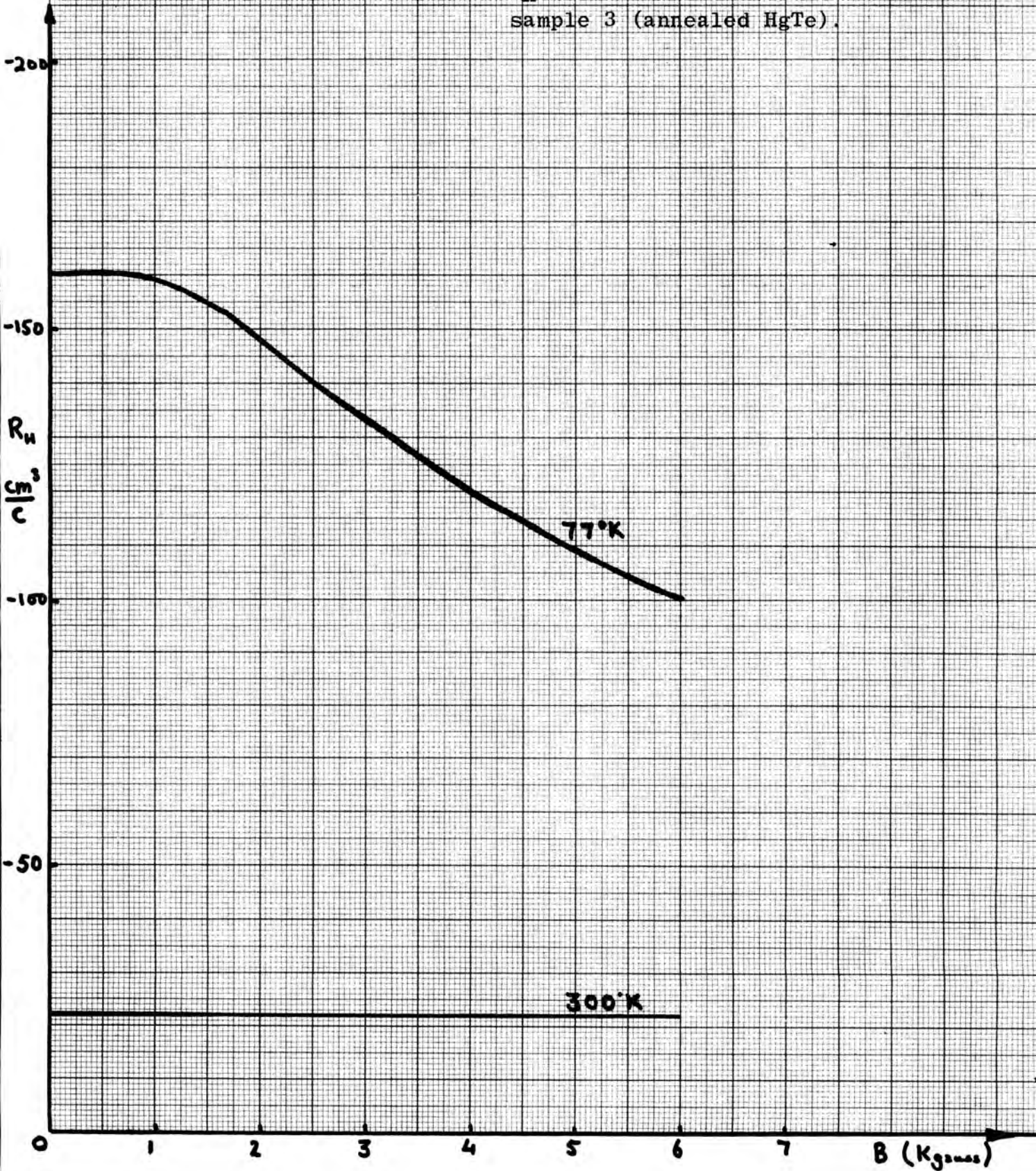
Samples 2 and 3 were later both annealed for 100 hours at a temperature of 250°C in an atmosphere of mercury vapour, according to the work of Rodot and Triboulet (74) and of Giriat (77). They considered that the annealing process took place in two ways. In the first reaction microheterogeneous precipitates that were contained in the non-annealed samples are dissolved out, and in the second reaction mercury atoms enter the HgTe from the vapour. These processes ultimately make the compound stoichiometric, and from the work performed by Giriat on this problem stoichiometry is achieved after 100 hours of anneal at 250°C . According to this theory of the annealing process, if the anneal is continued beyond the optimum time for stoichiometry to be achieved, the HgTe will begin to contain excess mercury, which should result in a reduction of conductivity due to the increased scattering associated with the mercury atoms, and a reduction of R_H , especially at the lower temperatures. To check if this actually did happen, sample 3 was annealed in mercury vapour for a further 100 hours, giving it a total of 200 hours anneal. The results of the electrical measurements carried out on these annealed samples are presented in Figs. (28), (29), and (30). As a comparison the results for sample 3 before annealing are included in these diagrams.

After the first anneal of 100 hours, the most noticeable change occurs in the variation of R_H with temperature (Fig. 28). The Hall coefficient no longer exhibits a maximum in the temperature range investigated and for both samples the variation of R_H with temperature is identical. The value of R_H at 77°K is about $-100\text{cm}^3/\text{C}$ which falls to the value of $-23\text{cm}^3/\text{C}$ at room temperature, above which

temperature the values are identical to those of the unannealed samples. For sample 3 the conductivity was noticeably improved at all temperatures, the value increasing from 65 to 145 mho/cm at 77°K and from 500 to 1400 mho/cm at 300°K (Fig. 29). However, the conductivity of sample 2 was not found to be improved by the anneal, remaining identical to the values obtained previously, which were a little higher than the values obtained for the other three unannealed samples. Unlike the results obtained by Giritat, the Seebeck coefficient still reversed sign in the temperature interval investigated, near to 77°K in each case (Fig. 30). This indicates that the two annealed samples are still p-type, as the sign reversal occurs close to where the Hall coefficient is flattening off to a broad maximum. Compared to the results of Giritat it would seem that the anneal was not continued long enough to allow stoichiometry to be achieved, for at 77°K the Hall coefficient, as measured by Giritat, is still rising and the Seebeck coefficient was still negative, indicating that it would have reversed sign at a much lower temperature, possibly in the region of 50°K. A slightly lower temperature of anneal may account for the fact that the samples did not quite reach stoichiometry during the same time as those annealed by Giritat. At higher temperatures the Seebeck coefficient of both samples tends to saturate at a value of about $-150 \mu\text{V}/^\circ\text{K}$, and for sample 2 this value was constant in the temperature range 170°K to 455°K. This behaviour is identical to that found by Giritat for his annealed samples and Dziuba who has measured the electrical properties of intrinsic HgTe from 20°K to 400°K and found that

Fig. 31.

Variation of Hall Coefficient R_H with magnetic field for sample 3 (annealed HgTe).



in this range HgTe has a constant Seebeck coefficient of about $-135\mu\text{V}/^{\circ}\text{K}$.

The results for sample 3 after its double-anneal are also to be found in Figs (28), (29), and (30). It is seen that R_H has been much reduced in value at all temperatures below 330°K and lies below the curve for the unannealed case. The conductivity has also decreased, and at lower temperatures becomes independent of the temperature. The sign reversal of the Seebeck coefficient is again close to the Hall coefficient maximum, which is now near to room temperature. From this behaviour it must be assumed that an excess of mercury in HgTe causes the material to become more p-type than stoichiometric material, although such behaviour is difficult to explain. However, the value of the Seebeck coefficient, although still rising at the highest temperature reached, indicates that it will saturate out at a value close to that of the stoichiometric material. The decrease observed in the conductivity must be due to the increase in scattering caused by the excess of mercury atoms in the material, which would also cause the value of R_H to fall at the lower temperatures.

The variation of the Hall coefficient, with magnetic field strength for the singly-annealed sample 3, is shown in Fig. (31). Similar to results found by Giriat, R_H varies quite strongly with magnetic field at 77°K , although no variation was found at room temperature. This is to be expected, since the electrical results on this sample in Figs. (28) and (30) indicate that the sample although annealed to near-stoichiometry, is still strongly p-type at 77°K , and that conduction processes at this temperature are

essentially by two carriers. This result is in contradiction to the work published by Rodot and Triboulet (74) and Quillet et al (76) both of whom found that, after annealing, the variation of R_H with magnetic field at 77°K was negligible.

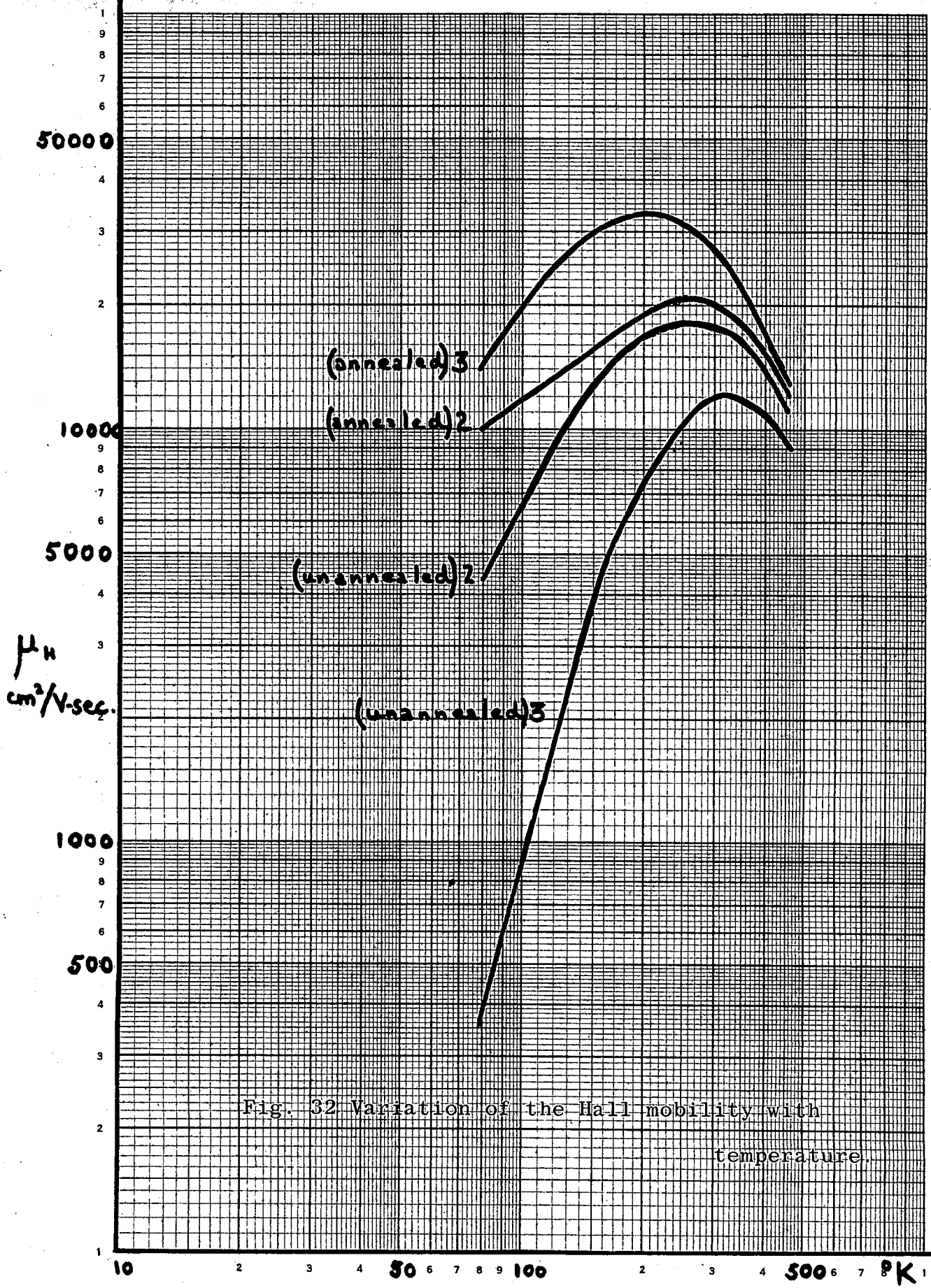
The electrical properties of the annealed samples at a temperature of 300°K are given in table 2, and at a temperature of 77°K in table 3.

Sample	θ	σ	R_H	$R_H \sigma$	n	Remarks
	$\mu V/^\circ K$	mho/cm	cm^3/C	$cm^2/Vsec$	per c.c.	
2	-160	810	-24	19500	$2.6 \cdot 10^{17}$	Anneal 100 hrs at 250° C
3	-150	1400	-23	32200	$2.7 \cdot 10^{17}$	Anneal 100 hrs at 250° C
3	-50	500	-20	10000	$3.1 \cdot 10^{17}$	Anneal 200 hrs at 250° C

Table 2. Room temperature electrical properties of annealed HgTe.

Sample	θ	σ	R_H	$R_H \sigma$	n	Remarks
	$\mu V/^\circ K$	mho/cm	cm^3/C	$cm^2/Vsec$	per c.c.	
2	+ 13	100	-110	11000	$5.6 \cdot 10^{16}$	Anneal 100 hrs at 250° C
3	0	150	-110	16500	$5.6 \cdot 10^{16}$	Anneal 100 hrs at 250° C
3	+ 60	220	- 2	440	$3.1 \cdot 10^{18}$	Anneal 200 hrs at 250° C.

Table 3 Electrical properties of annealed HgTe at 77°K.



The Variation of the Hall Mobility with Temperature

The logarithmic plots of the variation of the Hall mobility $R_H \sigma$ with temperature are shown in Fig. (32). The four curves correspond to the measurements taken on samples 2 and 3 when both unannealed and annealed, and are typical of all the samples. At both high and low temperatures the variation of $R_H \sigma$ tends to become linear with the temperature and so in these regions the relationship between $R_H \sigma$ and T can be expressed in the form

$$R_H \sigma = K T^a$$

For extrinsic conduction or for intrinsic conduction where the mobility ratio is large, as is found in HgTe, the value of the exponent a can be related to the scattering process at that temperature.

Above 300°K the conditions obtained above apply, namely intrinsic conduction with a large mobility ratio, and thus some information on the scattering process can be elicited. Although the linear region is not very extensive at these temperatures, and only an estimate for the value of the exponent a can be obtained for each sample, all the values lay between -1.5 and -2.0, in both the unannealed and annealed cases. The actual values are given in Table 4.

Sample	1	2	2	3	3	3	4
Remarks	Not Anneal	Not Anneal	Annealed	D. Annealed	Not Anneal	Anneal	Not Anneal
a	-1.8	-2.0	-2.0	-1.8	-1.9	-1.8	-1.5

Table 4. The exponent a , from the temperature variation of Hall mobility $T > 300^{\circ}\text{K}$.

From simple theory for non-degenerate semiconductors a value of the exponent of -1.5 is indicative of acoustic mode lattice scattering, so the values obtained are strongly suggestive that this process is the predominant scattering mechanism in HgTe above room temperature. The fact that most of the values were not exactly -1.5 probably means that the scattering mechanism is not purely acoustic mode but perhaps is coupled with some optical mode scattering, or even inter-valley and intra-valley scattering. Very few semiconductors measured exhibit pure lattice scattering, and values of the exponent a less than -1.5 are commonly met with in practice, but the assumption of acoustic mode scattering, whilst not leading to too great an error, can appreciably simplify the analysis of the results.

Below room temperature the logarithmic plot of $R_{\infty}\sigma$ rises to a maximum and then begins to fall again linearly, with temperature. The value of the exponent at these lower temperatures varied widely from sample to sample. For the unannealed samples the values lay between 3.7 and 1.8, but after annealing lower values than these were obtained, being 0.7 for sample 2 and 1.4 for sample 3. After sample 3 was annealed for the second time the value of the exponent rose again to its unannealed value of over 3. The extremely high values of the exponent a found in this region are almost entirely due to the fact that no one carrier predominates the conduction processes and that the effects of non-stoichiometry and inhomogeneity in the sample will be greatest in this region. This view is supported by the fact that the value of the exponent a tends to be reduced after annealing to achieve stoichiometry and homogeneity. From

the results of the electrical measurements it is also noted that, after annealing, the onset of the two carrier region occurs at a lower temperature than previously. However, even for the annealed samples, no information concerning the scattering process can be deduced from these results as it is obvious that, in the temperature range where the exponent a can be measured, two carrier conduction is definitely taking place.

The Effective Mass

In the samples measured, for temperatures at room temperature or above, the material is becoming intrinsic and thus the carrier density is given by equation (73) in which τ the scattering factor is $\frac{3\pi}{8}$ as acoustic mode lattice scattering predominates at these temperatures. As the mobility ratio of the material is known to be quite high at these temperatures, equation (73) will simplify to

$$n_0 = - \frac{3\pi}{8eR_H} = \frac{-73.6 \times 10^{17}}{R_H} \text{ per c.c.} \dots\dots(104)$$

From the values of R_H at these temperatures it will be seen that the carrier densities are all in excess of 10^{17} per c.c., and the material is partially degenerate. The formulae for the Seebeck coefficient and the carrier density in the case of partial degeneracy are given, from Fermi-Dirac statistics, as (155),

$$\theta = - \frac{k}{e} \left[\frac{(5/2 + s) F_{3/2 + s}(\eta)}{(3/2 + s) F_{1/2 + s}(\eta)} - \eta \right]$$

$$n_0 = 2 \left(\frac{2\pi kT}{h^2} \right)^{3/2} \cdot \left(\frac{m^*}{m_0} \right)^{3/2} \cdot F_{1/2}(\eta).$$

where $\eta = \frac{E_F}{kT}$ is the reduced Fermi energy.

For $s = -1/2$ acoustic mode lattice scattering, and after the numerical

constants have been substituted, these become

$$\theta = -86.5 \left(\frac{2 F_1(\eta)}{F_0(\eta)} - \eta \right) \mu V \text{ } ^\circ K \dots\dots\dots(105)$$

$$n_0 = 4.831 \cdot 10^{15} \left(\frac{m^*}{m_0} \right)^{3/2} T^{3/2} F_{3/2}(\eta) \text{ cm}^{-3} \dots(106)$$

Using the value of n_0 obtained from equation (104) and η from equation (105) gives an estimate of the value of the electron effective mass ratio when they are substituted in equation (106). Table 5 gives the results of these calculations on the measured samples of HgTe.

Sample	1	2	2	3	3	3	4
Remarks	Not Annealed	Not Annealed	Annealed	Not Annealed	Annealed	Double Annealed	Not Annealed
Temp. $^\circ K$	300	300	300	300	300	-	300
$\eta = E_f/kT$	0.5	1.4	0.8	1.8	1.1	-	1.5
$\frac{m^*}{m_0}$.048	.036	.044	.059	.035	-	.028
Temp. $^\circ K$	454	454	454	454	454	454	454
$\eta = E_f/kT$	0.2	0.8	0.8	1.1	1.1	1.5	0.6
$\frac{m^*}{m_0}$.056	.045	.043	.045	.045	.038	.041

Table 5. The Effective Mass of HgTe at 300 $^\circ K$ and 454 $^\circ K$.

The average value of $\frac{m^*}{m_0}$ for electrons from these results is 0.045 at both 300°K and 454°K. Giriat (77) gives a value of 0.035 for $\frac{m^*}{m_0}$ which is constant over the temperature range 215 - 400°K. This value must be increased to 0.045 when exact statistics are used on his results, and then the agreement between the two sets of values is quite good. The value of $\frac{m^*}{m_0}$ of 0.045 is rather higher than the values obtained by recent workers, but it is in agreement with the value of 0.04 deduced by Black et al. (72). It is stressed that the value is only an estimate as the conditions under which equations (104) (105) and 106) can be used are not strictly obtained in the case of HgTe. Even though at room temperatures and above the mobility ratio is quite high, the effect of the two carriers on the value of $\frac{m^*}{m_0}$ obtained by this method can not be neglected.

Magnetoconductivity Measurements

The variation of the electrical conductivity of several unannealed and annealed samples of HgTe with magnetic field strength was investigated at both 300°K and 77°K. Care was taken to check that the value of the Hall coefficient, and hence the carrier density, was the same at two points along the sample length, and that the conductivity of the sample was identical when measured from two sets of ~~probes~~ ^{probes} on the sample. This was to ensure that no anomalous results would be obtained due to carrier density variations along the length of the sample, as reported by Beer (48). It will be noted that such effects, if they do exist, are much more serious in materials having large carrier mobilities.

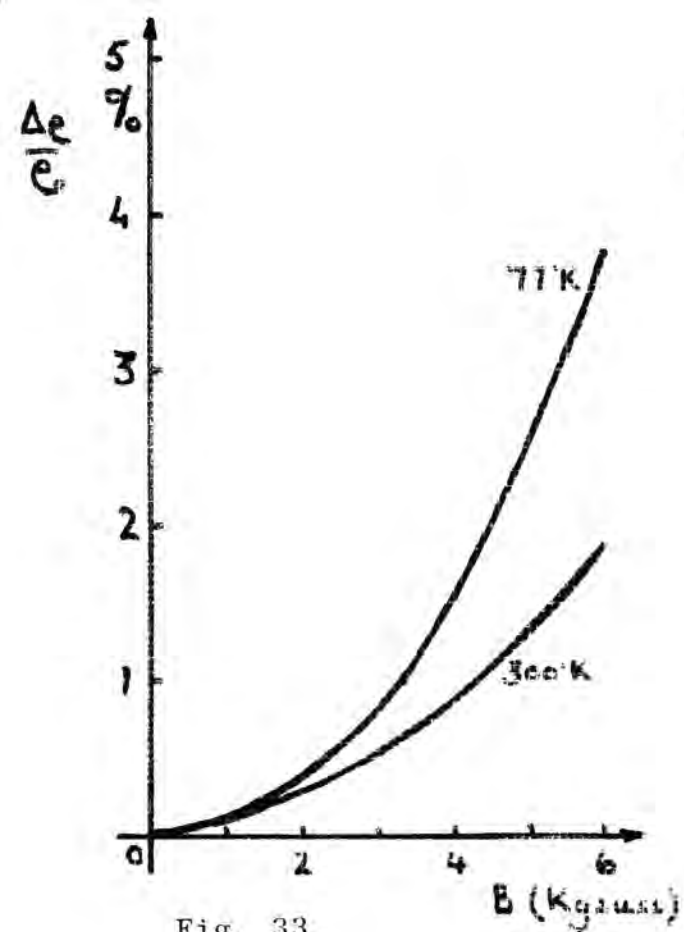


Fig. 33

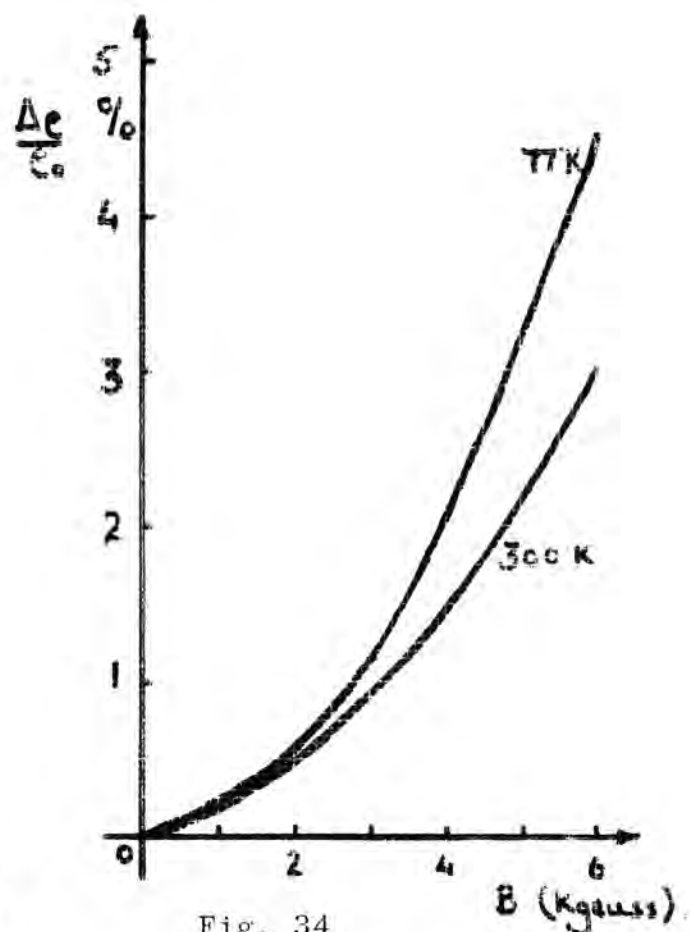


Fig. 34

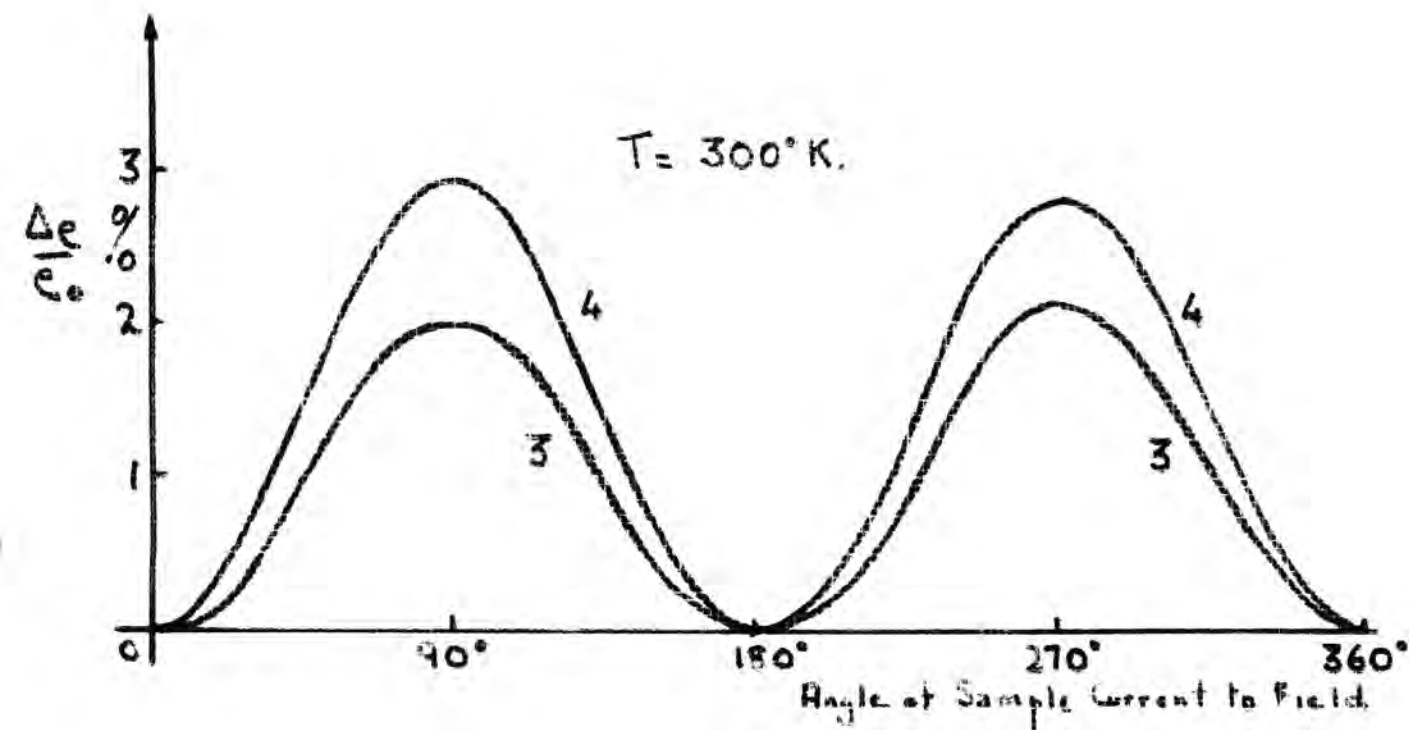


Fig. 35.

Even after such precautions, only a few samples were found which behaved according to the simple theory when the conductivity was measured in a magnetic field. (Fig. 33) shows the variation of the transverse magnetoconductivity of sample 3 with magnetic field strength, and Fig. (34) is for sample 4. Fig. (35) gives the variation of the ~~longitudinal~~ magnetoconductivity with orientation of the sample for samples 3 and 4. The curves shown could all be obtained when the magnetic field was reversed and no asymmetrical effects were observed. The transverse magnetoconductivity can be shown to obey the law

3
 left of
 after
 a-
 ?

$$\frac{\Delta\sigma}{\sigma} \sim B^n$$

where n lies between 1.65 and 2. However the absolute values of the magnetoconductivities, for a given value of the Hall mobility and the magnetic field strength, were much less than predicted using equation (86),

$$\frac{\Delta\sigma}{\sigma} = \mu_H^2 B_z^2 \left(\frac{8}{\pi} - 2 \right)$$

It would seem that the low values obtained are due to the fact that the material is partially degenerate, equation (86) being valid only for the case of non-degeneracy. As the magnetoconductivity of completely degenerate materials is zero, some reduction in the value given by equation (86) would be expected for the case of partial degeneracy. The situation is also complicated by the fact that conduction takes place by both holes and electrons, equation (86) being derived for the single carrier case.

The longitudinal magnetoconductivity, the results of which are presented in Fig. (35) is effectively zero, showing no variation

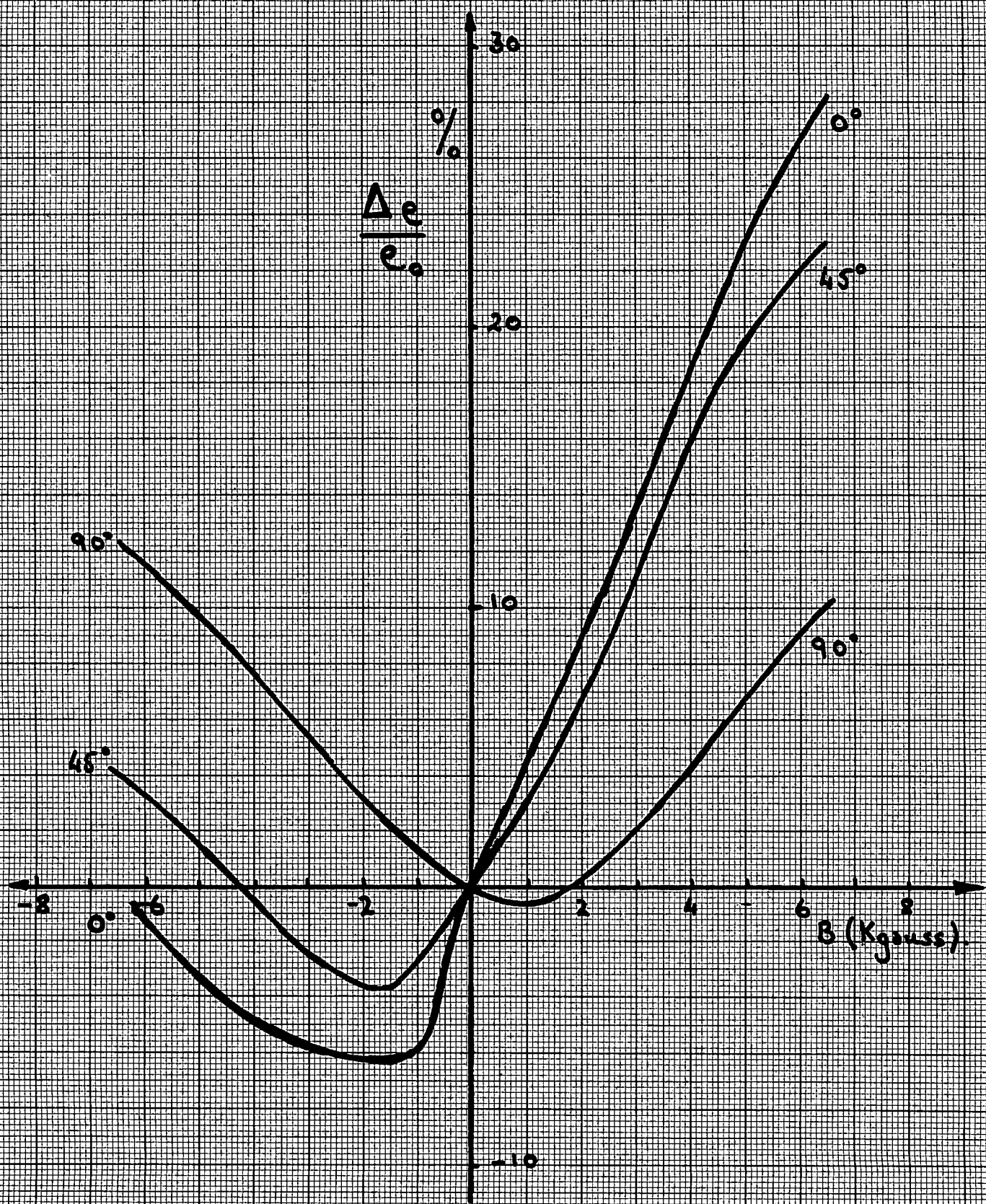


Fig. 36.

Anomalous Magnetoconductivity Variation with Magnetic Field for HgTe

with the strength or the orientation of the magnetic field . This result agrees with the findings of Rodot (87), (88), and indicates that the material has an isotropic band structure, with spherical constant energy surfaces in k -space.

The rest of the samples investigated, even after the precautions mentioned above were carried out to ensure homogeneity throughout the sample, were found to exhibit anomalous magnetoconductivity phenomena. The behaviour of each measured sample is given in Table 6, for both the magnetoconductivity and the magnetosebeck coefficients. It can be seen that there is not immediately apparant pattern to be discerned in these results, either with temperature or with annealing procedure. A typical variation of transverse magnetoconductivity with magnetic field strength for such a sample is shown in Fig. (36). It will be immediately noticed that the curves obtained are not symmetrical with respect to the direction of the magnetic field, but that reversal of the magnetic field causes the sample to exhibit the phenomenon of negative magnetoconductivity. For certain orientations of the sample with respect to the magnetic field, the negative magnetoconductivity reverts to positive magnetoconductivity at some magnetic field strength. For other orientations of the sample the negative magnetoconductivity increases almost linearly for low magnetic field strengths and has a maximum value of negative magnetoconductivity at some higher value of the magnetic field strength.

Temp

In general, larger but similar variations in the magneto-conductivity have been recorded for such samples at lower temperatures.

9TgH

Sample	Magnetoconductivity Measurement		Magnetoseebeck Measurement	
	300°K	77°K	330°K	77°K
2 (annealed)	Anom. Var ⁿ .	Anom. Var ⁿ .	Sym. Parab. Var ⁿ .	Not measured
3 (unanneal.)	Sym. Parab. Var ⁿ .	Sym. Parab. Var ⁿ .	Anom. Var ⁿ .	Sym. Parab. Var ⁿ .
3 (annealed)	Anom. Var ⁿ .	Sym. Parab. Var ⁿ .	Anom. Var ⁿ .	Not measured
3 (double- annealed)	Anom. Var ⁿ .	Sym. Parab. Var ⁿ .	Not measured.	Not measured
4 (unanneal.)	Anom. Var ⁿ .	Sym. Parab. Var ⁿ .	Sym. Parab. Var ⁿ .	Sym. Parab. Var ⁿ .

Table 6.

No satisfactory explanation for these results has yet been discovered or put forward. Most explanations fail to explain why the orientation of the sample with respect to the magnetic field should have any effect on its transverse magnetoconductivity. In fact, such behaviour patterns as found in these samples are extremely difficult to rationalise, and can not be safely ascribed to any of the usual mechanisms, such as probe effects, or inhomogeneities, producing negative magnetoconductivity phenomenon, as described by Beer (48). Surface recombination effects are also not thought to be the cause, since, in a recent experiment, Mr. Dahake in this laboratory has also obtained such phenomenon even after etching his samples. Woods and Chen (156) in a paper reporting the existence of negative magnetoconductivity in Cd-doped Ga-As, P-doped Ge and n-type GaAs, show curves of the magnetoconductivity with magnetic field strength for some of their samples. These curves are almost identical to the ones obtained on various samples of HgTe, but only the variation with one particular direction of the magnetic field is shown - that giving the negative variation in magnetoconductivity.

A tentative explanation has been offered by Tryozawa (157) and is referred to by Woods and Chen, () in terms of a two-energy state model of impurity conduction, the higher state having a higher mobility. Further work is essential before it is profitable to discuss the validity of this model.

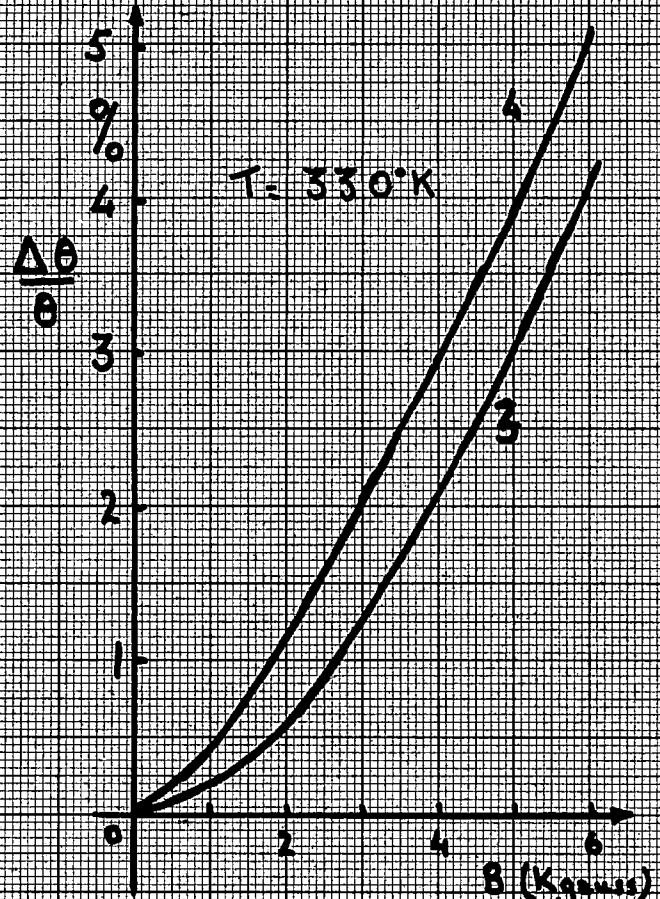


Fig. 37

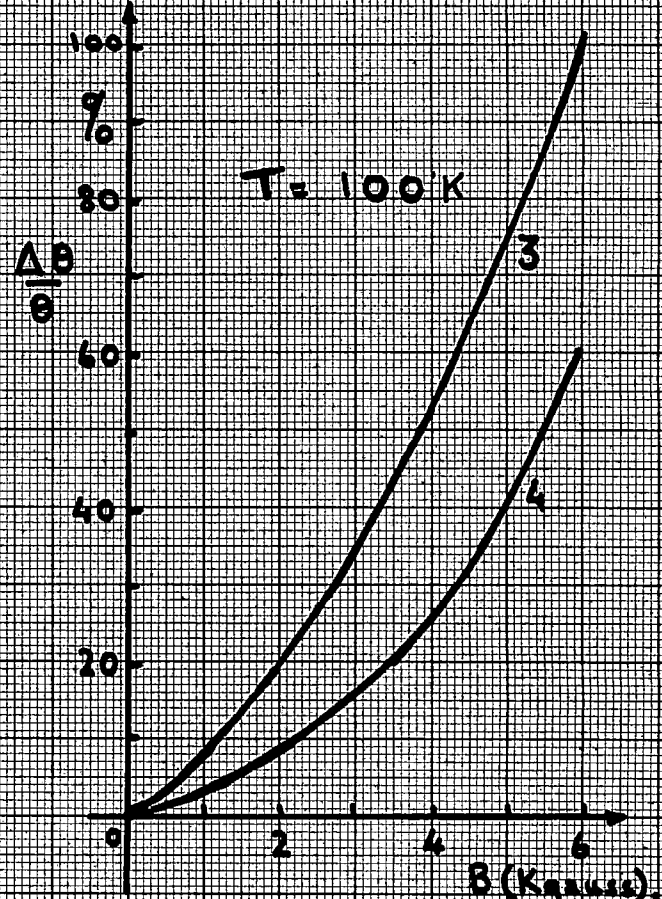


Fig. 38

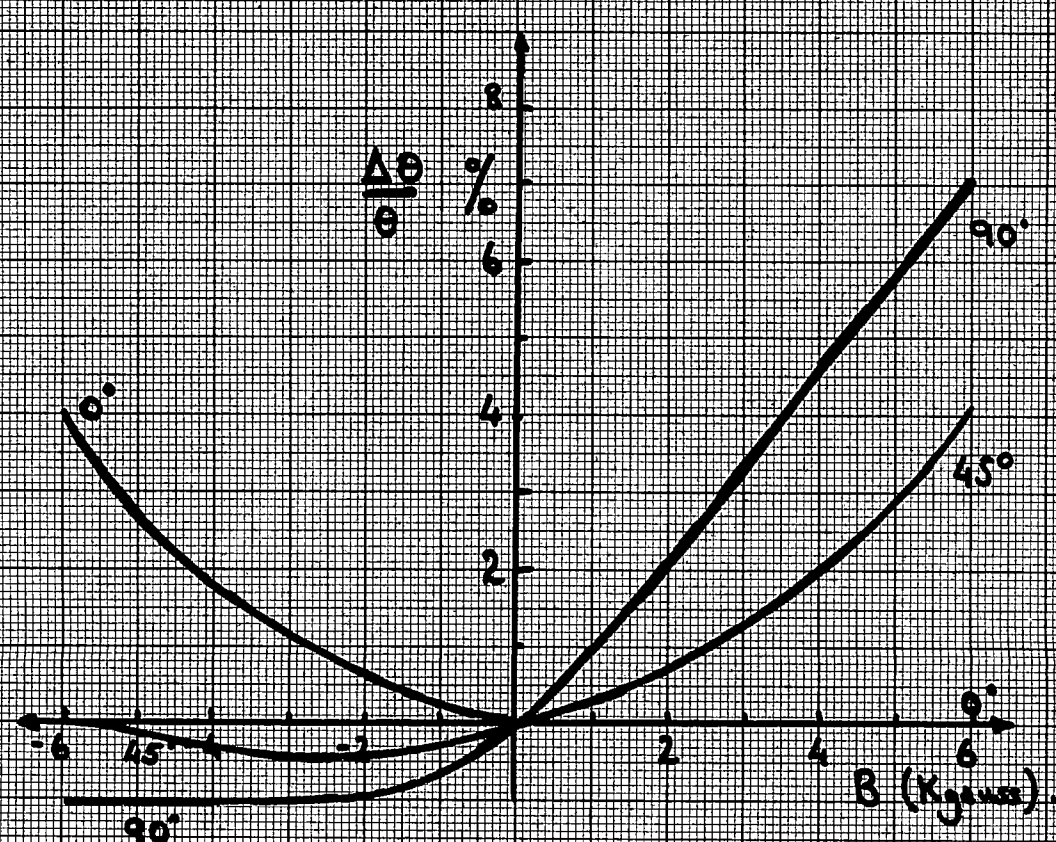


Fig. 39

Magnetoseebeck Measurements

Due to the anomalous behaviour found in the magnetoconductivity measurements of some of the samples of HgTe, it was decided that the variation of the Seebeck coefficient with the magnetic field strength should also be measured on these samples. Puri and Geballe (44) have pointed out that this effect (also known as the longitudinal Nernst coefficient) should be less affected by inhomogeneities in the sample or probe effects than in the case of the magnetoconductivity. If the anomalous behaviour found in certain samples for the magnetoconductivity was reduced or absent when the variation of the magnetoseebeck coefficient with magnetic field was measured, then it could be safely assumed that such behaviour was due to these effects. Theory predicts that the magnetoseebeck effect should vary as the square of the magnetic field strength for low inductions and should saturate for extremely high inductions. This behaviour is similar to that for the magnetoconductivity. The actual analysis is extremely complex, especially for low magnetic field strengths, but it has been carried out by Tsidil'kovskii (46).

Behaviour similar to that predicted by theory was found for certain samples, yet again others were investigated which gave completely anomalous results. It should be noted that samples which exhibited normal magnetoconductivity behaviour did not necessarily exhibit normal magnetoseebeck behaviour. Samples were also measured with anomalous magnetoseebeck effects after having shown normal magnetoconductivity behaviour.

Figs. (37) and (38) show the results of the variation of the magnetoseebeck effect with magnetic field strength for two

samples of HgTe, at both 100°K and 350°K. The variations, for magnetic field strengths less than 6,000 gauss, were found to obey the law

$$\frac{\Delta\theta}{\theta} \sim B^n$$

where n lies between 1.5 and 1.9. The samples measured at the higher temperature have an absolute Seebeck coefficient of about -150 $\mu\text{V}/^\circ\text{K}$ and the material at this temperature is intrinsic, but having a large mobility ratio. At 100°K, however, the value of the Seebeck coefficient is only +20 $\mu\text{V}/^\circ\text{K}$, and the effect of the holes, as they are the majority carrier at this temperature, is more noticeable. The large variation of the Seebeck coefficient with magnetic field strength at this temperature is due to this two carrier conduction process, and is analagous to the variation of the Hall coefficient with magnetic field strength also found when conduction is by two carriers.

Fig. (39) shows the variation in the magnetoseebeck coefficient with magnetic field strength for a typical sample which displays anomalous behaviour. As with such behaviour for the magnetoconductivity, no meaningful pattern can be seen in these results, and as the magnitude of the effect is approximately the same as in the case of the magnetoconductivities, the effect can not be solely due to inhomogeneities, or probe effects. Any variations due to changes in the carrier recombination ratio on the surface of the sample should also be smaller than for the magnetoconductivity. Finally, no one sample could be found which, at a particular temperature, exhibited both an anomalous magnetoseebeck effect

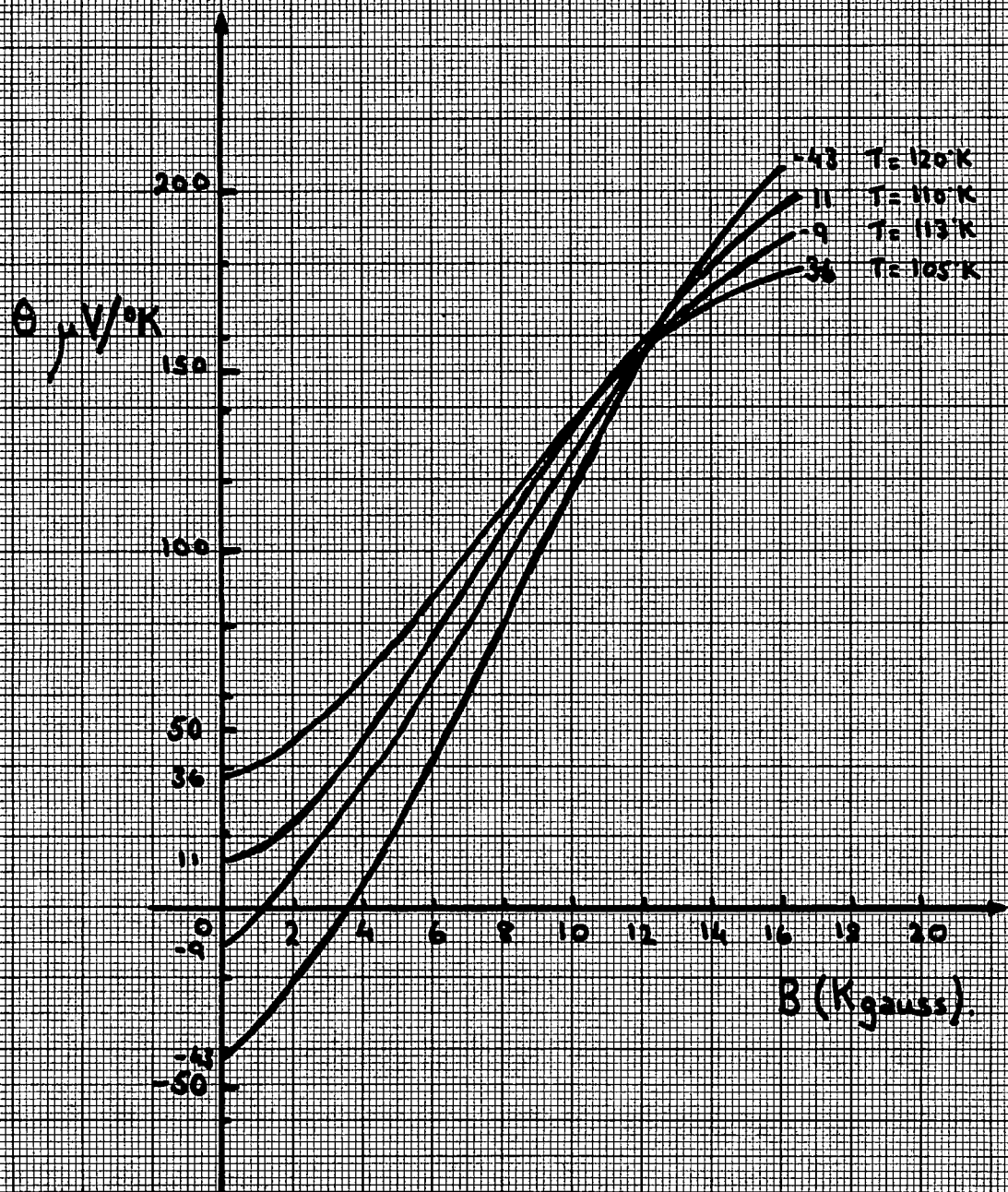


Fig. 40.

Absolute Variation of Seebeck Coefficient with Magnetic Field
for sample 4 (HgTe)

and an anomalous magnetoconductivity, as would be expected if they were caused by inhomogeneities or carrier recombination rates. Some samples were measured which though having a normal magnetoconductivity behaviour, exhibited quite anomalous magnetoseebeck variations with magnetic field.

The variation of the Seebeck coefficient with magnetic field strength at temperatures close to where it was zero was further investigated in the case of sample 4. The variations at four different temperatures corresponding to four different values of the Seebeck coefficient, were measured in magnetic field strengths up to a maximum value of 15,000 gauss. These variations are shown in Fig. (40), which depicts the variation in the absolute values at each temperature, and in Fig. (41), p. 127, which shows the corresponding percentage changes at each temperature. Large percentage changes in the value of the Seebeck coefficient with magnetic field strength were recorded, the largest changes occurring when the zero field Seebeck coefficient was zero. This pattern of behaviour is similar to that found in the variation of the Hall coefficient with magnetic field in the case of mixed conduction, and it is evident that mixed conduction is also the cause of these variations. It can be seen that there is a parabolic variation only for low magnetic field strengths, changing to a linear variation at intermediate field strengths. At very high inductions the effect tends to saturate out at some positive value of Seebeck coefficient. Within the limits of the experiment, this saturation value can be taken to be approximately $+200 \mu\text{V}/^{\circ}\text{K}$. Since the material has

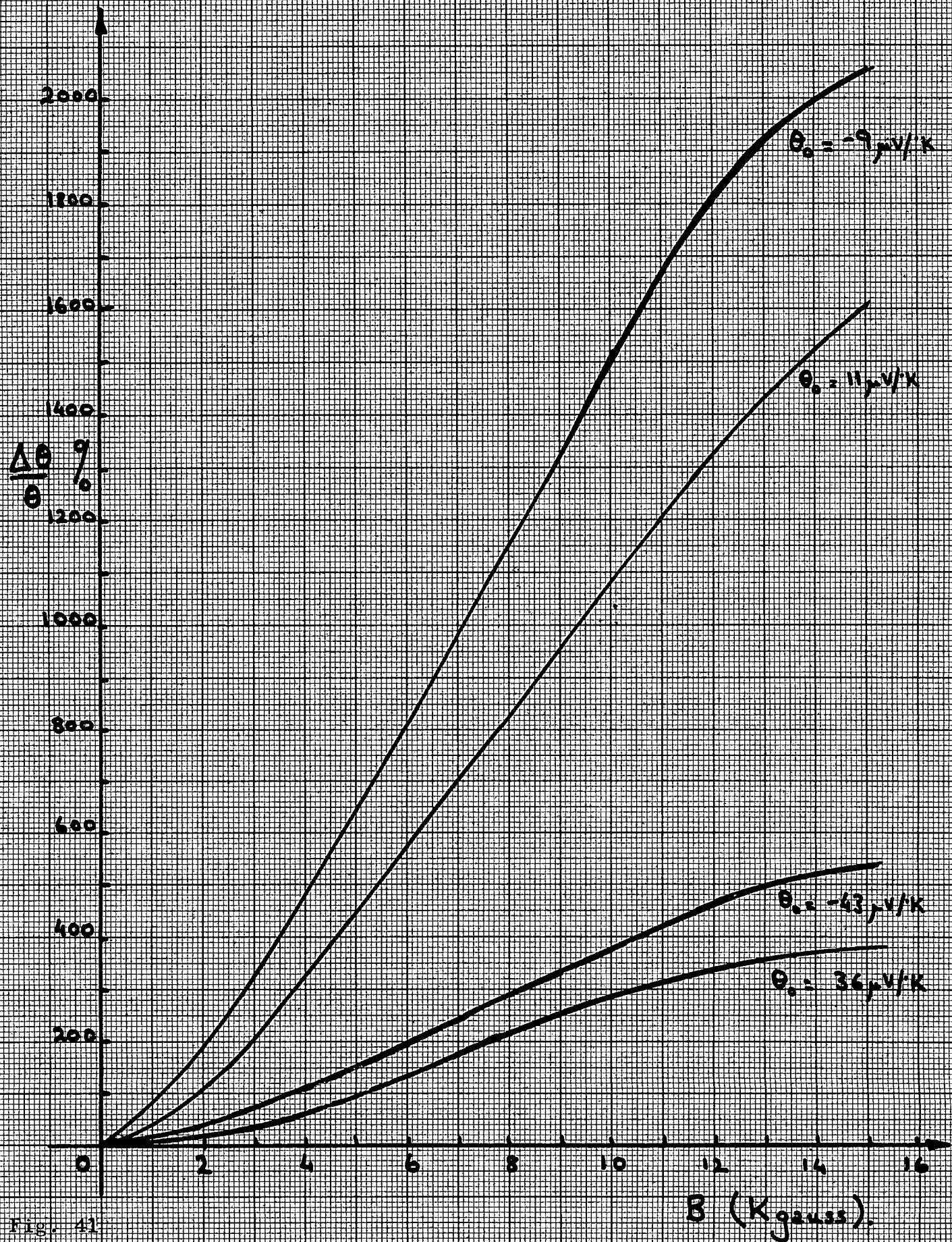


Fig. 41

Percentage Variation of Seebeck Coefficient with Magnetic Field for HgTe

a large mobility ratio at these temperatures, this value can be taken to be the zero magnetic field hole Seebeck coefficient. Assuming a value of 0.02 eV for the energy overlap at these temperatures and using the formulae for mixed conduction, a value of the mobility ratio can be deduced from these data. The most satisfactory fit occurs when the mobility ratio is about 20 which is rather lower than the generally accepted value at these temperatures, but it compares favourably with the value of 10 obtained by Black (72) on single-crystal material.

CHAPTER 5

The Properties of Some Alloys of HgTe and In_2Te_3

Introduction

The chapter is concerned with the work carried out on various alloys of HgTe and In_2Te_3 . The first part of the chapter deals with the measurement of the conductivities, Hall coefficients, Seebeck coefficients, and other related topics.

The results for each alloy composition are given under separate headings together with a short discussion on these results. The second part of the chapter deals with the galvanomagnetic and thermomagnetic measurements made on these alloys, after which the system is treated as a whole, including HgTe, and a discussion is made of the system.

The alloy compositions investigated were 7 molecular % In_2Te_3 in HgTe, 10%, 30%, 37.5%, 40% and 50 molecular % In_2Te_3 in HgTe. Only the 37.5% and 50% compositions were compounds, the 37.5% being a peritectic compound $\text{Hg}_5\text{In}_2\text{Te}_8$. The formula of the 50% composition is $\text{Hg}_3\text{In}_2\text{Te}_6$. The rest, as far as could be ascertained, were single-phase solid solutions. Altogether sixteen samples were investigated and measured, details of which are given in table 7, overleaf.

Sample No.	Alloy Composition	Remarks
5	7%	Good quality.
6	7%	" "
7	7%	" "
8	7%	" " oriented in [001] direction.
9	10%	" "
10	10%	" "
11	10%	" "
12	10%	" "
13	10%	" " oriented in [001] direction.
14	30%	Poor quality, shows some ordering.
15	37.5%	Good quality, shows strong ordering.
16	37.5%	" " " " "
17	37.5%	" " " " "
18	40%	Poor quality, ordering present
19	40%	" " " " }
20	50%	Good quality, shows strong ordering.

Table 7. Details of Alloy Samples Measured.

The preparation and production of these samples has been described in detail in chapter 3. All the samples were single crystal material and in the case of two samples, one of 7% the other of 10% composition, the geometric axis of the sample was oriented in a known crystallographic direction, the [001]. As in the case of HgTe, it was found that samples were extremely brittle and consequently few samples survived a full programme of measurements without small chips flaking from their surface, so deforming them. Some annealing treatment was carried out, mostly on the 10% alloy composition. Annealing in mercury vapour

at a temperature of 250°C even for periods as short as 10 hours caused the material to exhibit high carrier density ($\sim 10^{19}/\text{cm}^3$) presumably due to excess mercury entering the material from the vapour. Annealing in vacuum, at about 250°C, on the other hand, caused several of the samples to decompose. The samples, when examined, were found to be deformed and very porous, disintegrating under finger pressure. Annealing of the alloys in vacuum was discontinued for this reason and work has yet to be carried out on this topic.

The samples, except for the 30% and 40% compositions, appeared to be homogeneous and of good quality, no cracks or pits being noticeable on their surfaces, even under magnifications of 100 x. Homogeneity was checked by measuring the Hall coefficient along the samples, and by visual examination for two phase regions or other inhomogeneities. All samples were found to have good uniformity as judged in this way. X-ray powder photography confirmed this judgement, as extremely well resolved powder photographs were obtained from each sample. An accurate measurement of the lattice parameter of each composition was made from these photographs, the results of which are quoted in the relevant sections. The values compare well with those obtained by Spencer on his samples, which were generally polycrystalline and of poor quality. As noted by previous workers, (133), (134), (135), the 37.5% composition $\text{Hg}_5\text{In}_2\text{Te}_8$, was strongly ordered, as shown by the extra lines present on its powder photograph. Evidence of ordering was also found in the powder photographs of the 50% composition $\text{Hg}_3\text{In}_2\text{Te}_6$, as strong as that in the 37.5% composition. This is

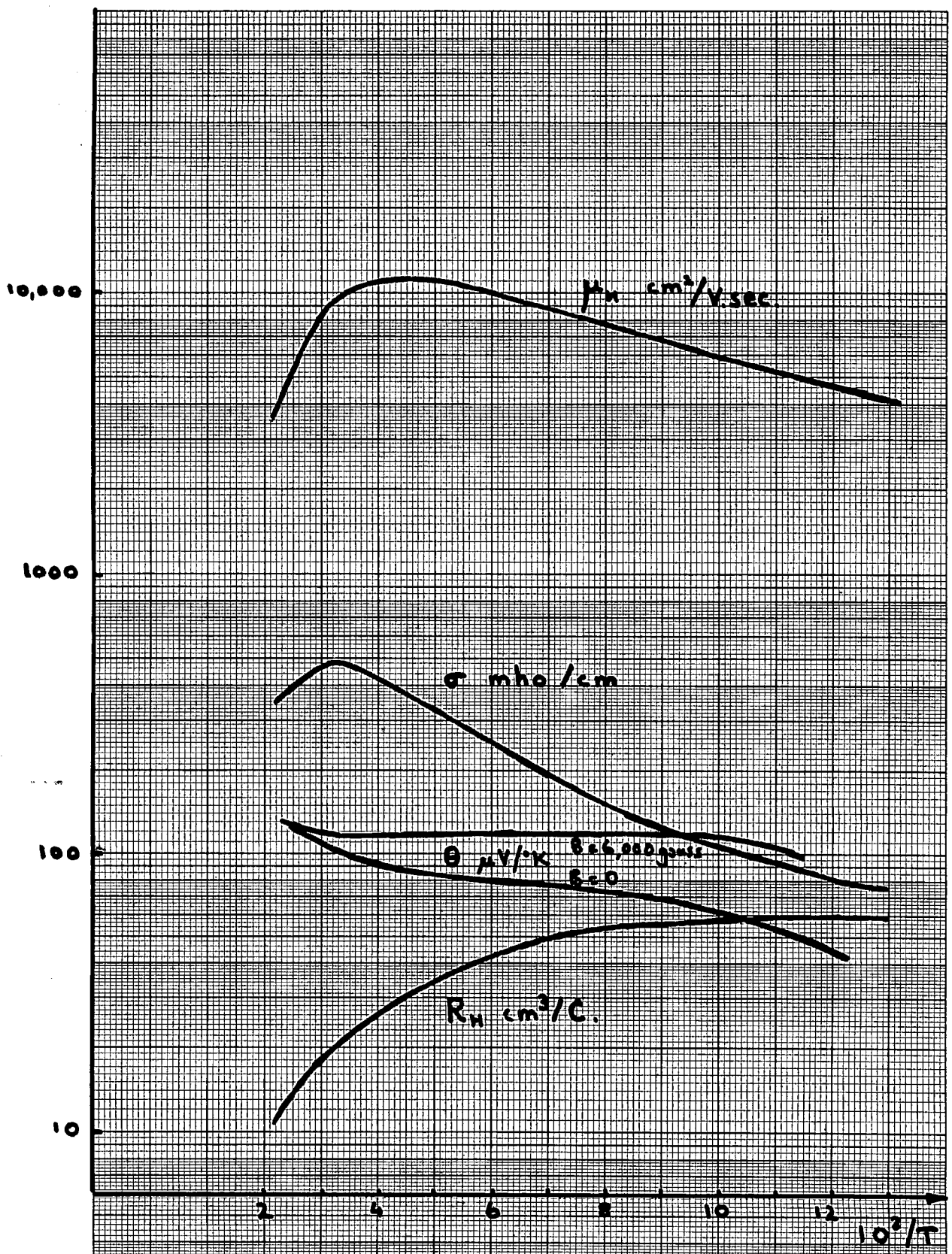


Fig. 42. Electrical results for sample 6 (7% In_2Te_3 in HgTe).

in agreement with Woolley and Ray (133), who first investigated the limits of the solid solubility of the system, and disagrees with Spencer's report that $\text{Hg}_3\text{In}_2\text{Te}_6$ is disordered (146).

The 30% and 40% samples, although single crystals, were not cut from nearly so good material as the other samples. The surfaces of these samples contained numerous cracks and a fine polished surface was unobtainable. The X-ray powder photographs contained diffused lines, even at the low angle side, but it would seem that these are due to the onset of ordering in the system rather than the effect of multiple regions in the material.

Electrical Properties of the Alloys

The Hall coefficient, the electrical conductivity and the Seebeck coefficient, were all measured on the alloy samples in the temperature range $77^\circ\text{K} - 455^\circ\text{K}$, the Hall coefficient being measured at a magnetic field strength of 6000 gauss. To avoid confusion each composition is treated separately in sections, and the properties of each composition are given in tabular form at the end of each section.

7% In_2Te_3 in HgTe

Four samples of this composition were measured, details of which appear in table 7. Except for sample 7 the variations of the Hall coefficient, conductivity, and Seebeck coefficient with temperature are essentially similar for the samples, and the results for sample 6, shown in Fig. (42) are typical of the other samples.

Sample 7 had a carrier density about an order of magnitude larger than in the other samples. Its Hall coefficient was constant

with temperature at $-6 \text{ cm}^3/\text{C}$ and the conductivity σ slowly decreased from 1700 mho/cm at 77°K to 1000 mho/cm at 300°K . The Seebeck coefficient θ , $-15 \mu\text{V}/^\circ\text{K}$ at 77°K increased to a value of $-60 \mu\text{V}/^\circ\text{K}$ at 300°K and was still rising at 455°K , having reached $-100 \mu\text{V}/^\circ\text{K}$.

The results of sample 6, shown in Fig. (42) are typical of the other samples. The conductivity has a low value of about 80 mho/cm at 77°K which increases steadily with rising temperatures to a maximum value of around 500 mho/cm close to room temperatures, after which it decreases, due to a change in the scattering mechanism. The properties of the oriented sample 8 showed similar variations but the values were somewhat higher, the maximum value of being close to 1000 mho/cm, just below room temperature. The variation of the Hall coefficient with temperature is similar for all samples, having its lowest value at 455°K , where the material is becoming intrinsic, and reaching a maximum value at or just above 77°K . The value of 77°K naturally depends on the purity of the sample, but above room temperature the values tend to converge as the intrinsic conduction region ~~was~~^{is} reached. The Seebeck coefficient θ was negative for all the samples in the temperature range investigated, rising from $-50 \mu\text{V}/^\circ\text{K}$ at 77°K to around $-100 \mu\text{V}/^\circ\text{K}$ at 300°K . On two of the samples, 5 and 6, the Seebeck coefficient was measured in a magnetic field strength of 6000 gauss, and increases of 100% at 77°K and 20% at 300°K were recorded. The result obtained for sample 6 is also shown in Fig. (42).

It would seem from these results that the material is n-type extrinsic except at temperatures close to 455°K , where the material is just becoming intrinsic. However, even at these temperatures

the effect of the holes on the properties is only slight, as the mobility ratio in this material must still be quite large. Thus the Hall mobility, $R_H \sigma$, the variation of which with temperature is also shown in Fig. (42) can be taken to be the electron mobility of the material in this temperature range, and from its variation with temperature the nature of the scattering mechanisms in the material can be deduced. The logarithmic plot of $R_H \sigma$ versus T yielded extremely high values of the exponent $|a|$ values of which are given below in table 8. However, from calculations of the effective mass of the carriers $\frac{m_e^*}{m_0}$ it was found that the value varied appreciably with temperature in the case of sample 8, from a $\frac{1}{T}$ variation at low temperatures to a T^2 variation at temperatures between 350°K and 455°K . When allowance is made for these temperature variations of $\frac{m_e^*}{m_0}$ which must be due to a non-parabolic band structure, the temperature variation of mobility is closer to the value predicted by simple theory for ionised impurity scattering, at temperatures below 130°K , and for acoustic mode lattice scattering for temperatures above 350°K . It would seem, then, that these are the dominant scattering mechanisms in this material in the temperature range $77^\circ\text{K} - 455^\circ\text{K}$. The properties of this material are listed, for both 77°K and 300°K , in table 8 below. In table 9, values of the effective mass at 77°K , 300°K and 455°K are given for each sample, together with the power dependence p of the mass on temperature at high and low temperatures. Also given are the values of the power dependence a of the Hall mobility at these temperatures, and in the final column the power dependence a' of the mobility is given when corrected for the variation of the effective mass.

Sample	θ	σ	R_H	$R_{H\sigma}$	n	θ	σ	R_H	$R_{H\sigma}$	n
	$\mu V/^\circ K$	mho/cm	cm^3/C	$cm^2/Vsec$	cm^{-3}	$\mu V/^\circ K$	mho/cm	cm^3/C	$cm^2/Vsec$	cm^{-3}
5	-100	230	37	8500	$2.01 \cdot 10^{17}$	-80	48	-95	4600	$.775 \cdot 10^{17}$
6	-105	465	-21	9750	$3.5 \cdot 10^{17}$	-36	77	-58	4100	$1.27 \cdot 10^{17}$
7	-58	900	-6.8	5220	$1.0 \cdot 10^{17}$	-14	1700	-6.1	10000	$12.1 \cdot 10^{17}$
8	-80	900	-25	22500	$2.95 \cdot 10^{17}$	-40	200	-42	8000	$1.75 \cdot 10^{17}$
300°K										
77°K										

Table 8 Electrical properties of 7% In₂Te₃ in HgTe Alloy at 77°K and 300°K.

Sample	$\frac{m_e^*}{m_0}$	$\frac{m_h^*}{m_0}$										
	455°K	100°K	77°K	77°K	400°K	100°K	400°K	100°K	400°K	100°K	400°K	100°K
5	.037	.018	.025	.025	2.0	-1.0	-3.0	2.3	-1.0	1.3	-1.0	1.3
6	.037	.026	.034*	.034*	1.0	0	-2.8	1.4	-1.8	1.4	-1.8	1.4
7	.040	.029	>.04*	>.04*	1.0	> 0.5	-	-	-	-	-	-
8	.037	.018	.021	.021	2.0	-1.0	-3.8	2.1	-1.8	1.1	-1.8	1.1

Table 9 Effective Masses and Scattering Parameters of 7% Alloy.

* signifies an approximate value.

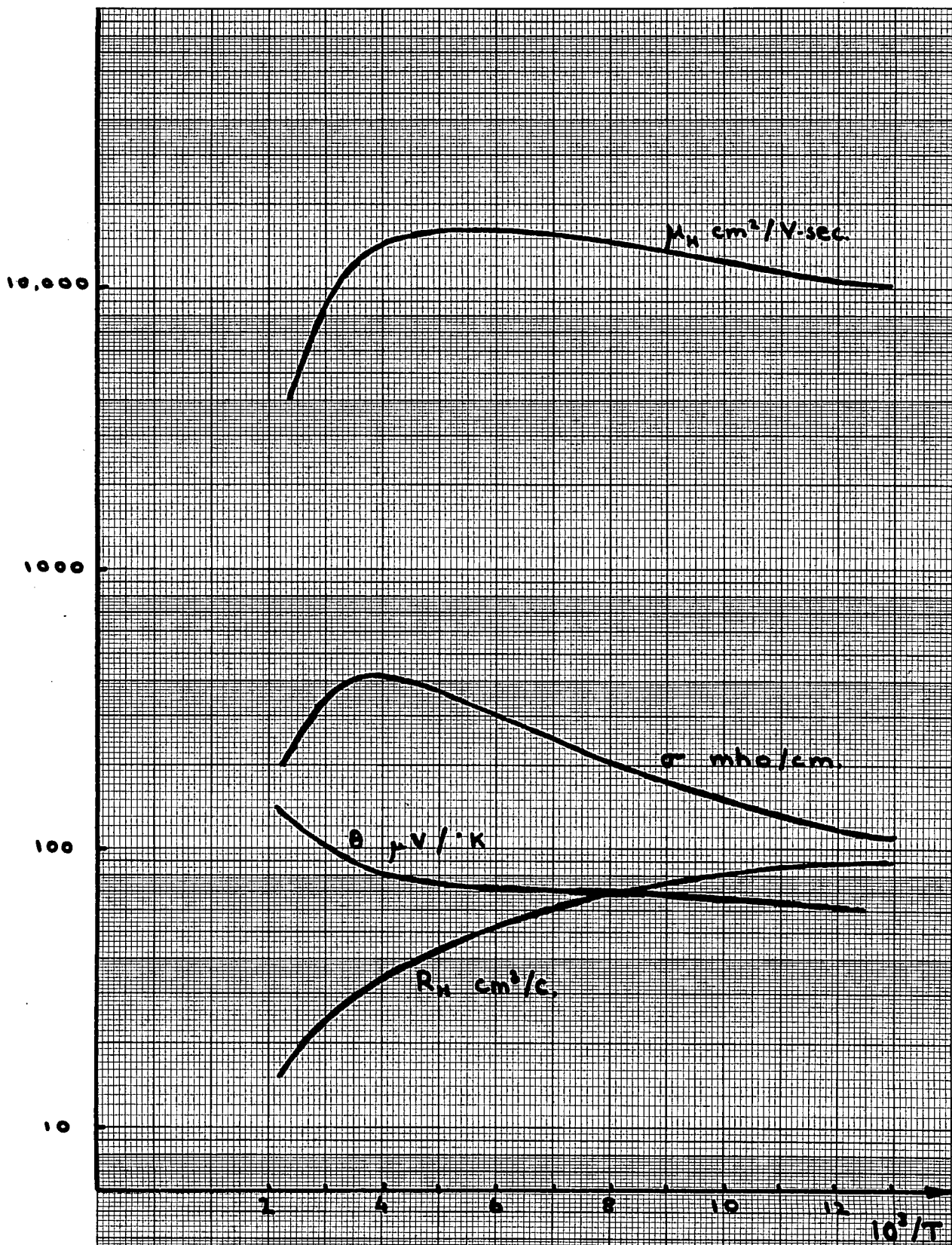


Fig. 43
 Electrical results for sample 13 (10% In₂Fe₃ in HgTe).

10% In₂Te₃ in HgTe.

Five samples of this composition were measured, details of which appear in table 7. As with the 7% composition, all the samples except sample 9 showed similar variations of the measured properties with temperature, and the results for sample 13, shown in Fig. (43) are typical of the other samples. Sample 9, the exception to this pattern of behaviour, showed properties similar to those described for the 7% composition sample 7, in that it had a constant high carrier density, about an order of magnitude greater than the carrier densities in the other samples, of $7.4 \cdot 10^{17} \text{ cm}^{-3}$, and that its conductivity slowly decreased as temperature increased, from 800 mho/cm at 77°K to 150 mho/cm at 455°K . The Seebeck coefficient was not measured in this samples. Some work on annealing these samples has been done, details of which were given in the introduction to this chapter. A summary of these results will be given at the end of this section.

The results for sample 13 are shown in Fig. (43). The variations of the properties with temperature are very similar to those found in the 7% composition. The conductivity σ has a low value of about 110 mho/cm at 77°K which increases with temperature to a maximum value of 400 mho/cm just below room temperature, after which a decrease occurs, associated with a change in scattering mechanism. The Hall coefficient, in general, fell in value as the temperature increased, from a value for sample 13, of $-90 \text{ cm}^3/\text{C}$ at 77°K , to a value of $-16 \text{ cm}^3/\text{C}$ at 455°K . At these higher temperatures the material was beginning to go intrinsic. For some samples a maximum occurred in the Hall coefficient just above 77°K , although this was not very pronounced.

The value of the coefficient at 77°K depended on the purity of the sample measured, but the different values obtained for each sample tended to converge above room temperature as the intrinsic conduction region was approached. The Seebeck coefficient θ was always negative in this region of temperature, rising from -60 $\mu\text{V}/^\circ\text{K}$ at 77°K to about -100 $\mu\text{V}/^\circ\text{K}$ at 300°K.

The results indicate that all the samples are n-type extrinsic, becoming intrinsic at temperatures above 455°K. As for the 7% composition, the effect of the holes on the properties at the higher temperatures can be neglected, as the mobility ratio is quite large. The Hall mobility can be taken to be the electron mobility of the material in this temperature range and deductions about the scattering mechanisms can be made from its variation with temperature, as in the case of the 7% composition. Again this variation with temperature is quite large but it was also found that the electron effective mass also varied appreciably with temperature. When allowance was made for this variation the Hall mobility was found to vary at close to the rate expected from simple theory, assuming acoustic mode lattice scattering at temperatures above 300°K and ionised impurity scattering at temperatures below 130°K. The properties of the material are listed in tables 10 and 11, and they include information on the variation of the electron effective mass and the Hall mobility with temperature. Table 12 gives a summary of the annealing carried out on this composition.

Sample	θ	σ	R_H	$R_H \sigma$	n	θ	σ	R_H	$R_H \sigma$	n
	$\mu V/^\circ K$	mho/cm	cm^3/C	$cm^2/Vsec$	cm^{-3}	$\mu V/^\circ K$	mho/cm	cm^3/C	$cm^2/Vsec$	cm
9	-	350	-10	3500	736.10^{17}	-	800	-10	8000	736.10^{17}
10	-160	560	-16	9500	461.10^{17}	-110	110	-43	4700	171.10^{17}
11	-118	330	-18	6000	409.10^{17}	-80	170	-22	3900	335.10^{17}
12	-125	40	-135	5400	$.55.10^{16}$	-28	30	-235	7000	$3.13.10^{16}$
13	-92	400	-29	12000	$2.54.10^{17}$	-61	110	-90	10000	$8.18.10^{17}$
300°K										
77°K										

Table 10 Electrical Properties of 10% In₂Te₃ in HgTe at 77°K and 300°K.

Sample	$\frac{me}{mo}$	$\frac{me}{mo}$	$\frac{me}{mo}$	$\frac{me}{mo}$	$\frac{me}{mo}$	$\frac{me}{mo}$	$\frac{me}{mo}$	$\frac{me}{mo}$	$\frac{me}{mo}$	$\frac{me}{mo}$	$\frac{me}{mo}$
	455°K	300°K	77°K	P400°K	P100°K	a _{400°K}	a _{100°K}	a _{400°K}	a _{500°K}		
10	-	-	.071	-	0	-2.8	1.0		1.0		
11	.043	.035	.079	.8	-.9	-2.2	1.2	-1.4	.3		
12	.023	.010	.015*	2.0	-.5	-2.2	2.1	-1.2	1.6		
13	.032	.019	.021	1.4	-.15	-3.3	.73	-1.9	.6		

Table 11 Effective Masses and Scattering Parameters of 10% Alloy.

* signifies an approximate value.

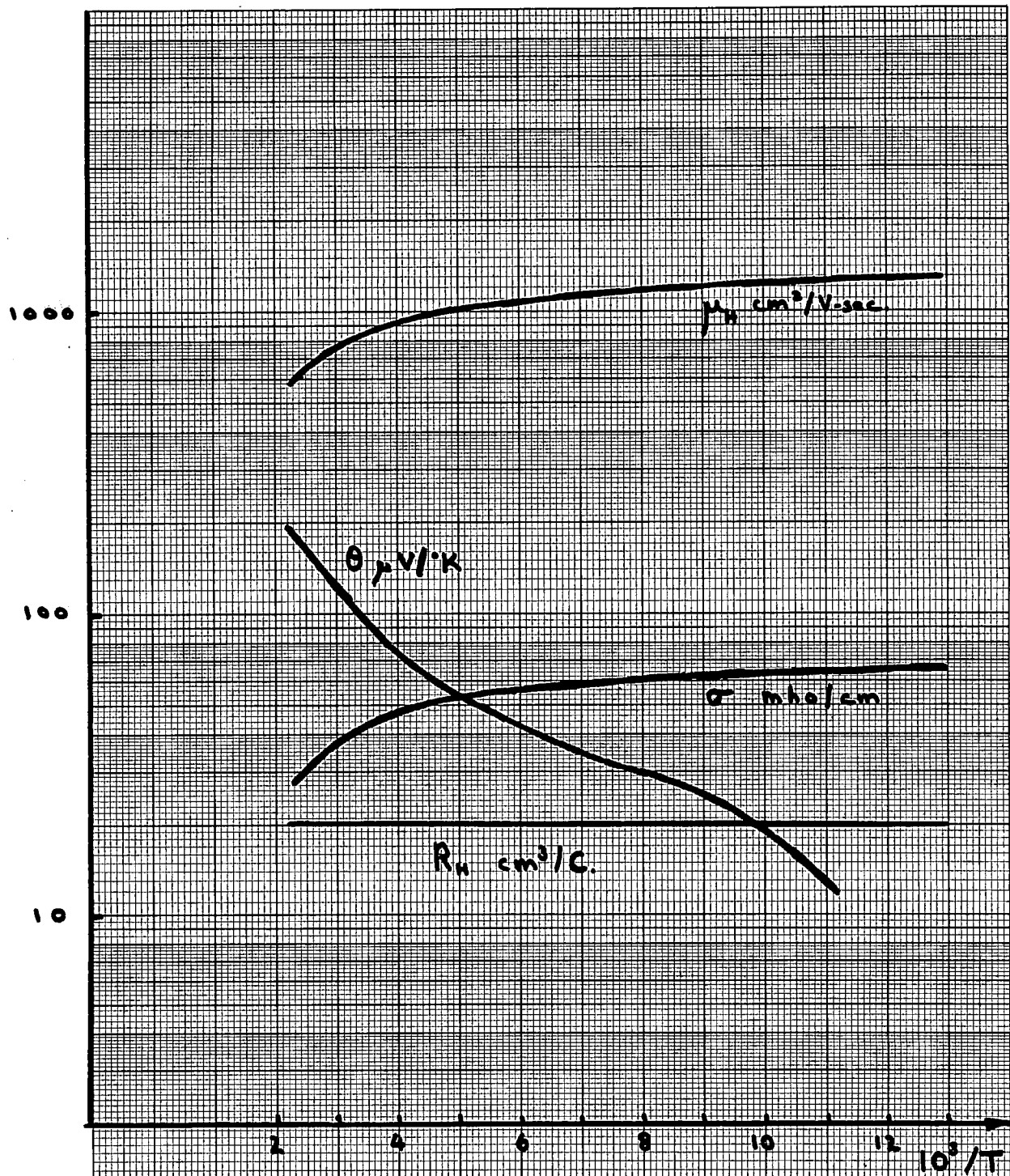


Fig. 44.

Electrical results for sample 14 (30% In_2Te_3 in HgTe).

Sample	Anneal Temp.	Anneal Atmos.	Anneal Period	Remarks
11	250°C	Hg Vapour	< 10 hours	High carrier density; excess Hg.
12	250°C	Vacuum	~ 10 hours	Decomposition of sample.

Table 12 Annealing Procedures on Two Samples of 10% Alloy.

30% and 40% In₂Te₃ in HgTe.

The samples of 30% and 40% alloys were prepared from inferior quality ingots as it was found that, by the usual method, good quality material was impossible to produce at these two compositions. From the X-ray powder photographs, which are somewhat blurred, there is reason to believe that ordering is taking place in the system at these compositions, although this ordering is not nearly as strong as occurs at the 37.5 and 50% compositions.

Only one sample of the 30% composition was prepared, the results of which are shown in Fig. (44). The Hall coefficient is constant with temperature at $-20 \text{ cm}^3/\text{C}$, a carrier density of about $3.68 \cdot 10^{17} \text{ cm}^{-3}$ electrons, a figure similar to that obtained in the lower composition alloys. The material is still extrinsic at the highest temperature reached, 454°K, the Hall coefficient showing no signs of decreasing. The conductivity, however, is much lower than the value obtained in lower compositions, due most probably to the poor quality of the material. The Hall mobility of the sample is thus an order of magnitude less than in these other samples being about $1000 \text{ cm}^2/\text{V-sec}$ at 300°K. At high temperatures it was found to vary as the inverse square of the temperature. The

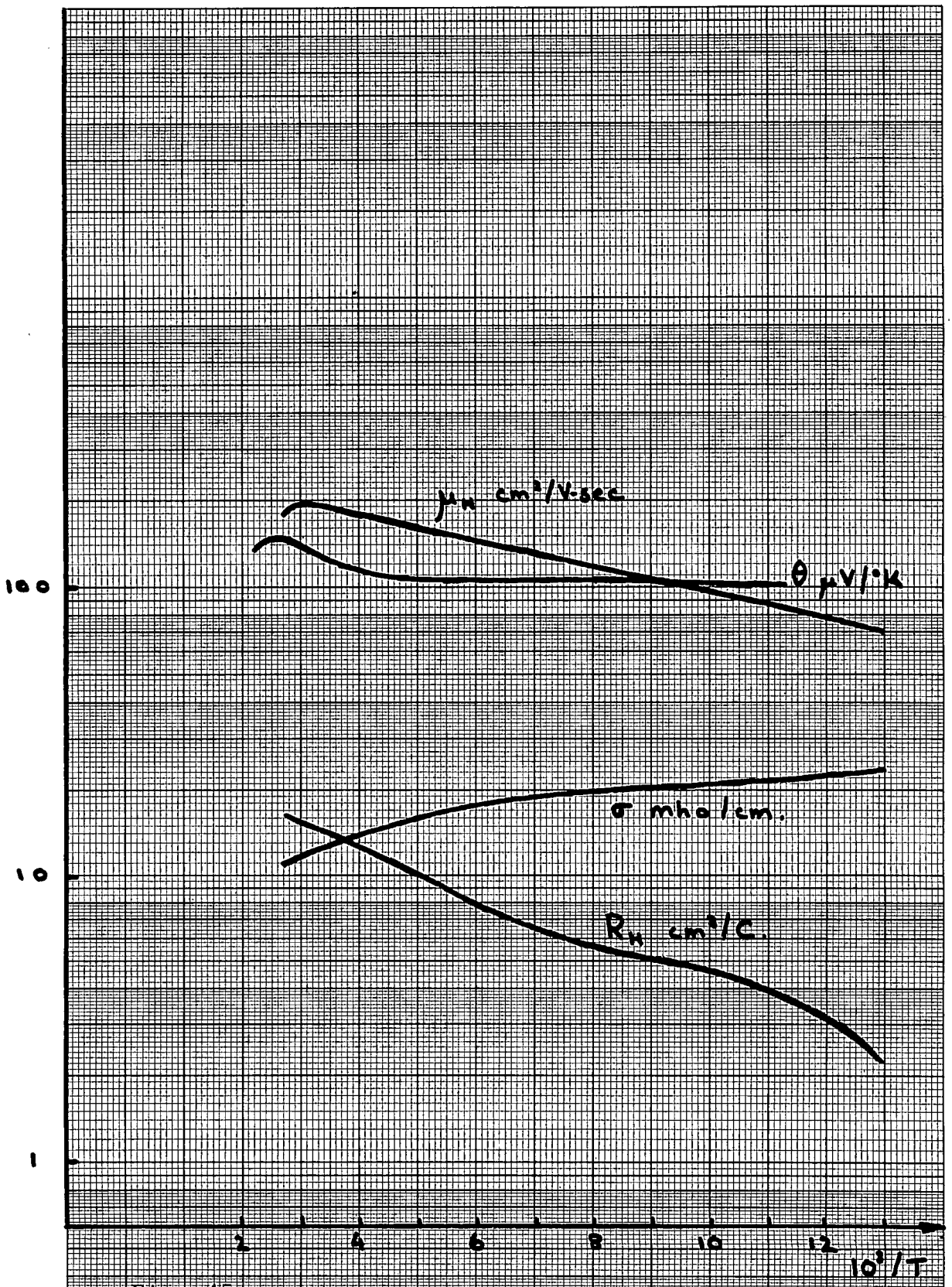


Fig. 45.

Electrical results for sample 19 (40% In_2Te_3 in HgTe).

Seebeck coefficient at 77°K is also somewhat low, being $-10 \mu\text{V}/^\circ\text{K}$, but by 454°K it has reached values comparable to those found in the previous alloys. The value of the electron effective mass is thus of the same magnitude as in the previous compositions being .026 at 300°K. Again this effective mass varied with temperature, and for temperatures greater than 200°K the variation is proportional to the (temperature)^{1.25}.

The properties of this sample are summarised in tables 13 and 14, below, page 140.

Two samples of the 40% composition were prepared, both being p-type extrinsic. The results for sample 19 are shown in Fig. (45). The Hall coefficient reversed sign at 77°K for sample 18, a little below 77°K for sample 19. In both cases the Hall coefficient increases monotonically with temperature, being $-16 \text{ cm}^3/\text{C}$ at 454°K, at which temperature the material is still extrinsic. The conductivity is lower than that found in the 30% composition, its maximum value being 20 mho/cm. Hence the Hall mobility, the maximum value of which was $200 \text{ cm}^2/\text{V-sec}$, was also lower than in the 30% composition. As the material is p-type, the Hall mobility can not be taken to be the majority carrier mobility, for in the temperature range measured the material is affected by both carriers. The Seebeck coefficient is constant in value from about 100°K to 300°K at a value of $-100 \mu\text{V}/^\circ\text{K}$, rising to a slight maximum above 300°K. No information can be elicited about the scattering mechanisms involved in this composition, or about the effective mass of the carriers, as the material was in the mixed conduction region at the temperatures investigated. The properties of the material are given in tables 13 and 14, overleaf.

Sample and Composition	θ	σ	R_H	$R_H \sigma$	n	θ	σ	R_H	$R_H \sigma$	n
	$\mu V/^\circ K$	mho/cm	cm^3/C	$cm^2/Vsec$	cm^{-3}	$\mu V/^\circ K$	mho/cm	cm^3/C	$cm^2/Vsec$	cm^{-3}
14(30%)	-97	43	-20	860	$3.68 \cdot 10^{17}$	-13	65	-20	1300	$3.68 \cdot 10^{17}$
18(40%)	-165	8.5	-13.5	115	$5.46 \cdot 10^{17}$	-	15	~ 0	-	-
19(40%)	-128	± 12.8	-14.5	190	$5.07 \cdot 10^{17}$	-	23	~ 2	~ 50	-
			$300^\circ K$							$77^\circ K$

Table 13 Electrical Properties of 30% and 40% In_2Te_3 in HgTe at $77^\circ K$ and $300^\circ K$

Sample and Composition	$\frac{m_e^*}{m_0}$	$\frac{m_e^*}{m_0}$	$\frac{m_e^*}{m_0}$	$\frac{m_e^*}{m_0}$	$p_{400^\circ K}^*$	$p_{100^\circ K}^*$	$a_{400^\circ K}$	$a_{100^\circ K}$	$a_{400^\circ K}^*$	$a_{100^\circ K}^*$
	455 $^\circ K$	300 $^\circ K$	77 $^\circ K$	77 $^\circ K$	400 $^\circ K$	100 $^\circ K$	400 $^\circ K$	100 $^\circ K$	400 $^\circ K$	100 $^\circ K$
14(30%)	.043	.026	-	-	1.25	-	~ 2.0	-	$\sim .75$	-
18(40%)	-	.067	-	-	-	-	-	-	-	-
19(40%)	-	.045	-	-	-	-	-	-	-	-

Table 14 Effective Masses and Scattering Parameters of 30% and 40% Alloy.

* signifies approximate value.

Due to mixed conduction few parameters could be evaluated.

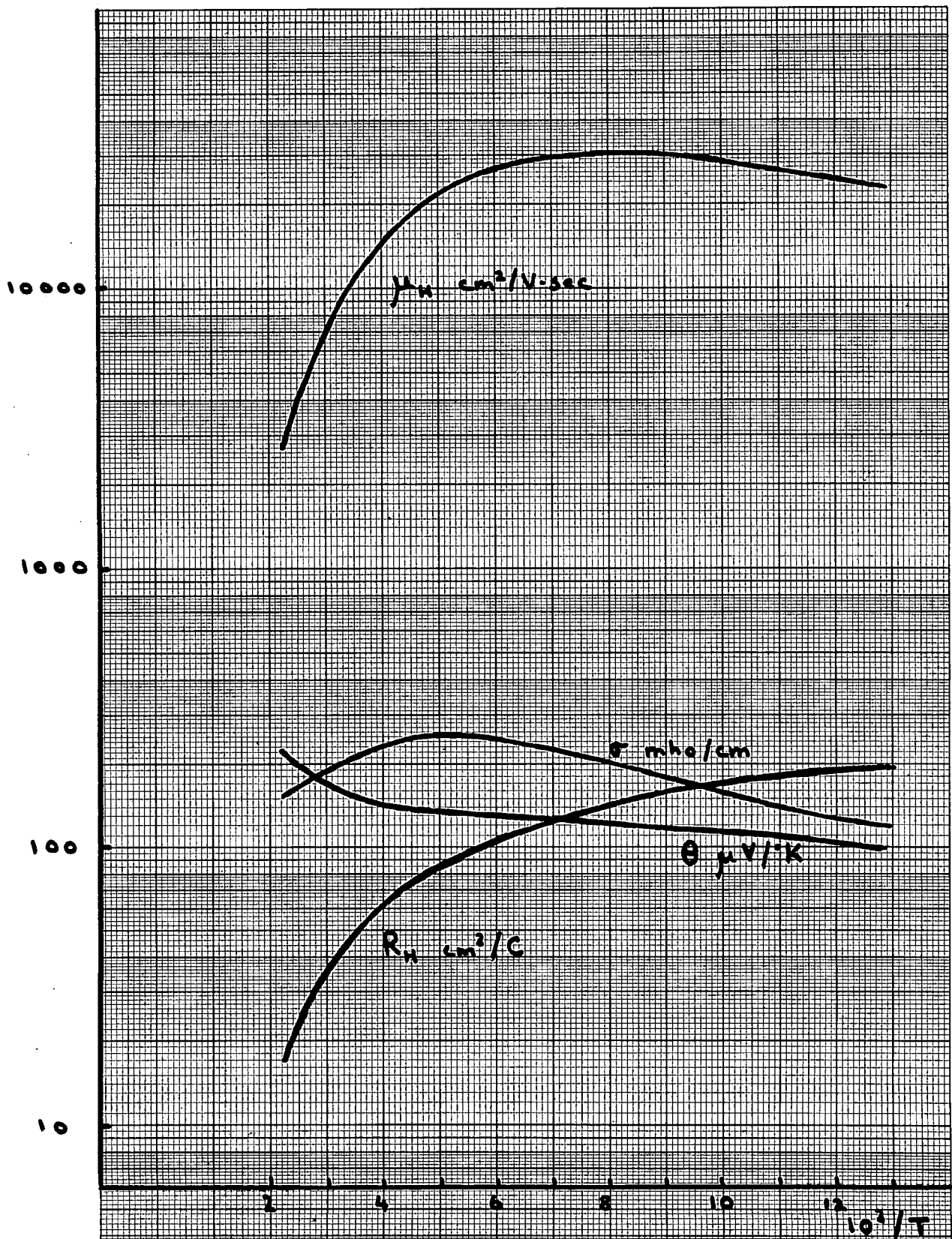


Fig. 46.

Electrical results for sample 17 (37.5% In_2Te_3 in HgTe).

37.5% In₂Te₃ in HgTe

Three samples of this composition were measured details of which appear in table 7. This composition is the peritectic compound, of Hg₅In₂Te₈, and good quality single crystal ingots were invariably obtained. From the evidence of X-ray powder photographs of the samples, the composition is always strongly ordered when prepared in the manner previously described, a slow cooling from the melt.

The variations of the electrical properties with temperature are similar for all three samples, and closely resemble the results obtained for the low indium content alloys, the 7% and 10% In₂Te₃ in HgTe compositions.

Typical variations of the electrical properties with temperature are shown in Fig. (46), which is the results for sample 17. The conductivity σ , 120 mho/cm at 77°K, reaches a broad maximum just below room temperature, and then slowly begins to fall in value as high temperatures are reached. The Hall constant R_H , drops in value, from -200 cm³/C at 77°K to below -20 cm³/C at 455°K, at which temperature intrinsic conduction is just beginning. The low temperature value of R_H depends on the impurity concentration in the original ingot, and so varies from sample to sample, whereas at 455°K the values for each sample tend to be much closer. The Seebeck coefficient, -100μV/°K at 77°K slowly reaches -150 μV/°K at room temperature, then rises more sharply at the higher temperatures. It can be seen from these properties that the material is n-type extrinsic in the measured temperature range and the Hall mobility $R_H \sigma$ which is extremely

Sample	θ $\mu\text{V}/^\circ\text{K}$	σ mho/cm	R_H cm^3/C	$R_H\sigma$ cm^2/Vsec	n cm^{-3}	θ $\mu\text{V}/^\circ\text{K}$	σ mho/cm	R_H cm^3/C	$R_H\sigma$ cm^2/Vsec	n cm^{-3}
15	-92	400	-31	12000	$238 \cdot 10^{17}$	-30	320	-40	13000	$1.84 \cdot 10^{17}$
16	-	240	-44	11000	$1.67 \cdot 10^{17}$	-	50	-115	5500	$6 \cdot 4 \cdot 10^{16}$
17	-150	210	-48	10000	$1.53 \cdot 10^{17}$	-100	120	-195	23000	$3.78 \cdot 10^{16}$
										77°K
										300°K

Table 15 Electrical Properties of 37.5% In_2Te_3 in HgTe at 77°K and 300°K

Sample	$\frac{m_e}{m_0}$ 455°K	$\frac{m_e}{m_0}$ 300°K	$\frac{m_e}{m_0}$ 77°K	p 400°K *	p 100°K *	a 400°K	a 100°K	a' 400°K *	a' 100°K *
15	.055	.018	.02*	2.5	0	-3.5	1.5	-1.0	1.5
17	.060	.025	.02	2.5	0	-3.4	1.1	-.9	1.1

Table 16 Effective Masses and Scattering Parameters of 37.5% Alloy.

* signifies approximate value.

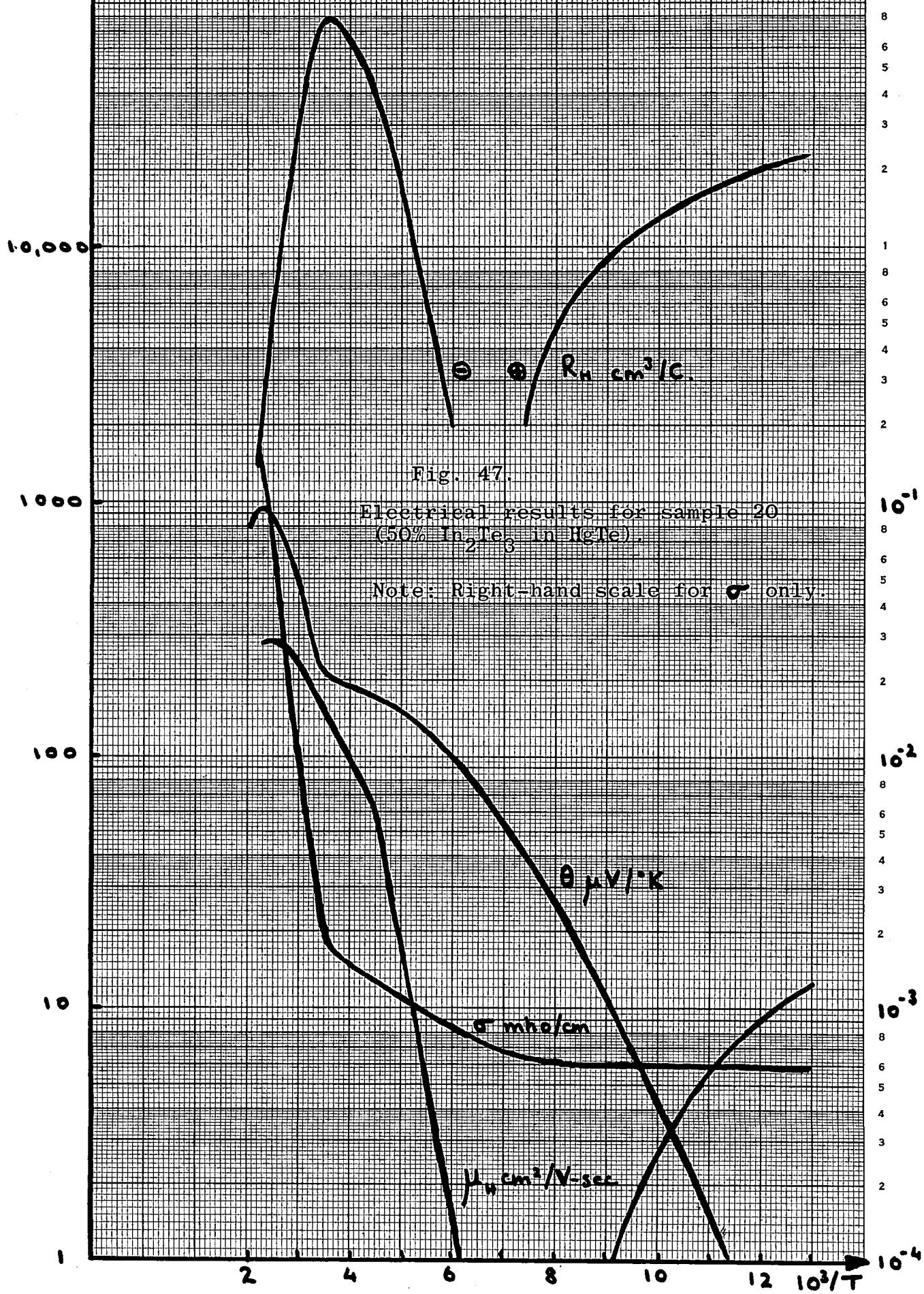
large, is essentially the electron mobility. The maximum mobility recorded was over 30,000 cm²/V-sec in sample 17, at 125°K. As with previous compositions, this mobility varied quite steeply with temperature, being almost entirely due to the effective mass of the carriers varying with the temperature. When allowance is made for the effective mass, the variation of the mobility is not so great with temperature, indicating that acoustic mode lattice scattering predominates at the higher temperatures. The properties of the material are summarised in tables 15 and 16 on facing page.

50% In₂Te₃ in HgTe

Only one sample was measured of this composition, due to the difficulties presented in measuring a high resistivity material. The composition is a true compound, being Hg₃In₂Te₆, and good ingots were obtained. The material was always found to be strongly ordered as prepared, similarly to the 37.5% composition.

The results for the sample, number 20, are shown in Fig.(47)p.143. The material is p-type extrinsic, and from the variation of the Hall coefficient, the mobility ratio b is found to be 14.5.

The conductivity σ which is constant at low temperatures at a value of 6.10^{-4} mho/cm, rises gradually to $1.7.10^{-3}$ mho/cm at 278°K. At that temperature it increases steeply by two orders of magnitude, reaching 2.10^{-1} mho/cm at 454°K. A marked increase in the Seebeck coefficient is also obtained at 278°K and both effects are thought to be due to a second heavy mass band being activated at this temperature. The large increase is the density of states available for conduction processes at temperatures above 278°K is reflected in the Hall coefficient measurement, R_H



falling sharply above this temperature, as the carrier density rises. The material can be considered as single carrier above 250°K, with electrons as the dominant carrier, due to the large mobility ratio of the material. The effective mass of the electrons as calculated from non-degenerate statistics, shows a marked dependence on temperature, being only 0.003 m_0 at 250°K, rising sharply to 0.5 m_0 at 400°K. These values are only approximate, as the effects of the holes on these properties have been neglected in obtaining them. From Fig. (47) this is not strictly justified, as both R_H and μ_H are varying considerably at these temperatures, due to the holes. Bearing this in mind, the rather low value of 0.0003 m_0 for the electron effective mass at 250°K could well be considerably underestimated. However, as further information is lacking, this value will be quoted as the effective mass of the electrons at that temperature. The value of 0.003 m_0 for m_e^* at 250°K is that near the bottom of the light mass band, equivalent to a carrier density of 10^{14} electrons -cm^{-3} . This band must be similar to that in HgTe. The value of 0.5 m_0 for the electron effective mass at 400°K is that for the heavy mass band, which is activated at temperatures above 280°K, and corresponds to a carrier density of $2 \cdot 10^{15}$ electrons -cm^{-3} . The Hall mobility, $R_H \sigma$, also shown in Fig. (47) agrees with this band model. At temperatures just above the Hall coefficient zero the mobility is rising at such a rate that by room temperature it would be of the order of 10,000 $\text{cm}^2/\text{V-sec}$, the mobility associated with HgTe and the lower indium percentage alloys. However, at a temperature

just below 250°K the rate of increase of mobility with temperature alters noticeably, and the final maximum mobility obtained is only 300 cm²/V-sec, much lower than that observed in good quality HgTe. The reduction in mobility must be due to the activation of the heavy mass band at about 250°K.

The properties of this sample are summarised in table 17, facing page. The values of the effective mass of the electrons are only given for temperatures above room temperature, values being unobtainable at low temperatures due to the effect of the two carriers. These are given in table 18, facing page.

Magnetoconductivity and Magnetoseebeck Measurements

Due to the anomalous magnetoconductivity and magnetoseebeck behaviour of many of the samples of HgTe, similar measurements were carried out on some of the alloy compositions. The samples investigated were numbers 7 and 8 (7% comp.) 12, and 13 (10% comp.), and 15 and 17 (37.5% comp.). Samples 8 and 13 were oriented in a known crystallographic direction and longitudinal as well as transverse magnetoconductivity measurements were made on them.

Before measurements were carried out on these samples all the precautions mentioned in the relevant sections dealing with these topics in the chapter on HgTe (page 120 and page 124) were taken. In each case the carrier density, as indicated by Hall effect measurements, was uniform along the length of the sample. This would eliminate the spurious effects due to nonuniform

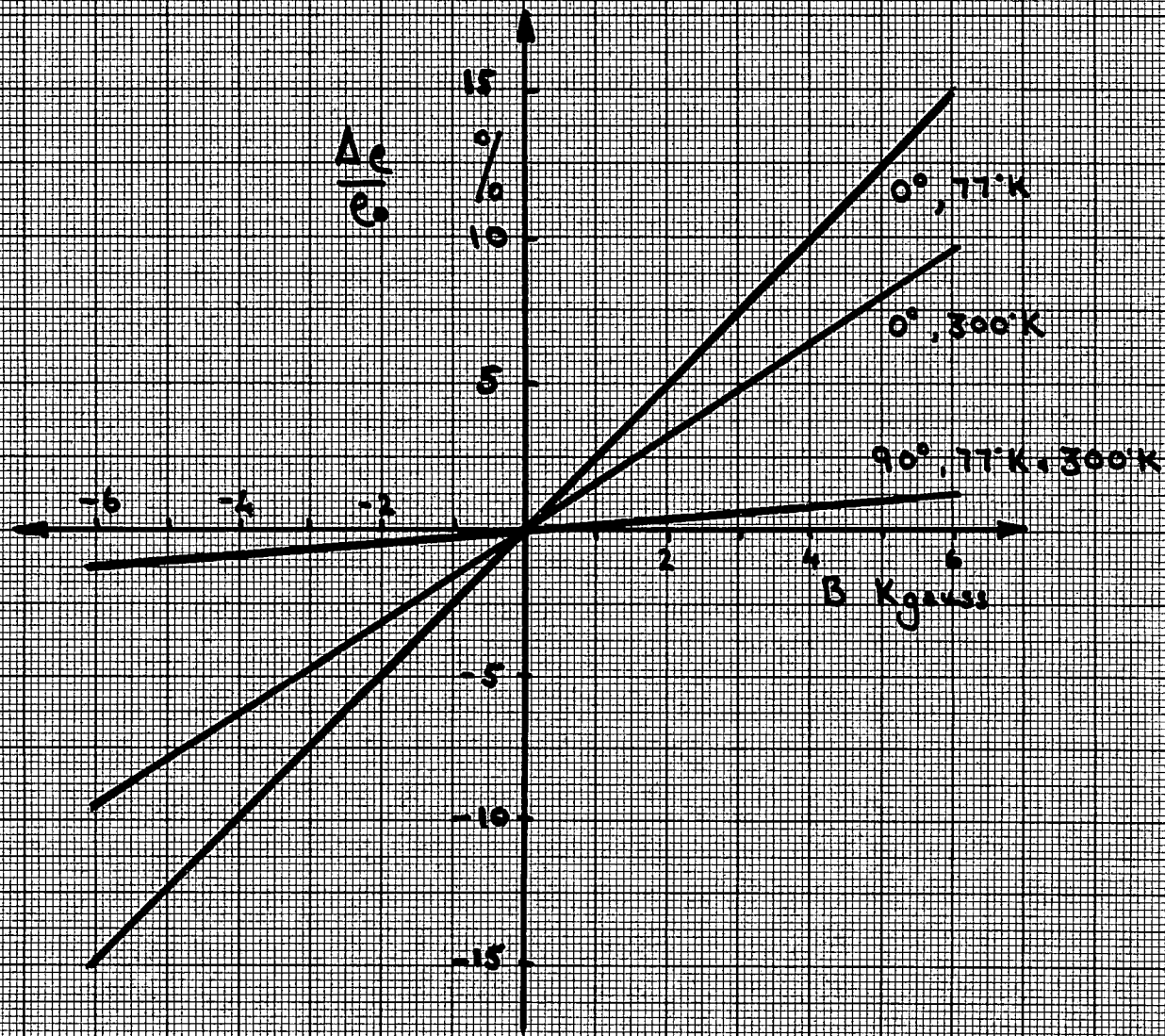


Fig. 48.

Anomalous Magnetoconductivity Variation with Magnetic Field for Sample 7 (7% In_2Te_3 in HgTe).

densities on the magnetoconductivity, as reported by Beer (48).

Anomalous behaviour, similar to that found in HgTe, was found in all the samples measured, except for the magnetoconductivity of sample 12 (10% comp.) and the magnetosebeck coefficient of samples 15 and 17 (37.5% comp.). However, anomalous behaviour existed for the magnetosebeck coefficient in sample 12 and in the magnetoconductivity in samples 15 and 17. For sample 12, the magnetoconductivity at 77°K varied parabolically for low magnetic field strengths and tended to saturate at the higher fields. At the maximum fields used, it was still rising quite rapidly, having reached a value of 40%. For samples 15 and 17 the magnetosebeck coefficient varied parabolically over the whole range of magnetic field strength, reaching a value of 6% at 6,000 gauss.

All the rest of the samples behaved anomalously, exhibiting negative coefficients for certain magnetic field strength directions, which on reversal of the magnetic field became positive. Such typical behaviours of the magnetoconductivity and the magnetosebeck coefficient are shown in Figs. (48) and (49), being the results for sample 7 (7% comp.). It will be seen that the magnetoconductivity is linear with magnetic field strength, from -6,000 gauss to +6,000 gauss, changing from a value of -15% to +15% in that interval, at a temperature of 77°K. These values were reduced slightly to -10% to +10% when the temperature was raised to 300°K, but at that temperature the mobility of the material is less than at 77°K. For the 37.5% samples even larger variations were recorded, from -21% at -6000 gauss to +21% at +6,000 gauss, the mobility of this material being higher than

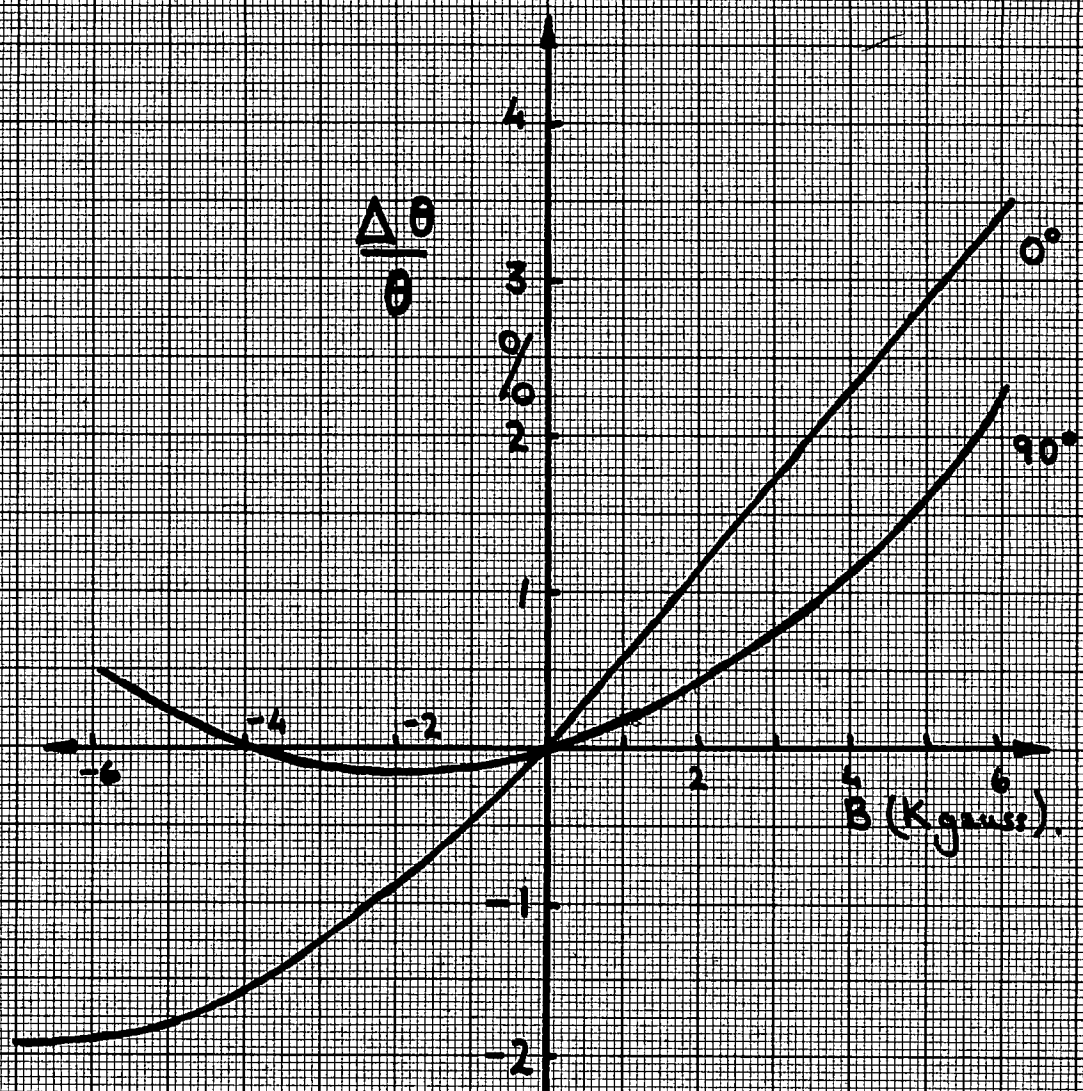


Fig. 49.

Anomalous Magnetoseebeck Variation with Magnetic Field for
 Sample 7 (7% In_2Te_3 in HgTe).

that of the 7% sample. The magnetoseebeck coefficient also tended to vary linearly with magnetic field strength, but only over a smaller range, from -2,500 to +2,500 gauss. For the negative magnetic field strength the coefficient tended to saturate out at -2%, but for the opposite direction the coefficient began to increase at a rate greater than unity for the larger magnetic field strengths.

The longitudinal magnetoconductivity was measured on samples 8 and 13, which had been cut so that their geometrical axis was parallel to the $[001]$ direction. Although for oriented HgTe the longitudinal magnetoconductivity was zero, for these alloys (7% and 10% comp.) non-zero coefficients were measured. The values obtained were much smaller than the corresponding transverse coefficients, being of the order of 3% to 5% at 6,000 gauss. Moreover, in both cases, reversal of the magnetic field caused the coefficient to become negative, as in the transverse case.

No satisfactory explanation for these results can be put forward as yet, but in view of the precautions taken and the reproducibility of the results, it would seem that the phenomena are genuine properties of these materials. A tentative explanation based on a two energy state model of impurity conduction has been offered by Tryozawa (157), but further work must be done before the validity of this model can be checked.

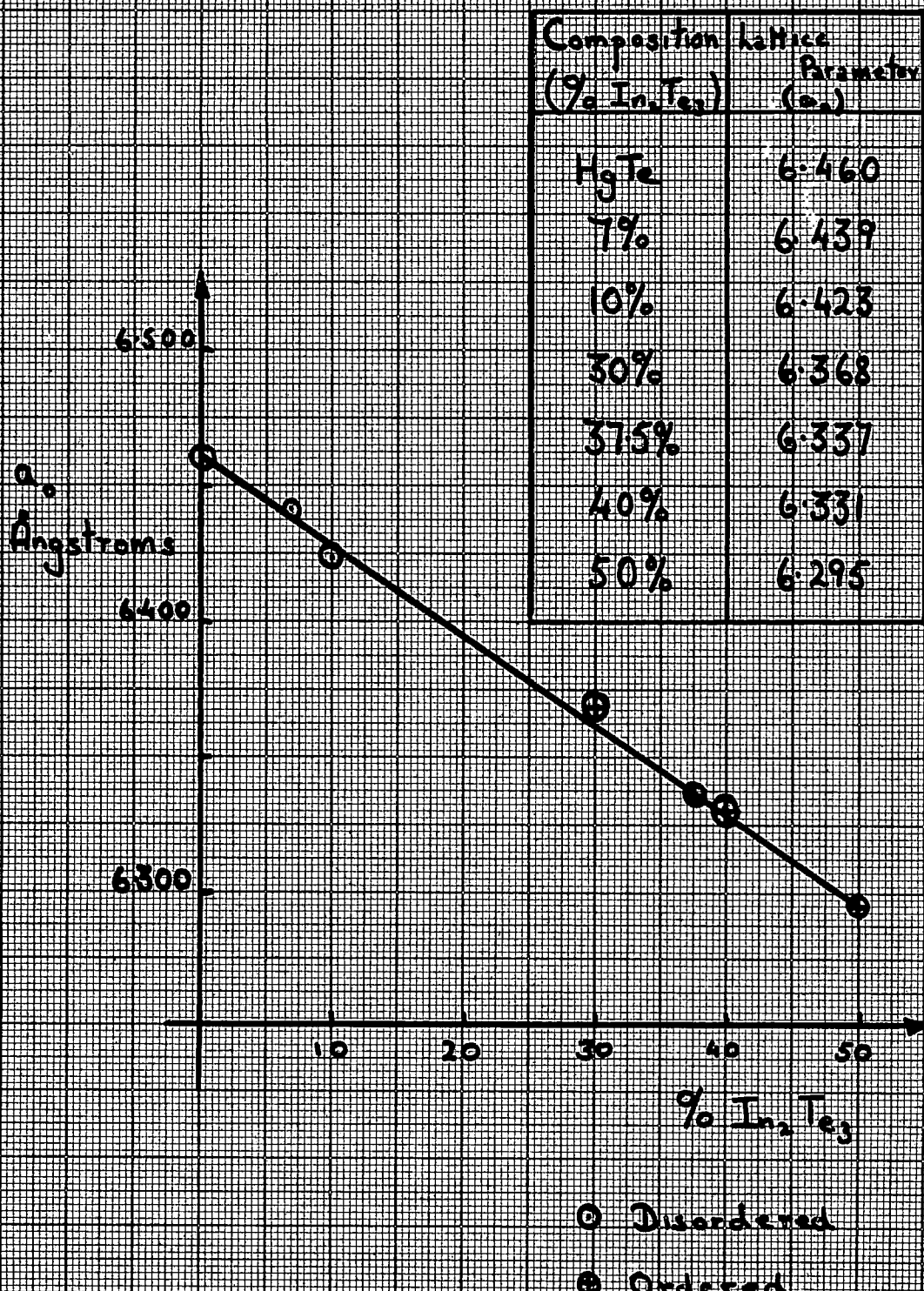


Fig. 50

Variation of Lattice Parameter with Composition for
 HgTe - In₂Te₃ Alloy System.

The Alloy System HgTe - In₂Te₃

The lattice parameter and limits of solid solubility of this system were first described by Woolley and Ray (133), who found that a central miscibility gap extends from about 50% to 60% compositions. On either side of this two phase region, there exist regions in which an ordered structure, a superlattice, is superimposed on the zincblende phase. The first region is centred around the peritectic compound Hg₅In₂Te₈ and extends from about 30% to 50% compositions. The other region is centred around the peritectic compound HgIn₂Te₄ and has been investigated by Hahn (158). In the present study of the system only compositions up to the miscibility gap were prepared, from HgTe to Hg₃In₂Te₆.

The lattice parameter, a_0 of each composition was obtained from X-ray powder photographs by the standard procedure. Except for the 30% and 40% compositions, the parameter could be measured to a high degree of accuracy. These parameters are shown in Fig. (50), plotted against composition. The results are in agreement with previously published results, the plot being linear with composition as far as the 50% composition Hg₃In₂Te₆, when the two phase central miscibility gap intervenes.

The properties of the various compositions of the system have been given in the appropriate sections. It would seem, on the evidence of the electron effective mass and the electron mobility, that the HgTe band structure extends, with slight modifications, at least as far as Hg₅In₂Te₈, the 37.5% composition. The main feature of this band structure is a non-parabolic, light electron effective mass conduction band. As the band is non-

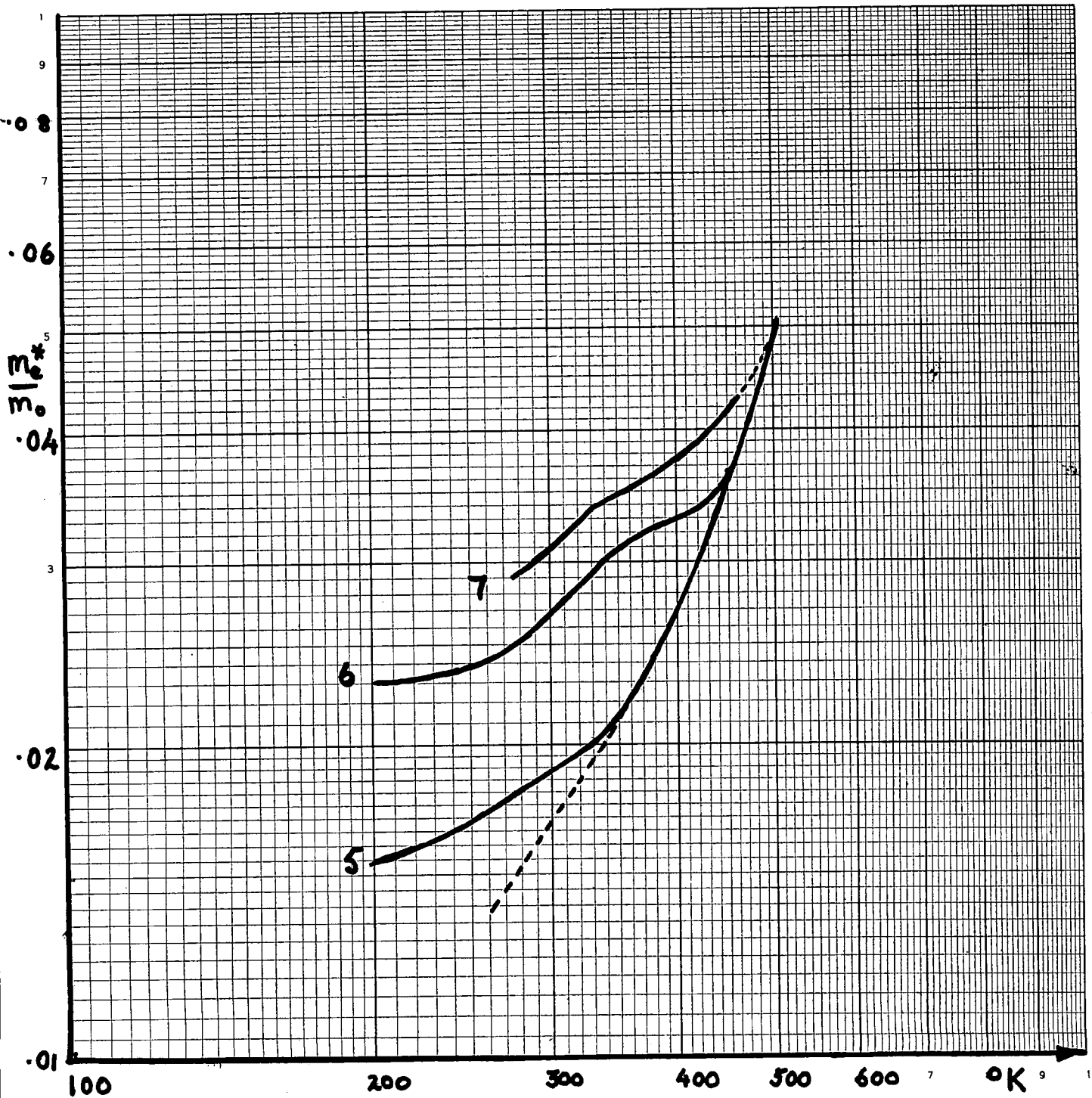


Fig. 51

Variation of the Effective Mass with Temperature for 7% In_2Te_3 in $HgTe$

parabolic, the value of the effective mass will vary according to the level of occupancy of the band, the lowest value of the effective mass occurring at the bottom of the band. On this model the effective mass of the carriers should increase as temperature increases, due to the conduction band being progressively filled.

This phenomena is to be seen in the variation of the effective mass of the electrons with temperature for all the alloy compositions up to 37.5%, $\text{Hg}_5\text{In}_2\text{Te}_8$. A typical variation is shown in fig.(51) for samples 5, 6 and 7, the 7% compositions. Only values of the effective mass above 200°K are plotted, the temperature range in which acoustic mode lattice scattering is the dominant mechanism. For lower temperatures, below 150°K , ionised impurity scattering predominates and the form of equations (104), (105), and (106), used in evaluating the effective mass, must be changed. Even so, the pattern of behaviour at these lower temperatures is not so coherent which could possibly be due to two-carrier effects becoming important, and accordingly were not plotted. It is seen that for an n-type extrinsic composition a family of curves exists, and this family of curves, depending on the temperature, at which each curve becomes intrinsic, run together, the effective mass increasing rapidly with temperature due to the non-parabolic conduction band. As plotted on log-log scales, the intrinsic curve has a curvature. This is most probably due to the error introduced in the value of the effective mass by assuming a single dominant scattering law. This error will be greatest at the lower temperatures. All these

features are to be seen clearly in Fig. (51) in which three of the family of curves appear.

The 50% composition is more complicated than the others in so far as a second heavy mass band is activated, before the material becomes intrinsic. This causes the effective mass to increase by many orders of magnitude in a short temperature interval. The value of the effective mass was extremely small before this occurred, and coupled with a small carrier density, would indicate that the primary band is the same as occurs in all the other compositions, being similar in form to the HgTe band structure. The second heavy mass band would seem to lie 0.03 eV above this light mass band, being activated by just below room temperature.

It would seem, then, that the band model for HgTe - In_2Te_3 alloys follows the general lines set out by Wright (159), the model being based on the Groves and Paul band model for grey tin. However, in the paper, Wright indicates that the heavy mass band is level with the light mass band at the 37.5% composition. It would now seem that this occurs nearer to the 50% composition, since no heavy electron effective masses were found in the 37.5% composition, unlike in the 50% composition.

References

1. Suchet J.P. Chemical Physics of Semiconductors pp. 3-6 (1965).
2. Smith R.A. Semiconductors p.57 (1961).
3. Heitler W., and London F. Zeitschrift für Physik 44 p.455 (1927).
4. Kröger F.A. The Chemistry of Imperfect Crystals pp.194-214(1964).
5. Spenke E. Electronic Semiconductors pp.29-33 (1958).
6. As (5) p.30. See also Wannier G.H. Phys. Rev. 52 p.191 (1937).
7. As (1).
8. Slater J.C. Quantum Theory of Matter (1951).
9. As (2), pp. 45 - 73.
10. As (5), pp. 29 - 53.
11. As (4).
12. Sommerfeld Zeitschrift für Physik 47 p.1 (1928).
13. Bloch F. Zeitschrift für Physik 52 p.555 (1928).
14. Pincherle L. Course 22 Semiconductors p.9 (1963).
15. As (14) pp. 26. - 41.
16. Jenkins D.P. Physica 20 p.967 (1954) for Si.
17. Bell, D.G. et al. Pro. Roy. Soc. A.217 p.71 (1953) for PbS.
18. Herman F. Phys. Rev. 93 p.1214 (1954) for Ge and Si.
19. InSb was once considered to have such a band structure but recent work on spin-orbit coupling, important in InSb, has shown that InSb has an extremely complex band shape at $\underline{k} = 0$ See (14) p.47.
20. Pincherle L. Proc. Int. Conf. Semiconductors, Exeter, p.541 (1962).
21. As (14) pp. 41 - 48.
22. Krömer H. Progress in Semiconductors 4 (1960).
23. Kohn W. Phys. Rev. 105 p.509 (1957).

References - continued

24. As (5) p.218.
25. As (2) p.81.
26. As (2) p.99.
27. Wannier G.H. Elements of Solid State Theory p.199 (1960).
28. Lax B., and Mavroides J.G. Solid State Physics 11 (1960).
29. As (2). p. 332.
30. As (2) p.36 and p.77.
31. Ehrenberg W. Proc. Phys. Soc. A. 63 p. 75, (1950).
32. As (2) p. 81.
33. As (2) p. 82 ff.
34. Putley, E.H. The Hall Effect and Related Phenomena p.122 ff. (1960).
35. As (2) p. 91 and p. 334.
36. As (34) and (35).
37. Sondheim D.J. and Howarth E.H. Proc. Roy. Soc. A. 219 p. 53, (1953).
38. Kohn W. and Luttinger J. M. Phys. Rev. 108 p.590 (1957).
39. As (34) p.80.
40. As (34) pp. 88 - 89.
41. Chambers, R.G. Proc. Phys. Soc. (London) A65 p.903 (1952).
42. As (35) p. 120.
43. Amir Khanov Kh. I. et al. Fiz. Tver. Tela. 3 p.3743 (1961),
trans: Sov. Phys. Sol. State 3 p. 2713 (1962)
44. Puri S.M. and Geballe T.H. Phys. Rev. Letters 9 p.378 (1962).
45. Beer A.C. Galvanomagnetic Effects in Semiconductors pp.336-
339 and pp. 348 - 353 (1963).
46. Tsidil'kovskii I.M. Thermomagnetic Phenomena in Semiconductors
(1962).
47. As (45) pp. 308 - 328.

References - continued

48. As (45) p. 315.
49. As (45) p. 278 ff.
50. Blatt, F.J. Solid State Physics Vol. 4. p. 198 (1957).
51. Heikes R.R. and Ure R.W. (Jr.) Thermoelectricity p. 53 ff(1961)
52. As (45). p.99.
53. Enz. Ch. Physica 20 p. 983 (1954).
54. Ioffe A.F. and Stil'bano L.S. Reports of Progress in Physics 22 p. 167 (1959).
55. As (45) p. 111.
56. Read W.T. (Jr.) Phil. Mag. 45 p. 775 and p. 1119 (1954);
46 p. 111 (1955).
57. Nordheim L. Ann. Phys. 9 p. 641 (1931).
58. Hansen M. and Andenko K. Constitution of Binary Alloys
p. 840 (1958).
59. Delves R.T. and Lewis B.J. J. Phys. Chem. Solids 24 p.549(1963).
60. Lawson W.D. et al. J. Phys. Chem. Solids 9 p. 325 (1959).
61. Krucheanu Ye et al. Kristallografiia 9 no. 4 p.537 (1964).
62. Kuchanu Ye and Nistov N. Phys. Stat. Solidi 7 no. 1.
p. K9 - K 10, (1964).
63. Blum A.I., and Regel A.R., Zhur. Tekh. Fiz. 21 p.316 (1951).
64. Nikol'skaya E.I. and Regel A.R. J. Tech.Phys. U.S.S.R., 25
p. 1347, p. 1352 (1955).
65. Elpat'evskaya O.D. and Regel A.R. J.Tech. Phys. U.S.S.R. 27
p. 45 (1957). (trans: Sov.Phys.(Tech.Phys.)2 p.35 (1957)).
66. Tsidil'kovskii I.M. J. Tech: Phys. U.S.S.R. 27 p.1744 (1957).
(trans: Sov.Phys. (Tech.Phys.) 2 p. 1622 (1957)).
67. Harman T.C. and Logan M.J. Bull.Am.Phys.Soc.Ser.II. 3 p.15
(1958).
68. Black J. et al. Bull. Am. Phys. Soc. Ser.II, 3 p. 15 (1958).

References - continued

69. Carlson R.O. Phys. Rev. 111 no. 2. p. 476. (1958).
70. Lagrenaudie J. J. Chimie Phys. 55 p. 175 (1958).
71. Bell R.L. J. Elect. Control 3 p. 487 (1957).
72. Black J. et al. J. Elect. Chem. Soc. 105 p. 723 (1958).
73. Harman T.C. et al. J. Phys. Chem. Solids 7 p. 228 (1958).
74. Rodot H. and Triboulet R. Comptes Rendus, Paris, 254
p. 852, (1962).
75. Rodot, H. J. Phys. Chem. Solids 25 p. 85 (1964).
76. Quillet A., et al. Proc. Int. Conf. Semiconductors Exeter
p. 711 (1962).
77. Giriat W. Brit. J. App. Phys. 15 p. 151 (1964).
78. Kot, M.V. and Meronchuk Yu-Ye. Tr.Po.Fiz. 1 pp 77-84 (1962).
79. Ivanov-Omskii V.I. et al. Izv.Akad.Nankusse Ser. Fiz. 28
no. 6 p. 1057 (1964).
80. Tovstymk K.D. et al. Izv. Akad. Nank. U.S.S.R. Ser. Fiz. 28,
no. 6 p. 1048 (1964).
81. Strauss, A.J. et al. Proc. Int. Conf. Semiconductors Exeter
p. 703 (1962).
82. Dziuba Z. and Zakrzewski T. Physica Stat. Solidi 7, no.3,
p. 1019 (1964).
83. Kolodziejczak J. Acta.Phys.Polon. 20 p. 379 (1961).
84. Byszewski P. et al. Phys. Stat. Solidi 3 p. 1880 (1963).
85. Dziuba Z. Acta Phys. Polon. 26, no. 5 p. 897 (1964).
86. Dziuba Z. Acta Phys. Polon. 25 no. 5 p. 757 (1964).
87. Rodot H. and Rodot M. Comptes Rendus, Paris 248 p. 937 (1959).
88. Rodot H. and Rodot M. Comptes Rendus, Paris 250 p. 1447 (1960).
89. Harman T.C. and Strauss A.J. J. App. Phys. Supp. 32
p. 2265 (1961).
90. Harman T.C. et al. Phys. Rev. Letters 7 p. 403 (1961).
91. Kane E.O. J. Phys. Chem. Solids 1 p. 249 (1957).

92. Harman T.C. et al. Sol. State Comm. 2 no. 10, p.305 (1964).
93. Groves S. and Paul W. Phys. Rev. Letters 11 p. 194 (1963).
94. Thomas D.G. J. App. Phys. 32 p. 2298 S (1961).
95. Mavroides J.G. and Dickey D.H. to be published.
96. Woolley J.C. and Ray B. J. Phys. Chem. Solids 13 p.151 (1960).
97. Harman T.C. et al. to be published.
98. Blair J. and Smith A.C. Phys. Rev. Letters 7 p. 124 (1961).
99. Kafakes J.A. et al. J. Phys. Chem. Solids 23 p.1541 (1962).
100. Sorokin O.M. Sov. Phys. So. State 2 p. 2091 (1961).
101. Braithwaite J. Pure Phys. Soc. B.64 p. 274 (1951).
102. Kruse P.W. et al. Infra-Red Physics 2 p. 53 (1962).
103. Quilliet A. et al. J. de Phys. et Rad. 23 p. 93 (1962).
104. Cardona M. and Harbeke G. J. App. Phys. 34 p. 813 (1963).
105. Cardona M. and Greenaway D.L. Phys. Rev. 131 p. 98 (1963).
106. Mavroides J.G. and Kolesar D.F. Solid State Comm. 2 no. 12
p. 363 (1964).
107. Ioffe A.V. and Ioffe A.F. Sov. Phys. Sol. State 2 p. 719 (1960).
108. Rodot M. et al. J. App. Phys. 32 p. 2254 (1961).
109. Spencer P.M. Thesis, Durham University p. 112 (1963).
110. Phillips F. C. An Introduction to Crystallography, p. 148 (1946).
111. As (110), p. 147.
112. Rodot H. et al. Comptes Rendus, Paris 256 p. 5535 (1963).
113. As (58) p. 863.
114. Holmes P.J. et al. J. Phys. Chem. Solids, 23 p.1 (1962).
115. Woolley J.W.C. and Pamplin B.R. J. Elect. Chem. Soc. 101 p.874 (1961).
116. Zaslavskii R.I. and Sergeeva V.H. Fiz. Tver, Tela 2 no. 11
p. 2872 (1960), trans. Sov. Phys. Sol. St. 2 no. 11 p. 2556 (1961).

References - continued

117. Zhuze V.P. et al. Fiz.Tuer Tela. 2 no 11 p. 2858 (1960),
trans.: Sov.Phys.Sol. State 2 no.11 p. 2545 (1961).
118. Woolley J.C. et al. J. Less. Comm. Metals 1 p.362 (1959).
119. Gasson D.B. et al. Proc.Int.Conf.Semiconductor Phys.Prague,
p. 1032, (1960).
120. Hahn H. and Klinger W. Zeit. Anog. Chem. 260 p. 97 (1949).
121. As (58) p. 864.
122. Inuzuka H. and Sugaike S. Proc. Acad. Japan 30 p. 383 (1954).
123. Petrushevitch V.A. and Seegeeva V.M., Fiz. Tuer Tela. 2,
no. 11 p. 2881, (1960).
trans.: Sov. Phys. Sol. State 2 no. 11. p. 2562 (1961).
124. Woolley J.C. et al. J. Phys. Chem. Solids 19 p. 147 (1961).
125. Ioffe A.F. Doklody Akad. Nauk U.S.S.R. 16, no. 10 (1952).
126. Ioffe A.F. Zhuz. Tekh. Fiz. 27 p. 1153 (1957).
trans.: Sov. Phys. Tech. Phys. 2 p. 1049, 1957.
127. Ioffe A.F. Fiz. Tuerd. Tela 1 p. 157 p. 160 (1959).
trans.: Sov. Phys. Sol. State 1 p. 139 p. 141, 1960.
128. Chizhevskaya S.N. and Glazov V.M. Doklody Akad.Nauk.S.S.S.R.
145 no. 1 p. 115 (1962).
129. Sergeeva V.M. and Shelykh A.I. Fiz. Tuer. Tela 2 no. 2
p. 347 (1960).
130. Zaslavskii A.I. et al. Fiz. Tuer. Tela 2 no. 11. p. 2885 (1960).
trans.: Sov.Phys. Sol. State 2 no. 11. p 2565 (1961)
131. Petrushevitch V.A. et al. Fiz. Tuer. Tela 2 no. 11 p. 2894
(1960), trans: Sov.Phys.Sol.State 2 no. 11 p.2573 (1961).
132. Spencer P.M. Thesis, Durham University p. 109, (1963).
133. Woolley J.C. and Ray B. J.Phys.Chem. Solids 15 p.27 (1960).
134. Pamplin B.R. Thesis Nottingham (1960).
135. Spencer P.M. et al. Proc. Int. Conf. Semiconductors,
Exeter p. 244 (1962).
136. Spencer, P.M. Thesis, Durham University (1963).
137. Mason D.R. and Cook J.S., J.App. Phys. 32 p. 475 (1961).

138. Lawson W.D. and Nielsen S. Preparation of Single Crystals (1958)
139. The Art and Science of Growing Crystals, 1963).
140. Methods of Experimental Physics 6 B pp. 145 - 170 (1959).
141. As (140) pp. 147 - 153. (1959).
142. Stockbarger D.C. Rev. Sci. Ins. 7 p. 133.
143. As (34) p. 45.
144. As (136) p. 76, section 18.4.
145. As (136) p. 104, section 25.2.
146. As (136) p. 104 section 25.3.
147. As (110). p. 155.
148. As (110) p. 148.
149. Henry N.F.M. et al. Interpretation of X-ray Diffraction photographs ch. 13 p. 189. (1960).
150. As (149) ch. 13 p. 190 see also ch.11 p. 168 for the method of taking powder photographs and ch.6 p. 71 for Laue photographs.
151. As (34) p. 45.
152. As (45) p. 57 Fig. 4.
153. Drabble J.R. and Wolfe R. Journ.Electr.Controls III 3, p. 259 (1957).
154. As (34) p. 27 and p. 42.
155. Wilson A.H. Theory of Metals 2nd Edⁿ p. 204 and p.15 (1953).
156. Woods and Chen Phys. Rev. 135, 5A p. 1462 (1964).
157. Tryozawa Y., J. Phys. Soc. Japan 17, p. 986 (1962).
158. Hahn H. et al. Zeit. für Anorg.Chemic. 279 p.241 (1955).
159. Wright D. A. Brit. Journ. App. Phys. 16 p. 939 (1965).

